Structure-Property Relations of Imine-Linked Covalent Organic Frameworks

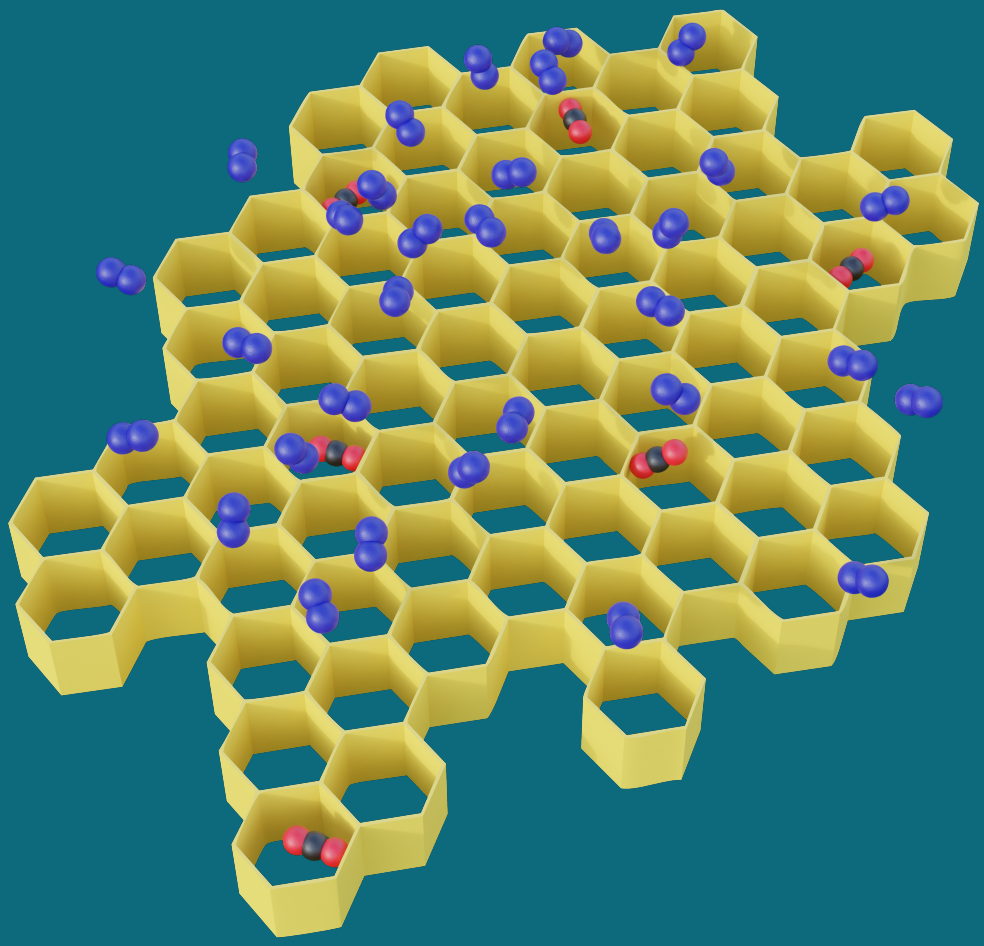

Ellen Dautzenberg

Propositions

1. Time-dependent solid-state NMR compensates for the inaccessibility of 2D solid-state NMR.
   (this thesis)

2. Stability is an overlooked topic in Covalent Organic Framework research.
   (this thesis)

3. Incentivising researchers to focus on number of publications and impact factors shifts the traditional understanding of academic qualification.

4. The results of computational chemistry are only as good as the chemists performing it.

5. Without knowledge diamonds are just rocks.

6. Practising karate would make the world more peaceful.

Propositions belonging to the thesis, entitled

Structure-Property Relations of Imine-Linked Covalent Organic Frameworks

Ellen Dautzenberg,
Wageningen, 14 March 2023

Structure-Property Relations of Imine-Linked Covalent Organic Frameworks

Ellen Dautzenberg

Thesis committee

Promotors

Prof. Dr L.C.P.M. de Smet

Personal Chair at the Laboratory of Organic Chemistry

Wageningen University & Research

Prof. Dr H. Zuilhof

Professor of Organic Chemistry

Wageningen University & Research

Other members

Prof. Dr H. Bitter, Wageningen University & Research

Prof. Dr A. Thomas, Technische Universität Berlin, Germany

Dr M.A. van der Veen, TU Delft

Dr R. Ameloot, KU Leuven, Belgium

This research was conducted under the auspices of VLAG Graduate School (Biobased, Biomolecular, Chemical, Food, and Nutrition Sciences).

Structure-Property Relations of Imine-Linked Covalent Organic Frameworks

Ellen Dautzenberg

Thesis

submitted in fulfilment of the requirements for the degree of doctor

at Wageningen University

by the authority of the Rector Magnificus,

Prof. Dr A.P.J. Mol,

in the presence of the

Thesis Committee appointed by the Academic Board

to be defended in public

on Tuesday 14 March 2023

at 4 p.m. in the Omnia Auditorium.

Ellen Dautzenberg

Structure-Property Relations of Imine-Linked Covalent Organic Frameworks, 162 pages.

PhD thesis, Wageningen University, Wageningen, the Netherlands (2023)

With references, with summary in English

ISBN: 978-94-6447-460-2

DOI: https://doi.org/10.18174/579409

Table of Contents

1 Introduction

1.1 General introduction

Porous materials are solid structures that permanently contain pores. On a macroscopic level, the porosity can be illustrated by a pumice (**Figure 1.1**), which rough surface with vesicles reflects the porosity that porous materials contain on a nanolevel. Based on the size/diameter of these pores, porous materials can be classified as macroporous (pore size >50 nm), mesoporous (2-50 nm) and microporous (<2 nm).[1] These pores lead to large, accessible surface areas, which make these materials interesting for, amongst others, energy storage,[2,3] catalysis,[2,4–6] sensing,[2,7] and gas separation (**Section 1.4.2**)[2,8]

Figure 1.1: Photograph of a pumice. The rough surface with its vesicles can be used to illustrate the porosity of nanomaterials on a macroscopic level.

The history of porous materials goes back into the 18^{th} century, when zeolites were discovered as natural minerals.[9] At that time, their porosity remained unknown and was only discovered later. Zeolites are inorganic materials, consisting of aluminosilicates, which are bridged by oxygen atoms. Based on the geometry, they can form several different types of pore architectures and pore sizes. Besides the naturally occurring minerals, zeolites have to date also been synthesised artificially.[9] In the 1990s, porous inorganic-organic hybrid materials were discovered, namely metal organic frameworks (MOFs).[10,11] They consist of metal ions that are coordinated by multivalent organic linkers. That way, one linker coordinates several metal ions, and a regular framework structure with voids is formed.[12] In 2005, Yaghi and co-workers designed covalent organic frameworks (COFs), which are the fully organic equivalent of MOFs.[13]

To this end, two or more multivalent building blocks react with each other forming the polymeric COF linkage. In this thesis, valency refers to the number of functional groups in building blocks that are used to form the COF linkages. The terms 'functionalised' and 'functionalisation' refer to any additional functional groups that are present in the COF but that are not involved the linkage formation. Other relevant terms that are part of the COF nomenclature are related to the position of the building block in the framework: linkers and nodes, which at least should be a combination of a divalent and trivalent building blocks to enable the formation of a framework.

1.2 Covalent organic frameworks

The first COFs consisted of boronic esters and boroxine anhydrides and were synthesised by dynamic covalent chemistry (DCC).[13–15] Dynamic covalent chemistry refers to reversible reactions carried out under thermodynamic reaction conditions. A requirement for a dynamic covalent reaction is a reaction rate high enough to have an equilibrium during the framework formation, but low enough to form stable products. Typically, dynamic covalent bonds are often only broken by a catalyst.[14] The constant cleavage and reformation of bonds can transform amorphous polymers and oligomers into to crystalline frameworks with long-range order. Alternatively, DCC enables the opportunity for exchange reactions with a different monomer to form new COFs.[16–18]

Powder X-ray diffraction (PXRD) measurements and high-resolution transmission electron microscopy (HR-TEM) images have revealed the crystalline nature of COFs and the regular structure of pores.[19,20] One advantage of COFs over MOFs is that they combine several advantages of dynamic chemistry with a high chemical stability due to the formation of covalent bonds. In more detail, the dynamicity enables error correction during the framework formation, which results in higher degrees of crystallinity, and it also opens the possibility for linker-exchange reactions. Based on their type of linkage (**Section 1.2.1**), COFs can retain their crystallinity and chemical composition in acidic and/or alkaline solutions.[21–24]

COFs can be synthesised based on tetravalent, tetrahedral building blocks to form a three dimensional (3D) framework.[25–29] Alternatively, aromatic building blocks, for example trialdehyde nodes and diamine linkers, are linked together, leading to two dimensional (2D) polymeric sheets, which form a 3D structure with channel-like pores due to π-π-stacking (**Figure 1.2**).[6,30]

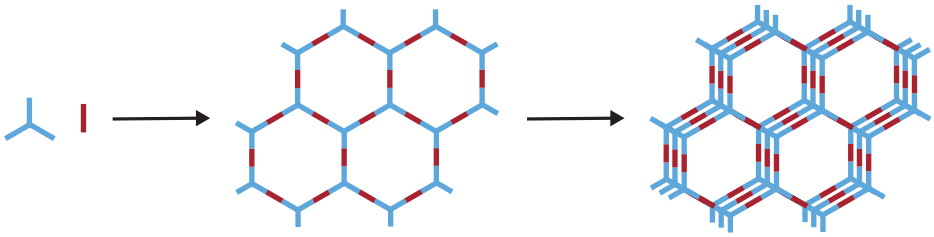

Figure 1.2: Schematic representation of 2D COF condensation. The building blocks react with each other, forming regular, 2D polymeric sheets, which stack upon each other by π-π-stacking.

Several different reaction conditions have been reported for COFs, including microwave-assisted synthesis, mechanochemical synthesis and solvothermal synthesis.[2] For many COFs, the reaction conditions — such as temperature, inert atmosphere, catalyst, solvents — have been optimised to achieve high porosity.[2,31–33]

Most COFs have been synthesised by via solvothermal synthesis.[2] The term 'solvothermal synthesis' refers to a synthesis in a closed reaction vessel under elevated temperatures, leading to a reaction under a higher than atmospheric pressure. Typically, the building blocks are dissolved in the optimised solvent mixture in the reaction vessel, subjected to three freeze-pump-thaw cycles and then often closed by flame sealing. As flammable organic solvents are used, the flame sealing requires special knowledge to perform it safely. The reaction is then mostly left for three several days to allow the reaction to reach the thermodynamic minimum for a high crystallinity and porosity.

These harsh conditions led to the development of milder methods. It was found that the reaction of a hydrazine COF at room temperature for three days led to a moderate Brunauer, Emmett, Teller (BET) surface area (S_{BET}) (**Section 1.2.1**) of 446 m^2/g.[34] Only 2 h at room temperature were needed when transition-metal nitrate catalysts were used to synthesise imine-linked COFs.[33] As an alternative to decrease reaction times, microwave-assisted synthesis can be employed. High surface areas (S_{BET} > 1000 m_2/g) were achieved within a reaction time of 3 h.[31]

The solvent-free mechanochemical synthesis, developed by Banerjee and co-workers, illustrates the large variety of synthetic methods to obtain COFs.[35] Grinding the building blocks in a mortar can lead to β-ketoenamine COFs with moderate crystallinity within 40 min. The reaction uses the mechanical energy instead of thermal energy and the absence of solvents is advantageous, as it is more environmentally friendly, and intrinsically leads to a high concentration of all reagents involved.

The variety of different linkage motifs, the large diversity of building blocks and the different synthetic methods illustrate the tuneability of COFs, which further shows their potential as promising candidates for many applications.

1.2.1 Linkage chemistry

The classification of COFs is not only based on the dimension (2D/3D), but also and mainly based on the linkage chemistry that connects the building blocks in COFs. Each different type of linkage has certain advantages and disadvantages, which can be explained by the COF trilemma.[36] Three different features are important to obtain ideal COFs: stability, crystallinity, and functionality. However, these features compete with each other. By employing reversible reactions, a higher crystallinity is achieved through a better reversibility of the reaction, as this enhances the correction of any crystallinity error to reach the thermodynamic minimum. Concomitantly, a higher reversibility means that the bonds are more easily cleaved, yielding structures that are more susceptible to hydrolysis, deteriorating the COF stability. Harsher reaction conditions, *i.e.*, higher reaction temperatures and pressures, can also enhance the reversibility of the reaction. Unfortunately, functional groups attached to the building blocks are often not compatible with these harsh reaction conditions. Therefore, a compromise must be found between stability, crystallinity, and functionality of the resulting COF.[36] This can be done by choosing a specific COF linkage. The most common COF linkages will be discussed in this section.

As already mentioned, Côté *et al.* synthesised the first COF in 2005, which was based on boronic esters or boroxine anhydrides.[13] Boronic esters are formed by the condensation of catechol units with a boronic acid or boroxines, also termed boronic anhydrides, are formed through dehydration of boronic acids. While boronic acids are attractive for the synthesis of COFs given their large diversity and commercial availability, boron based COFs suffer from hydrolytic instability, reducing their applicability (**Table 1.1**).[37] The BET surface area of the boroxine COF-1 and the boronic ester COF-5 were reported to be 711 m^2/g and 1590 m^2/g, respectively.

Covalent triazine frameworks (CTFs) can be considered as a subclass between COFs and porous organic frameworks (POFs), which are the non-crystalline equivalent of COFs.[38] CTFs are formed through the ionothermal synthesis of nitrile monomers in the presence of zinc chloride.[39] Ionothermal synthesis uses ionic liquids as solvents, but they can also function as template for the pre-organisation of monomers.[40] During the reaction, the nitrile groups react to triazine rings and form pores. The

high nitrogen content, which can interact with analytes, and the high chemical and thermal stability make this subclass of COFs interesting for a large variety of applications, such as gas adsorption and storage, heterogeneous catalysis and photocatalysis.[38] However, not all CTFs are crystalline, and the reaction conditions are usually very harsh, *i.e.*, > 400 °C or requiring superacids as catalysts (**Table 1.1**).[38]

One of the most common types of linkages in COF chemistry are imines.[2] Imines are synthesised via a condensation reaction from an aldehyde and an amine under acidic catalysis (**Scheme 1.1**), which is also known as Schiff base chemistry.[2,31,41,42] Schiff base chemistry was already developed in the 19^{th} century[42] and is therefore well known, and well understood. Furthermore, a large variety of aldehyde and amines are commercially or easily synthetically available, which results in a large number of different COF structures.

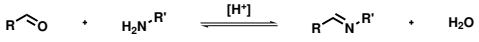

Scheme 1.1: General scheme for the condensation reaction of an aldehyde and an amine forming an imine.

The advantage of imine-based COFs compared to boron-based COFs is their increased hydrolytic stability (**Table 1.1**). Imine COFs are stable in most organic solvents, water and alkaline conditions.[2,43] The first imine COF was synthesised by Uribe-Romo *et al.* in 2009, via the condensation of tetrakis(4-aminophenyl)methane with terephthalaldehyde (PDA) using acetic acid as a catalyst.[25] The crystallinity was confirmed by PXRD measurements, and the BET surface area was determined to be 1360 m^2/g based on argon adsorption at 87 K.

Up to July 2022, the number of publications of imine COFs has reached over 650,[44] and a large variety of functionalised and non-functionalised building blocks has been employed, of which some are depicted in **Figure 1.3**. The building blocks vary in geometry, size, symmetry, reactivity, functionalisation, and valency.

The work on imine chemistry was the starting point to develop similar, yet different linkages such as azines,[37,45] hydrazones,[46–48] imides,[49–51] and β-ketoenamines for COFs (**Scheme 1.2**).[3,21,35,52] Azine COFs are of interest, because of their good chemical and thermal stability (**Table 1.1**). Moreover, the short hydrazine unit makes them interesting for applications that require small pores.[37] Hydrazone COFs possess weaker interlayer interactions, which makes it easier to exfoliate the stacked COF layers to achieve nanosheets.[48] Stegbauer *et al.* reported on a hydrazone COF that was the first

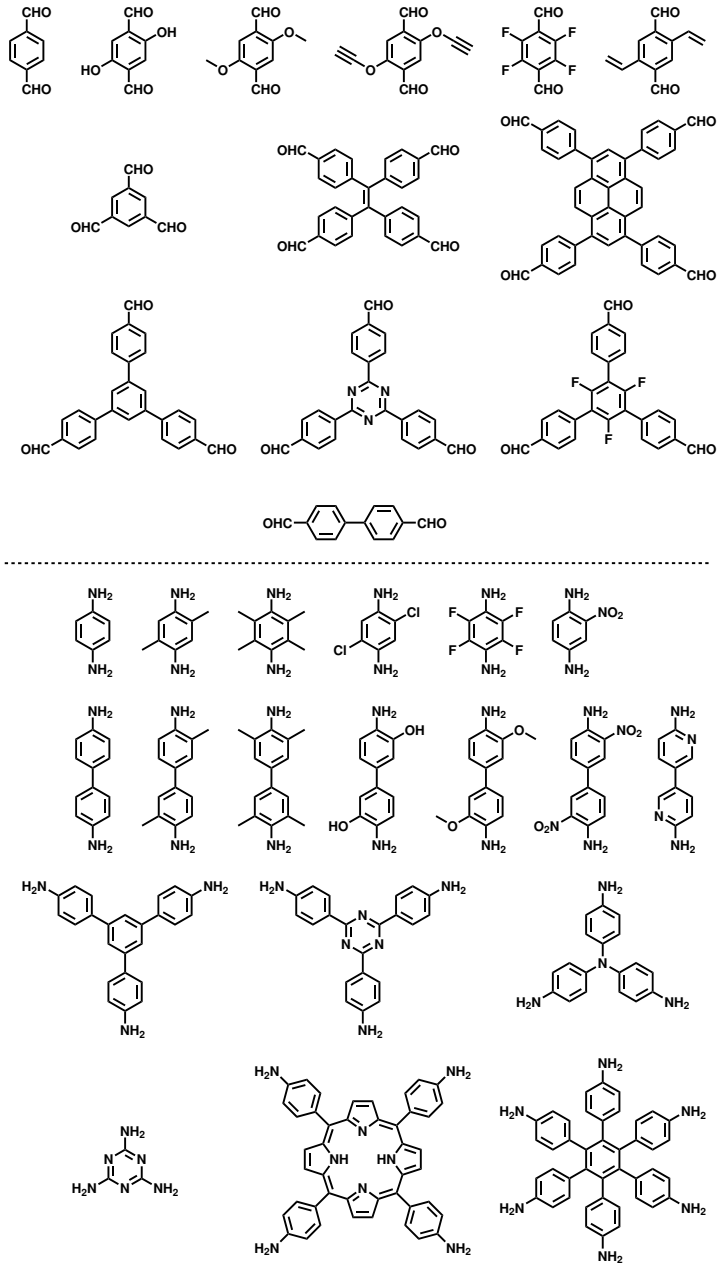

Figure 1.3: Selection of a series of aldehyde and amine building blocks to illustrate the variability of imine COFs.

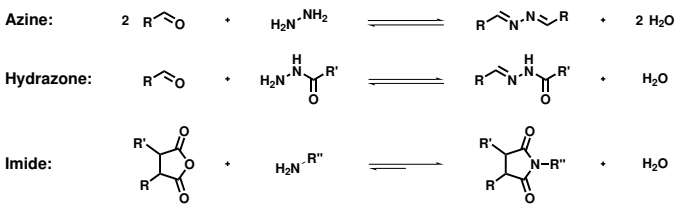

Scheme 1.2: Overview of the building blocks and the chemical structure of the azine, hydrazone, and imide linkages.

to produce hydrogen (H_2) from water under visible-light irradiation.[47] Imide COFs are known for their great chemical and thermal stability. However, the formation of high porosity imide COFs can be challenging because the reaction is limited in dynamicity (**Table 1.1**). Additionally, to form imine COFs harsh reaction conditions, *e.g.* temperatures up to 150-200 °C, are needed, which limits the compatibility with functional groups.[49–51]

β-Ketoenamine COFs are based on aldehyde-amine condensation, first forming an imine bond (**Scheme 1.3**). In contrast to imine COFs, the aldehyde building block is mostly 1,3,5-triformylphloroglucinol (TFP). The additional hydroxy groups tautomerise irreversibly to form β-ketoenamines. This irreversible tautomerisation leads to an enhanced chemical stability with respect to imine COFs (**Table 1.1**). At the same time, this irreversible step hampers the error-correction that is required to obtain a porous framework structure that is highly crystalline. The group of Banerjee of reported the first β-ketoenamine COF in 2012.[21] They used TFP, 1,4-phenylenediamine (PA) and 2,5-dimethyl-1,4-phenylenediamine (PA-2) as building blocks for their COFs. Both COFs showed an exceptionally strong resistance towards aqueous solutions of 9 N HCl and 9 N NaOH. Soon after, Banerjee and co workers reported on a possibility to synthesise these COFs via a mechanochemical synthesis.[35] Moreover, mechanical grinding can be used to delaminate the COFs into nanosheets.[53] Karak *et al.* further optimised the mechanochemical grinding by using *p*-toluenesulfonic acid.[52] The acid ensures the reversibility of the reaction and leads to higher crystallinity and porosity in comparison to grinding without acid. This process allows for large-scale synthesis of β-ketoenamine COFs with up to 10 g/s. The resulting COFs exhibit very high BET surface areas of approximately 3100 m^2/g after 60 s reaction time. The authors demonstrated that COFs could be processed *in situ* into a variety of different shapes.

So far, all examples for COF formation rely on the formation of different types of C-B, O-B or C-N bonds during the reaction. In 2016, the synthesis of fully C=C linked COFs was achieved by

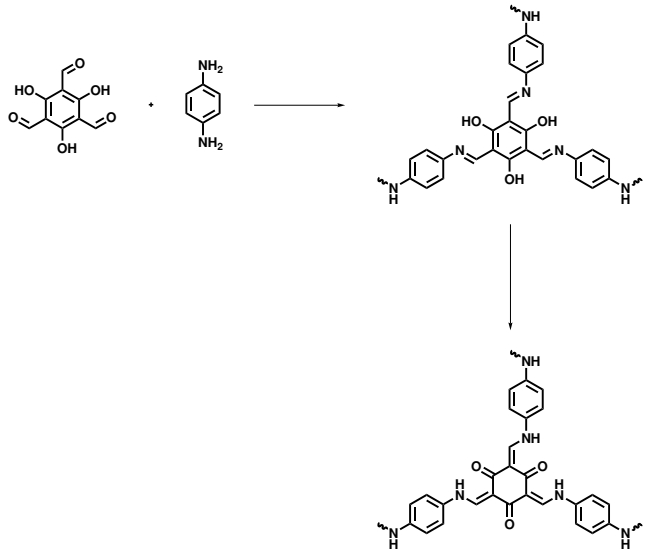

Scheme 1.3: 1,3,5 Triformylphloroglucinol reacts with 1,4-phenylenediamine forming an imine-linked COF, which can then tautomerise into the β-ketoenamine COF.

Knoevenagel polycondensation.[54] C=C bonds enhance the conjugation with respect to the C=N bonds of imines, which leads to a better ion conductivity.[55] On the one hand, the chemical stability of C=C bonds is much higher compared to bonds including heteroatoms, which makes vinylene COFs advantageous for applications. On the other hand, the synthetic control to achieve regular pores remains a challenge, because the C=C bond formation is less dynamic (**Table 1.1**).[56]

Table 1.1: Summarised overview of the advantages and disadvantages of COF linkages related to the COF trilemma.

COF	Chemical stability	Crystallinity	Functionality
Boronic ester	hydrolytically poor	high	high
Boroxines	hydrolytically poor	high	high
CTFs	good	varies	limited
Imines	good	high	high
Azines	good	high	medium-low
Hydrazones	great	high	high
Imides	great	low	low
β-Ketoenamines	great	low-medium	medium-high
Vinylene	great	low	medium

With respect to the COF trilemma and considering the advantages and disadvantages for all different linkages, we have chosen to focus on imine COFs. Compared to hydrazones — the type of linkage that shows the best specifications in **Table 1.1** — imines are more widely used, and their chemistry is well understood. Moreover, the large variety of potential building blocks (aldehydes and amines) also allows for a wider COF tuneability. With gas interactions and related applications in mind, we aimed for highly crystalline COFs in order to have many gas adsorption sites.

1.2.2 Pore architecture

Besides the type of COF linkage, also the pore size and pore geometry determine the COF structure and its properties to a large extent, which can be rationalised by their impact on the high surface to volume ratio of COFs. Control over pore size and pore geometry is therefore crucial.

Reticular chemistry is the concept to pre-design a framework/COF structure based on rigid building blocks by strong, covalent bonds. It is a prerequisite to use well-defined, rigid building blocks that maintain their structure during the reaction.[57] Therefore, COF synthesis makes usually use of aromatic building blocks. These conjugated molecules do not possess many degrees of freedom and maintain their structure. The valency of the building blocks and their angles predetermine the pore shape.[58] One of the most studied COFs — TFB-PA — is synthesised based on 1,3,5-triformylbenzene (TFB) and PA.[6] The combination of a (3,2)-connected 2D framework leads to the formation of hexagonal pores, forming a honeycomb (**hcb**) topology. The pore size can be varied by the size of the building blocks. In more detail, the use of benzidine (BD) instead of PA leads to larger pore sizes.[59] The **hcb** topology is also available from (3,3)-connected building blocks. In that case, the building block at the vertices alternate, and the resulting pores consist of less molecules per pore, which results in smaller hexagonal pore sizes. 4-Connected building blocks can form different types of topologies based on the angle between the linkages. A 4-connected porphyrine derivative, which has 90 °angles, can react with a ditopic linker. This geometry combination forms the rectangular 'square grid like' **sql** topology (**Figure 1.4**). However, a building block with 120 ° and 60 ° angles, such as tetraphenyl ethylene-based building blocks, would form the kagome (**kgm**) topology with a ditopic linker. The kagome topology consists of two different pore geometries, *i.e.*, triangular and hexagonal, and sizes.[58]

Reticular design refers to the pre-design of a preferred topology. The chosen topology is deconstructed into the underlying geometric units, for which then molecular equivalents can be found. This

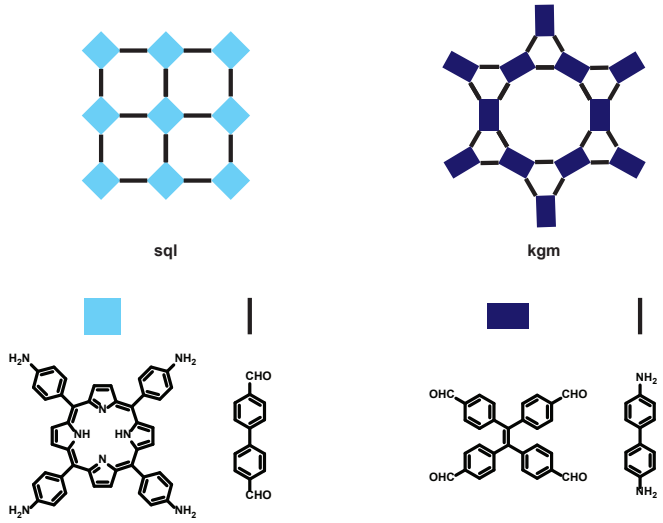

Figure 1.4: Schematic representation of square grid-like **sql** and kagome **kgm** topology and an example of the building blocks forming such a topology.

concept gave rise to the development of many different topologies with one, two or more different pore geometries.[58,60–62]

In this thesis, the honeycomb topology was chosen due to the commercial availability and facile synthesis of the respective building blocks.

1.2.3 Functionalisation

The advantage of COFs over other porous nanomaterials lies in the huge diversity of building blocks and synthetic possibilities to modify organic molecules. The aluminosilicates of zeolites consist of only three different atoms: aluminium, silica, and oxygen. In MOFs, the structural variety is already enhanced due to variation of the metal centres and due to the organic linkers, which are easily functionalised and varied. COFs possess an even broader building block library. Besides changing the valency and geometry of the respective building blocks, functional groups can be incorporated. The functional groups can enhance COF properties and additionally they can play an active role in the desired application and/or facilitate COF characterisation.[63] However, the use of functionalised building blocks in the synthetic scheme is limited by the tolerance to the reaction conditions and the reactivity of the building block itself. Two different ways to functionalise a COF can be differentiated: pre-synthetic and post-synthetic functionalisation (**Figure 1.5**). In pre-synthetic functionalisation,

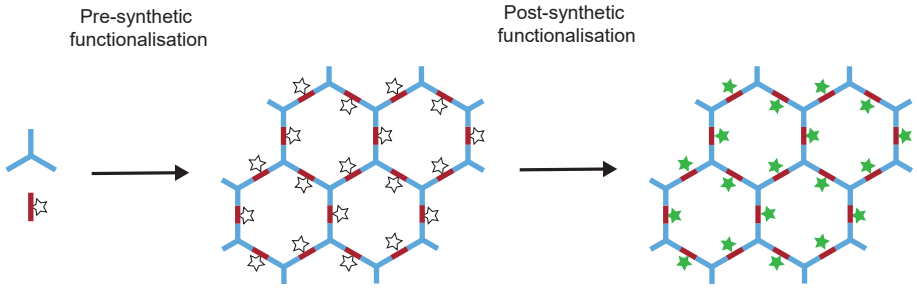

Figure 1.5: Schematic COF synthesis with a functionalised building block (step 1) and the post-synthetic conversion into different functionality (step 2).

the building blocks carry already the functional group of choice during the polymerisation and in post-synthetic functionalisation, the already existing COF is further modified.

The structural variety of potential building blocks is huge, and it is not possible to give a complete overview of all moieties involved. The standard phenyl substitutions such as hydroxy,[5] methoxy,[64,65] fluoride[66] or isopropyl[26,67] are the classical strategy for functionalisation as indicated in **Figure 1.3**. The hydroxy group was for instance employed to vary the push-pull electronic effect by tautomerisation in a series of imine- and β-ketoenamine-linked COFs.[5] The isopropyl substituent was used to tune the COF stacking to achieve staggered AB or ABC stacking in contrast to the usually obtained eclipsed AA stacking.[67] The hydrophobic isopropyl groups also protected the imine bonds from hydrolysis, leading to more chemically robust COFs. Recently, ionic COFs have been synthesised with guanidinium or sulfonic acid moieties.[68,69] Both moieties are known for their interaction with either cations[69] or anions,[70] which could be beneficial for ion sensing or desalination purposes. Next to ionic groups, functional groups can also possess redox activity.[3] A whole range of functionalised β-ketoenamine-linked COFs has been synthesised by Biswal *et al.* and studied for water adsorption.[71] The functional groups on the phenylenediamine or benzidine core included methyl, methoxy, tetrafluoro, and nitro groups. They also used azodianiline to incorporate a group that can isomerise upon irradiation.

The dynamic chemistry of COFs enables the use of monovalent building blocks, termed modulators. Due its monovalency, the modulator would terminate the reaction, but it can be replaced by a building block to continue polymerisation again. Mostly non-functionalised modulators were employed in studies and it was shown that they slow down the polymerisation, resulting in COFs with higher crystallinity and higher porosity.[72–80] Calik *et al.* studied the position of the modulator by using a thiol-functionalised modulator to enable staining with iridium clusters.[76] High-angle annular dark-field

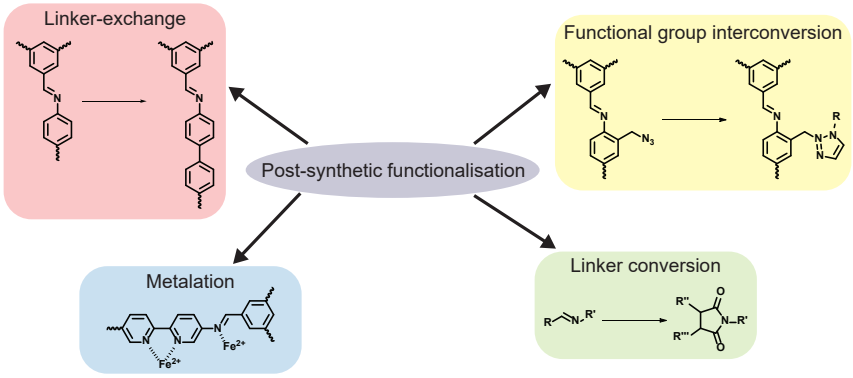

Figure 1.6: Schematic overview of the different post-synthetic functionalisation possibilities.

scanning TEM showed that the stained modulators were mainly located at grain boundaries. In addition, Lee *et al.* reported on modulators used for SO_2 capture.[81] In more detail, they synthesised imide COFs with a dimethylamine functionalised modulator and obtained a high uptake of 6.30 mmol/g, which equals 40 wt%.

Alternatively, the functionalisation can be achieved post-synthetically. The good stability of COFs is advantageous for one or more following reaction(s). Post-synthetic functionalisation has been widely studied and several different approaches have been reported.[63] Metalation is by far the most reported post-synthetic modification, but also linkage conversion, functional group interconversion or linker-exchange have been described (**Figure 1.6**). Imine linkages are the most extensively studied COFs for post-synthetic modifications.[63]

Post-synthetic metalation has been carried out with a large variety of different metal ions, such as main group elements (Ca,[82] Sr[82]), early transition metals (Ti,[83] V,[84] Mn,[82,85,86] Mb[87]), typical metals for heterogeneous catalysis (Fe,[88–90] Co,[85,88,90–92] Ni,[85,90,93] Cu,[85,94,95] Rh,[96] Pd[6,86,96–98]), and also rhenium,[88,99] and iridium[67] have been incorporated into the frameworks. The organic ligand can be the COF linkage with or without additional functional groups on the building blocks. Diaminobipyridines are typically used as building blocks for post-synthetic metalation. The diamine groups can react with the aldehyde groups of a second building block to form the imine linkages, while the bipyridine moiety can coordinate the metal ion.[91] Furthermore, porphyrin derivatives have been of particular interest, because the tetrapyrrole core can coordinate a large variety of metal ions and the framework pores can be doped with different metals.[63,88] Such bimetallic

doping has been utilised in cascade reactions.[86,96] In many cases, metalation is used to obtain heterogeneous catalysts. The applicability of COFs in catalysis has been shown by a variety of reactions, such as Suzuki-Miyaura and Heck cross couplings, addition reactions, cyclisation and one-pot cascade reactions, as well as oxidation and reduction reactions.[63] In more detail, metalated COFs can, for example, catalyse the reduction of carbon dioxide (CO_2) to carbon monoxide, which is an industrially used precursor for many processes.[99] Kushwaha *et al.* reported on an iron-metalated, azine linked COF.[100] This Fe-COF maintained the magnetic properties of iron and the large surface area allowed for a high level of dispersion of the magnetic iron particles within the COF. The Fe-COF was used as a coating of clothes to form a magnetic vest. Only 72 mg of Fe-COF were able to lift a mannequin doll of 10 g in weight, which is a 12-fold increase compared to the performance of pure nanoparticles. The authors suggest that such vests, which would contain 550 g Fe-COF for a 75 kg person, can be used to rescue people with a drone.

Post-synthetic modifications allow to change the COF linkage after the formation of a regular framework. This strategy can make inaccessible COF linkages accessible or it can be used to enhance the crystallinity and porosity of the COF. Amides, for instance, are stable bonds that are difficult to break, and therefore not good for the use in dynamic COF chemistry. One approach to generate highly crystalline COFs with amide linkages includes the syntheses of an imine-linked COF initially, which was then, in a second step, oxidised into its amide equivalent.[101] The symmetry and crystallinity as well as the porosity of the imine COF were retained during the oxidation step. Soon after, the same research group reported a strategy to access oxazole and thiazole COFs from imine COFs in a two-step reaction.[102] Again, an imine COF was synthesised in the first step. In a second step, the amine building block was exchanged by a hydroxy- or thiol-functionalised amine. The hydroxy or thiol group can react with the imine bond, followed by an oxidation to yield oxazole or thiazole linkages with retained porosity. The conversion was confirmed by solid-state nuclear magnetic resonance (ssNMR) and the new linkages were more stable compared to the pristine imine COF. A direct synthesis of crystalline COFs with oxazole and thiazole linkages is difficult due to the final irreversible oxidation step. The backbone modification is not limited to intramolecular reactions but can also involve additional molecules. For example, Li *et al.* locked the imine linkage through the subsequent reaction with phenylacetylene via an aza-Diels-Alder cycloaddition.[103] The obtained quinoline-linked COF displayed retained crystallinity and enhanced chemical stability in strong acidic and alkaline solutions and in redox environments compared to the pristine imine COF.

Functional groups in the COF building blocks can be further reacted after the polymerisation, which is often termed as 'pore-wall engineering' or 'channel-wall modification'. The functional group interconversion reactions require good conversions and high specificities to ensure that most functional groups have been transformed. The insolubility of COFs further complicates the analysis of the resulting material so that the material composition is not always unambiguously clear, which is a disadvantage of post-synthetic modifications. Click reactions are known for their good yields as well as their regio- and stereospecificity and therefore they are an attractive tool in post-synthetic functionalisation.[104] The first example of a copper(I)-catalysed alkyne-azide cycloaddition (CuAAC) for the post-synthetic modification of a COF was reported in 2011 by Jiang and co-workers.[105] They employed an azide-functionalised building block for their boronic ester COF, which could click with different alkynes to show the large diversity of the modification. Huang *et al.* employed an alkyne-functionalised porphyrin COF in a CuAAC reaction to incorporate different functional groups (Et, EtOH, AcOH, MeOAc, $EtNH_2$) into the pores.[106] Besides the widely used CuAAC reaction, strain-promoted cycloadditions, and also addition and substitution reactions were used in pore wall engineering.[63,107] Next to click reactions, etherifications can be employed to attach, for instance, zwitterionic molecules or tetraethylamine bromide containing moieties at the pore walls.[108,109] The resulting COFs catalyse the reduction of CO_2 in the presence of N-methylaniline and phenylsilane, or the formylation of amines with CO_2 and phenylsilane.

The dynamic chemistry also allows COF-to-COF transformations by building block exchange. This strategy offers the possibility to enhance the crystallinity of COFs or to obtain COFs that were not accessible via direct synthesis.[16–18] Qian *et al.* reported the first COF to COF linker-exchange by replacing PA with BD in an imine linked COF, which yielded an almost complete transformation.[110] This way, pristine imine COFs have been exchanged to oxazole,[102] thiazole,[102] imide,[16] azo[111] and amide COFs.[112] A varied size of the building block molecule changes the pore size of the COF. Cao *et al.* exchanged PA with hydrazine to obtain smaller pore sizes to enhance the sieving properties of their pristine COF.[113] The reversibility of this exchange becomes apparent through the reversible linker-exchange in which hydrazine got replaced by PA.[114] The authors reported on a time-dependent linker-exchange. As long as not all linkers were exchanged, the effective pore size was narrowed, allowing them to control the pore size needed for the desired membrane separation. Ma *et al.* exchanged C_{2v}-symmetric building blocks for C_3-symmetric ones.[115] This difference in building block symmetry expanded the scope of the linker-exchange strategy. Furthermore, this

linker-exchange strategy can be used to incorporate functional groups into the framework or transform a 3D COF into a 2D COF by varying the geometry of the building block.[116,117] This approach has also been employed to transform linear polymer into 2D COFs.[118,119]

To conclude, functionality plays an important role in COF design, because it can enhance the material quality and tailor the structure towards the desired application. Expanding the scope of COF functionalisation enhances the understanding of structure-property relationships and can help to improve the already existing COFs.

1.2.4 Stability

As discussed in the COF trilemma, stability is one of the key aspects for COFs. Stability refers to several different aspects: chemical, thermal, activation stability and stability over time (**Figure 1.7**).

The chemical stability was discussed in **Section 1.2.1** to illustrate the advantages and disadvantages of the different linkages. The thermal stability refers to the temperature at which the material degrades, *e.g.* the covalent bonds are broken. COFs usually start decomposing at temperatures of 300 °C or higher, indicating high thermal stability.[6,59,120] Evans *et al.* found that the thermal degradation of boronate and imine COFs occurs in two steps.[121] First, at a certain temperature, the COF loses its crystallinity before the chemical decomposition starts at a higher temperature. Additionally, boronate COFs were found to be more robust compared to imine COFs and smaller pore sizes lead to higher thermal stability. While Evans *et al.* report on a decreased thermal stability for functionalised COFs, Emmerling *et al.* found a beneficial effect of methoxy groups on the thermal stability.[122] They specifically studied the thermal stability and the slipped layer stacking of COFs with large pore sizes

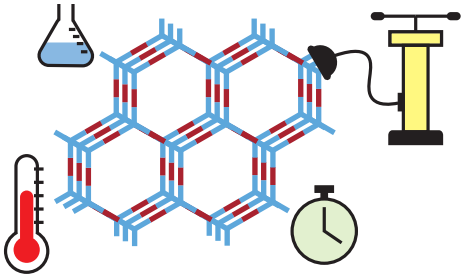

Figure 1.7: Schematic illustration of the four different aspects of COF stability: chemical stability, thermal stability, stability against pore collapse, and bench (time) stability.

(4.8 nm and 5.8 nm). They concluded that methoxy groups act as anchors by strengthening the interlayer interactions to prevent a slip between the COF sheets. Thereby, the accessibility of the pores and therefore large surface areas were maintained. Moreover, the increase in interlayer interaction was beneficial for the thermal stability.

Activation stability refers to the stability of the crystalline framework and possible pore collapse. In that case, the chemical bonds are not broken, but distorted and the COF sheets misalign. Such distortions and shifts lead to a loss of crystallinity and the pore collapse affects the pore shape, pore size and the surface area. Spectroscopic techniques like Fourier-transform infrared spectroscopy (FT-IR) or ssNMR, allow one to obtain information on the chemical structure of the COF sample and can therefore not display the distortions and misalignments of the COF sheets. For nearly 15 years, the synthetic reaction conditions and careful optimisation have been considered as most important for high-quality COFs. Only recently, the phenomenon of pore collapse has attracted attention in COF research, and by thorough analysis of the BET surface area it was found that the work-up and drying (referred to as COF activation) conditions are important to obtain high surface areas and crystallinity.[64,65,123]

Pore collapse is mainly caused by capillary forces. Capillary forces do not only increase with decreasing pore sizes, but also increase with increasing surface tension. This means that the commonly applied process of vacuum drying to remove solvent molecules damages the pores.[64,65,123] Zhu *et al.* have developed a washing protocol that uses solvent exchange from polar solvents to wash out oligomers and impurities to apolar solvents, ending with perfluorohexane, which has a low surface tension.[65] A similar, yet different, approach uses supercritical CO_2. The supercritical conditions remove the surface tension and clean, intact pores can be obtained.[64,123] Both methods rely on the reduction of surface tension to reduce capillary forces during COF activation.

Furthermore, the degree of pore collapse depends on the type of COF. A conclusive picture of what makes a COF more robust or fragile with respect to another COF is still not known and remains research of interest. It has been hypothesised that the interlayer interactions are important for the stability of COFs. To stabilise the interlayer interaction, Braunecker *et al.* employed C_3 aldehyde and amine building blocks of the same core; the aldehyde was fluorinated while the amine was not.[66] The resulting **hcb** COF can stack via an eclipsed stacking, where fluorinated molecules and non-fluorinated building blocks alternate along the stacking axis. This leads to an enhanced face-to-face π-π-stacking and therefore to an enhanced interlayer interaction. It was found that

with this improved stacking the COFs had higher BET surface areas and crystallinity. Employing intermolecular hydrogen bonds is an alternative way to lock the COF in a more planar structure, which also enhances the interlayer interaction and therefore leads to higher crystallinity and porosity.[124] Feriante *et al.* found that methoxy-substituted terephthaldehyde (OMePDA) formed a more robust COF (TAPB-OMePDA) with 1,3,5-tris-(4-aminophenyl)benzene (TAPB) in terms of vacuum activation compared to the unsubstituted equivalent, *i.e.*, the TAPB-PDA COF.[64] The reason why the methoxy group leads to a more robust framework is still not fully known, but it is assumed that a stronger interlayer interaction and steric hinderance of the methoxy groups stabilise the COF during vacuum activation. The same study shows that a larger extended π-system serves as a better docking site for adjacent sheets and reduces the interlayer distance, which makes the COF more robust.[64]

These few studies show that research on the structure-stability properties of COF is still in its infancy. Systematic, in-depth studies in this field would facilitate the optimisation of COF synthesis and activation and could provide a guideline for the development of pre-designed building blocks that would form more robust frameworks by themselves. Additionally, to the best of our knowledge, it is still unknown whether — and how long — a specific COF is bench stable, which is a crucial parameter for all types of application, further motivating the need to explore COF stability in more detail.

1.3 COF characterisation

1.3.1 Physisorption

Knowledge on the material's porosity is an immediate need when characterising COFs. Porosity can be expressed by surface area and pore size distributions. Both play an important role in tuning material properties for desired applications. Both are determined by nitrogen (N_2) physisorption measurements at 77 K. Physisorption refers to weak, unspecific interactions of an adsorptive with the adsorbent, mainly covered by Van der Waals forces.[1] The adsorbed molecules are called adsorbates. In a physisorption measurement the adsorptive will adsorb to and desorb from an adsorbent until an equilibrium is reached at which the adsorption rate equals the desorption rate (**Figure 1.8**). The quantity adsorbed is measured at different pressures at a constant temperature (isothermal) and the overall measurement gives the adsorption-desorption isotherm. During this physisorption process, N_2 will first be adsorbed at specific preferred adsorption sides, which leads to a monolayer formation. Continuous adsorption then leads to multilayer formation and eventually to pore filling. Based on the

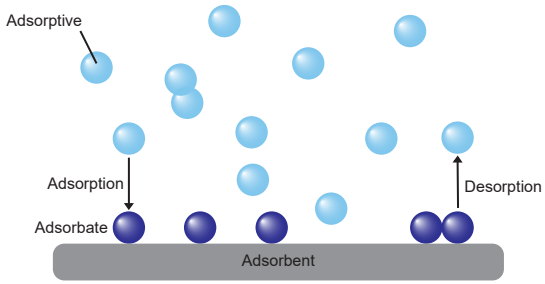

Figure 1.8: Schematic representation of the physisorption process. Adsorbed molecules in red, molecules in bulk in blue.

pore sizes present in the material, the isotherm has a certain shape that can be classified according to IUPAC convention.[1]

Furthermore, the surface area can be derived out of the isotherm. Several different theories have been developed to describe adsorption processes on surfaces. For the determination of surface area, two models are particularly important: the Langmuir model describes the monolayer formation and Brunauer, Emmett and Teller extended this theory for multilayer adsorption.[125,126] The multilayer has an infinite thickness and in each layer the adsorptive will need the same space to adsorb onto the already existing layer. It is also assumed that the enthalpy of adsorption for the first layer is larger than the second and higher layers. The enthalpy of adsorption of the second and higher layers equals the enthalpy of liquefaction.

Based on these assumptions, the BET equation (**Equation 1.1**) can be derived:

$$\frac{1}{v[(\frac{p^0}{p})-1]} = \frac{c-1}{v_m c}(\frac{p}{p^0}) + \frac{1}{v_m c} \tag{1.1}$$

where v is the quantity of adsorbed gas, p and p^0 are the equilibrium and saturation pressure of the adsorptive, respectively, c is the BET constant and v_m is the adsorbed quantity needed to form a monolayer.

This is the linearised version of the isotherm, and its plot contains a linear region, usually between 0.05-0.3 p/p^0. The surface area can be calculated out of the slope and intercept of this linear range.

In principle, the BET theory can only be applied to mesoporous materials. However, Rouquerol et al.[127] have developed criteria that make the BET theory applicable to microporous materials:

(a) The parameter c is related to the adsorption enthalpy and must therefore be positive;

(b) $v(1 - \frac{p}{p^0})$ must be continuously increasing;

(c) The pressure corresponding to the monolayer capacity (v_m) should be within the selected pressure range of the linear fit;

(d) The obtained value of $\frac{1}{\sqrt{c}+1}$ should not differ more than 10% from the relative pressure p/p^0 belonging to the monolayer capacity v_m.

It has recently been shown that the selection of the pressure range varies for different persons and that automated selection ranges can provide better tools for the selection of the appropriate pressure range.[128]

As a second key parameter for the characterisation of porous materials, the pore size distribution is of interest. Besides many classical models, that are all based on one single pressure to define the pore size, non-local density function theory (NLDFT) has been developed applied to compute adsorption isotherms.[129] For each pressure, a model isotherm is computed and several of those isotherms are collected in one Kernel that is used to fit the experimental isotherm. The development of more and newer DFT models for various adsorbents enhanced the quality of the fitted isotherms.

1.3.2 Powder X-ray diffraction

Powder X-ray diffraction (PXRD) is a technique that can be used to evaluate the crystallinity of a sample, and has proven to be an important, if not standard, technique in characterisation COFs. Max Laue discovered in 1912 that X-rays can diffract by crystalline materials.[130] Due to their long-range order, crystalline materials are acting as diffraction gratings with the atomic spacing as the spacing of the grating. In more detail, the X-rays can diffract at the atoms and constructively interfere when the Bragg equation[131] (**Equation 1.2**) is fulfilled:[132]

$$2d \times sin\theta = n \times \lambda \tag{1.2}$$

where n is a diffraction order, λ is the wavelength of the X-ray, d is the distance between parallel lattice planes, and θ is diffraction angle (the angle between X-ray radiation and lattice plane).

In a measurement, the only detected lattice plane is the one parallel to the surface. The high surface area of a powder ensures that, theoretically, each lattice plane is represented, resulting in all lattice planes being detected. This can be used to, amongst others, identify the phase (specific atomic

arrangement), determine the unit cell dimensions and the crystalline domain size. Domains should not be confused with particles. A polycrystalline particle can consist of several crystalline domains. If the domain size equals the particle size, one obtained a single crystal.[133]

In a PXRD diffractogram the diffraction angle is plotted against the intensity of X-rays. The phase can be identified based on the peak positions, as well as by comparison with a reference structure or a modelled crystal structure. The relative intensities of the peaks can give information about the morphology of the material. The unit cell dimension can be obtained via Pawley refinement of the patterns.[133]

Besides obtaining structural information, the peak width can give information about the domain size of the material. The sharper the patterns, the larger the domain sizes within the material.[133] The Scherrer equation[134] (**Equation 1.3**) is used to calculate the domain sizes based on the full width at half maximum of a diffraction peak:

$$D = \frac{K \times \lambda}{\beta \times cos\theta} \tag{1.3}$$

where D is the crystalline domain size, K is the Scherrer constant (usually 0.9, but can vary depending on the morphology), and β is the full width of a peak at half maximum.

1.3.3 Solid-state nuclear magnetic resonance spectroscopy

Usually, the chemical structure of molecules is elucidated by NMR spectroscopy. However, COFs are insoluble in any solvent, which makes it impossible to perform solution NMR. The utilisation of solid-state NMR offers an alternative for such structural characterisation. As this technique does not belong to the standard methods in COF characterisation, the most important differences and features will be highlighted in this section.

NMR uses radiofrequencies that resonate with spin state transitions of certain nuclei that are exposed to an external magnetic field. NMR analysis relies upon the relative frequency shifts between nuclei with different chemical environments, usually expressed as the chemical shift (δ). Together with the difference in the relative integrated peak intensities and peak characteristics, which reveal spin-spin coupling effects, one can identify connections between atoms within a molecule at such a level of detail that has proven to be very powerful in elucidating the structure of a molecule. Therefore,

NMR has become one of the standard analysis techniques in organic chemistry. Most NMR analyses focus on the ^{1}H or ^{13}C, but also ^{19}F or ^{31}P can be probed with NMR.

To understand the differences between solution NMR and ssNMR, it is important to realise that the chemical shift depends on the orientation of the molecule in the magnetic field. This anisotropy is caused by the asymmetric distribution of electrons in a molecule, which interact with the applied magnetic field, affecting the effective magnetic field experienced by the probed nuclei. This leads to broad signals, which may negatively influence the interpretation of spectra and signal assignment. In solution NMR spectra, the Brownian motion averages this anisotropy out. In a solid sample, this is solved by using a fine powder to make sure that all crystal orientations are present. Not only electrons, but also nuclei, like ^{1}H and ^{13}C, interact with the magnetic field. Each nucleus is by itself a small magnet and influences therefore the surrounding nuclei, which is called 'dipolar coupling ' and is also orientation dependent. Therefore, also dipolar coupling broadens the signals of the spectra. The closer two nuclei are, the stronger is the dipolar coupling. By spinning the sample at a specific frequency, external motion is introduced, which can average out the chemical shift anisotropy as well as the dipolar coupling. The angle at which the sample is spun is ideal at $\sim$54.74°, which is also referred to as 'magic angle' and its use in NMR therefore as 'magic angle spinning ' (MAS). To average all anisotropic components out, the magic angle spinning must be performed at high spinning frequencies. If the frequency is not high enough, spinning side bands can appear in the spectrum. Spinning side bands appear as sharp and intense signals that are separated from the isotropic shift by exactly the spinning frequency (**Figure 1.9**). Therefore, they shift based on the spinning frequency applied during the measurement. By comparing spectra at two or more different spinning frequencies, the isotropic signals and the spinning side bands can be differentiated from each other.[135,136]

As it is difficult to obtain high-resolution ^{1}H ssNMR spectra, which can only be obtained at high spinning frequencies ($\sim$60 kHz), solid-state NMR measurements focus on the detection of ^{13}C spectra. However, the low abundancy of ^{13}C leads to a low signal to noise ratio and the relaxation time, *i.e.*, the time related to the process by which the magnetic nuclei reach thermal equilibrium, can be very long. Both together lead to long measuring times. A solution to reduce the measurement time and to enhance the signal-to-noise ratio is cross-polarisation (CP), in which the magnetisation of an abundant (often ^{1}H) nucleus is transferred to the dilute nucleus (^{13}C). Both magic angle spinning and cross-polarisation are combined in most of the ssNMR sequences, which are applied in ^{13}C CPMAS analyses.[135,136]

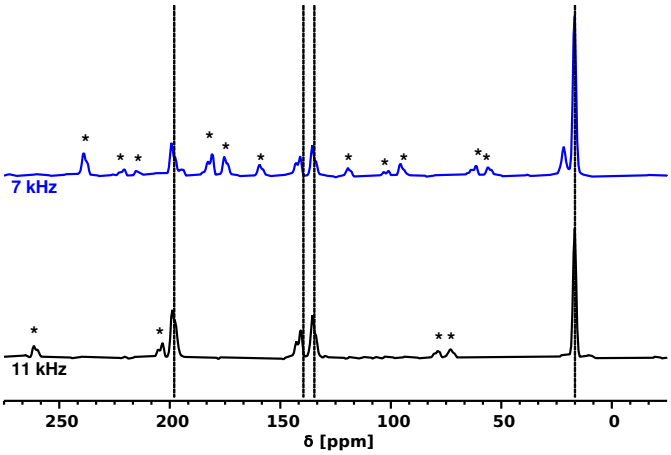

Figure 1.9: Solid-state NMR spectra at 7 kHz and 11 kHz spinning frequencies of the same compound. The chemical shift of the signal (dashed line) does not shift at different frequencies in contrast to the apparent chemical shift of the spinning side bands (asterisk).

Cross-polarisation can also be used to obtain additional information about the chemical structure, because it is dependent on the strength of the dipolar coupling between both nuclei. That is to say that a carbon atom bonded to one or more hydrogen atoms polarises faster compared to a quaternary carbon atom. Variation of the cross-polarisation time in the pulse sequence can probe the build-up rate of each atom and CP build-up curves can be obtained. Based on faster or slower build-up curves for the respective signals, the signals can be correlated to the chemical structure, enabling a more complete assignment.[136]

While the variation of the CP contact times is not yet frequently used in ssNMR analysis of COFs, in the timeframe of this PhD project, it has proven to provide advantageous information in the assignment of COF spectra. Samori and co-workers acquired 2D ssNMR spectra at two different contact times for the structural assignment of their imine COF.[137] This 2D experiment requires specialised ssNMR probes, which was overcome by Zhu *et al.* who measured spectra at 15 different CP contact times to assign a methoxy-functionalised, imine-linked COF.[33] The relative comparison of the signal build-up provided enough information for them to assign the COF structure. However, the analysis of the full CP build-up curve for structure elucidation of COF is still in its infancy.

1.3.4 Ideal adsorption solution theory

The ideal adsorption solution theory (IAST) was developed by Myers and Prausnitz to predict mixed gas adsorption behaviour.[138] To simulate the adsorption behaviour of gas mixtures, the pure component isotherms must be measured at the same temperature and on the same adsorbent. The basis of IAST is analogous to Raoult's law for vapour-liquid equilibrium.[138] For IAST, the adsorbed phase is assumed to behave like an ideal solution that is in an equilibrium with the bulk adsorptive. Furthermore, the underlying assumptions of the theory are:[138]

(a) The adsorbent is thermodynamically inert;
(b) The surface area is universally accessible and temperature invariant;
(c) The Gibbs definition of adsorption applies.

These assumptions apply to almost all theories of physical adsorption. The only difference between a fluid and an adsorbed phase is the substitution of spreading pressure for pressure and area for volume.[138] The spreading pressure can be interpreted as the negative surface tension,[139] and can be derived by integration of the adsorption isotherm. This integration is very sensitive at low surface coverage. Therefore, the adsorption isotherms have to be accurately measured in this regime. Based on these assumptions, thermodynamic equations can be derived to calculate the adsorbed solution equilibrium. In the end, seven equations are derived to solve nine unknown variables. Therefore, the pressure and the mole fraction must be defined prior to the calculations.[138] The simplicity of these calculations makes IAST a widely used method for selectivity determination in gas separation. The IAST selectivity (S) of a binary gas mixture is defined as the ratio of the mole fractions in the adsorbed state (q) over the mole fractions of the bulk phase (p) of components 1 and 2 (**Equation 1.4**).[140]

$$S = \frac{q_1/q_2}{p_1/p_2} \tag{1.4}$$

It must be noted that IAST is only of limited validity for polar adsorptive or mixtures, in which one component strongly adsorbs and the other one weakly. Other limitations are heterogeneous adsorbents and low loadings as they can lead to poor predictions of mixture adsorption. In more detail, for example, low loadings can lead to inaccurate spreading pressures, falsifying the selectivity calculation. If the fitted isotherms do not accurately reproduce the Henry constant for the specific adsorbate, the IAST calculation will predict incorrect selectivity values.[139]

1.4 COFs in applications

The large variety of functional building blocks to prepare COFs and the high porosities that can be obtained has led to the discovery of many applications for COFs. This ranges from the use of COFs as adsorbents, for example for heavy metal ions or toxic organic pollutants,[141] over catalysis[142] and chromatography[143] to even biomedical applications, such as cancer therapeutics.[144] This project focuses on studying the effects of functional groups in COFs on the properties of COF materials, mainly within the context of targeting COF-gas/vapour interactions. For that reason, the next paragraph focus on the role of COF in the fields of chemical sensors and gas separation.

1.4.1 Chemical sensors

Chemical sensors are needed to detect toxic or harmful compounds to prevent, for example, health problems or environmental damages. COFs can be employed as sensors, because the analytes can adsorb on the large surface area, which leads to a steep response in the read-out of the sensor. The read-out can be optical or electrical and for both, a variety of COF applications have been reported.[117,142,145,146]

A simple optical read-out or the detection via a change in fluorescence has been applied to sense Brønsted acids.[147–150] The proton attaches to a nitrogen lone pair of either the imine linkage or a bipyridyl moiety of the building block, which changes the absorption properties or switches fluorescence on/off, enabling acid detection. The sensing of iron[151] and nitroaromatic compounds works in a similar manner.[152] Additionally, solvents, for instance water, can be sensed by a colour change due to a solvatochromic response.[7]

Digital read-outs can be achieved by electrochemical sensors that either measure impedance,[153,154] the semiconduction behaviour of COFs,[155] resistance[156] or capacitance.[157] Impedance electrochemical spectroscopy has been used to build COF gas and vapour sensors that can detect ammonia and small amines. The β-ketoenamine COFs could sense those molecules without interference from CO_2, N_2, and methane (CH_4), which is an important property towards the development of real-life applications.[153] In another example, Zhang *et al.* used Ag-Pd interdigitated electrodes (IDEs) and coated them with an ionic β-ketoenamine COF for the detection of relative humidity.[154] A semiconducting gas sensor for the detection of nitrogen dioxide was built with exfoliated COF nanosheets and could detect the analyte down to 20 ppb unaffected by the relative humidity.[155]

More commonly known from daily life are resistance measurements, such as the resistance measurement of a light bulb. Ding *et al.* used this physical principle to construct an ammonia sensor.[156] In more detail, an Au-IDE was coated with a disordered COF. The sensor had a constant baseline, which changed upon exposure to ammonia with only short response time and large response value. Other gases (NO_2, NO, SO, H_2S, H_2, CO, CO_2) were tested, but the response was significantly lower, resulting in a good selectivity towards ammonia. Next to the resistance, also capacitance can be measured. When a gas or vapour gets adsorbed by the affinity layer, the dielectric constant of this sensor coating changes, which results in a change of the layer capacitance that can be detected by the underlying sensor platform. An imine-linked COF was grown on a Pt-IDE with integrated micro-hotplate.[157] The authors reported on the preferred detection of benzene vapour over CO_2, CH_4 and propane at room temperature. The applied COFs possess large π-systems with which aromatic compounds can interact via π-π stacking, explaining the differences in responses of the various analytes.

1.4.2 Gas separation

Gas separation is a process, in which a target gas is separated from a mixture of gases by, for example, a membrane or an adsorbent.[158] In order to achieve an efficient separation, the process needs to be selective towards the target gas, which can either mean to separate the desired product from the gas mixture or an unwanted gas from the mixture. COFs have been used for the separation of, amongst others, acetylene from propylene,[159] H_2 from CO_2, CH_4, propylene or propane,[8] CO_2 from H_2[140] or CO_2 from N_2.[160]

In particular, the separation of CO_2 from N_2 and the corresponding CO_2/N_2 selectivity is relevant as CO_2 is known for its contribution on global warming and N_2 is the most abundant gas in air (about 78%). The current concentration of CO_2 in the atmosphere is rather low with 0.042 vol% in 2021. However, it has considerably risen in the last 250 years by approximately 50% and is currently about 40% higher than the previously highest reported atmospheric concentration 300,000 years ago.[161,162] The low CO_2 concentration makes it difficult to capture it directly from the atmosphere. However, under flue gas conditions, the CO_2 concentration is significantly higher (10-25 vol%), which means it is advantageous to remove the CO_2 before its emission into the atmosphere.[163] For the materials involved in carbon capture it is relevant to have a large CO_2 uptake capacity and high CO_2 selectivity over other gases, for instance N_2. The material needs to be stable under the process conditions,

particularly also in humid atmospheres. The performance needs to be repeatable without a loss in performance and the regeneration should require only little energy.[164]

Several classes of porous materials have been studied for CO_2/N_2 gas separation. Herein, the focus will be on the separation under flue gas conditions (0.15/0.85 CO_2/N_2) of COFs and non-crystalline porous materials, such as benzimidazole-linked porous organic polymers and imine-linked networks.

Benzimidazole-linked porous organic polymers are promising candidates for CO_2/N_2 gas separation, because of their high CO_2 adsorption quantities (up to 5.19 mmol/g at 273 K and 1 bar for TLIP-2).[165] TBLIP-2 does not only contain the benzimidazole linkage, that can interact with CO_2, but also triazine rings, which are beneficial for CO_2 adsorption as the π-conjugated 1,3,5-triazine core acts as an electron donor, enhancing CO_2-COF interactions. The IAST CO_2/N_2 selectivity value was determined to be 63 at 298 K and 1 bar in a 0.1/0.9 mixture. Islamoğlu *et al.* have shown that post synthetic modification with nitro groups — which were subsequently also chemically reduced to amine groups — leads to an increase in CO_2 adsorption and CO_2/N_2 selectivity compared to the pristine porous polymer.[166] While the total CO_2 adsorption increased even further for COFs with amine groups compared to nitro-containing COFs, the CO_2/N_2 selectivity was better for the nitro-functionalised porous polymer.

Covalent triazine frameworks have also been studied for gas separation and are reported to have high CO_2/N_2 selectivity.[167] To the best of our knowledge, the highest CO_2/N_2 IAST selectivity value under flue gas conditions so far was reported by Mahato *et al.* to be 185.8 at 273 K with a CO_2 adsorption of 3.50 mmol/g.[168]

Imine-linked materials, which are comparable to the COFs presented in this thesis, often have CO_2/N_2 IAST selectivity values in the range of 10-30. Pore-wall functionalisation can enhance the CO_2/N_2 IAST selectivity significantly.[169,170] To give a few examples, Popp *et al.* studied a porous imine-linked network that adsorbs 1.8 mmol/g and 1 mmol/g at 273 K and 298 K.[171] The CO_2/N_2 IAST selectivity was determined to be 31 at 298 K and 1 bar. Another imine network, consisting of melamine and 1,4-piperazinedicarboxaldehyde, adsorbed 3.3 mmol/g CO_2 at 273 K, and 2.4 mmol/g CO_2 at 298 K. The CO_2/N_2 IAST selectivity was found to be 211 and 100 at 273 K and 298 K, respectively.[172] Huang *et al.* studied a channel-wall-functionalised, imine-linked, porphyrin COF.[173] Carboxyl groups were post-synthetically attached to the channel walls. The COOH-COF adsorbed

3.95 and 1.73 mmol/g of CO_2 at 273 K and 298 K, respectively, and the CO_2/N_2 IAST selectivity was found to be 77. Compared to the non-functionalised COF (S = 9), this was a ninefold increase.

Wang *et al.*, have revealed that a β-ketoenamine COFs outperforms imine COFs with similar pore sizes.[174] In their study, they did not find a direct relation between the CO_2 uptake and the pore size. However, by comparing different studies with each other, it becomes apparent that β-ketoenamine COFs adsorb higher CO_2 quantities compared to imine COFs.[140,175,176]

Recently, Yaghi and co-workers studied the incorporation of aliphatic amine groups into a tetrahydroquinoline COF, because amine groups are known for their interaction with CO_2.[160] They found high CO_2 adsorptions of 0.304 mmol/g at 0.4 mbar and 298 K, which are relevant conditions for direct air capture. 50% Humidity even enhances the CO_2 uptake to 0.393 mmol/g. Based on solid-state NMR, they could show that carbamates were formed during the adsorption, therefore confirming chemisorption interactions.

1.5 Aim and outline of the thesis

The different classes of dynamic covalent chemistry have enabled many different COF linkages and the variety of COF structures is large. A lot of research focuses on the applicability of the synthesised COFs to develop new or better catalysts, sensors, stationary phases for chromatography or make use of the large surface area for gas capture and separation. However, not much research has focused on the fundamental structure-property relationships, which is important to pre-design COFs. Especially, the knowledge about pore stability during the activation process and the stability of COFs over time is limited. Therefore, the aim of this thesis is to explore COFs with different functional groups and to thoroughly characterise them. The impact and tuneability of several functional groups on COF crystallinity, porosity, which includes surface area, and stability were studied. To this end, we have chosen imine COFs due to the good reversibility of the reaction and due to the easy accessibility and large diversity of building blocks. Several functionalisation strategies (pre-synthetic, modulators, linker-exchange) have been utilised and the resulting COFs were applied for vapour sensing and CO_2/N_2 separation.

In **Chapter 2** a new, trimethylated aldehyde building block was used to synthesise imine-linked COFs, which were studied in terms of thermal and activation stability and stability over four weeks. Unmethylated COFs were synthesised for comparison and the effect of the methyl groups on crys-

tallinity and porosity was investigated by density functional theory computations. In addition, the effect of the exposure of acid vapour onto the UV/vis absorbance properties of the COFs was examined. Furthermore, the reversibility of the sensor and its mechanism were investigated.

Chapter 3 builds on the results of **Chapter 2** and deepens the understanding of methyl-functionalisation by synthesising several imine-linked COFs with methylated and unmethylated building blocks. Thorough characterisation of similar, yet different COFs, revealed trends and tuneability based on the methyl substitution in terms of porosity, activation stability, UV/vis properties and optical band gaps. Additionally, the obtained COF series was analysed with solid-state NMR to facilitate the experimental assignment of the various carbons present in the COF structures.

Chapter 4 investigates functionalisation beyond methyl groups via the incorporation of a series of *para*-functionalised modulators (OMe, Me, F, Cl, CF_3, NO_2) into the COF structure. The crystallinity, porosity, the fraction of modulator incorporated in the COF, and the position of the modulator within the framework were analysed. The direct synthesis of functionalised COFs was explored, and the results were compared to the modulated COFs. Furthermore, the modulated COFs were explored for their ability to separate CO_2 from N_2 under flue gas conditions.

Amines are known for their interaction with CO_2. To optimise the CO_2/N_2 separation, an aromatic amine-functionalised COF was synthesised via linker-exchange in **Chapter 5**. This COF was not accessible via direct condensation. First, the linker-exchange was studied by FT-IR and solid-state NMR and the porosity was investigated. Then the CO_2/N_2 separation was studied under flue gas and direct air capture conditions.

The IAST calculations of the previous chapters required programming knowledge that not every material scientist has or has access to. Therefore, in **Chapter 6** a graphical user interface (GUI) software for IAST calculations is presented to predict IAST loading and selectivity of binary gas mixtures. The existing Python package was extended to three-dimensional selectivity predictions within a GUI and just a few clicks, providing a ready-to-use platform for non-programming scientists. This package was used in **Chapter 4** and **5**.

In **Chapter 7** the results of **Chapter 2-6** are summarised and discussed in a broader context. Based on these results, future research suggestions are outlined.

2 Enhanced surface area and reduced pore collapse of methylated, imine-linked covalent organic frameworks

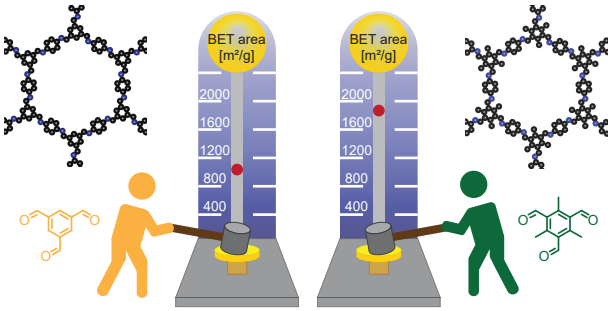

Ellen Dautzenberg, Milena Lam, Guanna Li, Louis C. P. M. de Smet

Nanoscale, **2021**, *13*, 19446-19452.

2.1 Abstract

Covalent organic frameworks (COFs) are thermally and chemically stable, nanoporous materials with high surface areas, making them interesting for a large variety of applications including energy storage, gas separation, catalysis and chemical sensing. However, pore blocking and pore collapse may limit their performance. Reducing the capillary forces by using solvents with low surface tension, like supercritical CO_2, for activation, and the introduction of bulky isopropyl/methoxy groups were found to reduce pore collapse. Herein, we present an easy-to-use alternative that involves the combination of a new, methylated building block (2,4,6-trimethylbenzene-1,3,5-tricarbaldehyde, Me_3TFB) with vacuum drying. Condensation of Me_3TFB with 1,4-phenylenediamine (PA) or benzidine (BD) resulted in imine-linked 2D COFs (Me_3TFB-PA and Me_3TFB-BD) with higher degrees of crystallinity and higher BET surface areas compared to their non-methylated counterparts (TFB-PA and TFB-BD). This was rationalised by density functional theory computations. Additionally, the methylated COFs are less prone to pore collapse when subjected to vacuum drying and their BET surface area was found to remain stable within at least four weeks. Within the context of their applicability as sensors, we also studied the influence of hydrochloric acid vapour on the optical and structural properties of all COFs. Upon acid exposure their colour and absorbance spectra changed, making them indeed suitable for acid detection. Infrared spectroscopy revealed that the colour change is likely attributed to the cleavage of imine bonds, which are only partially restored after ammonia exposure. While this limits their application as reusable sensors, our work presents a facile method to increase the robustness of commonly known COFs.

2.2 Introduction

Covalent organic frameworks (COFs) are a class of nanoporous materials first discovered in 2005 by Yaghi and co-workers.[13] Since then, COFs have gained increasingly more interest and a huge variety of different materials and applications have been reported.[2,43] COFs consist of fully organic building blocks linked by dynamic covalent chemistry.[14,15] Dynamic covalent chemistry refers to reversible reactions carried out under thermodynamic reaction conditions. This enables error correction, leading to crystalline frameworks with a long-range order. The symmetry of the building blocks is determining the crystal structure. In the case of 2D COFs, the third dimension is formed by π-π stacking. The layers usually stack in an eclipsed structure leading to channels in the framework which results in high surface areas. These high surface areas are of interest for, amongst others, energy storage,

gas separation, catalysis, and chemical sensing.[2,6–8] The variability in organic building blocks in terms of functional groups or symmetry allow a high control over the COF properties and thus leads to tailor-made materials. However, the boronic esters used to make the first COFs were susceptible to hydrolysis. This has been improved by using imine-linked COFs or even more stable β-ketoenamine COFs. The latter first forms imine bonds which then tautomerise irreversibly into the β-ketoenamine linkage. The irreversible tautomerisation results in a lower crystallinity and surface area compared to their imine counterparts.[43] The chemical stability of COFs does not only depend on the type of linking chemistry, but can also be affected by the nature of the core of the organic building blocks. Ma *et al.* reported two highly porous 3D COFs of terephthalaldehyde or 4,4'-biphenyldicarboxaldehyde and a tetrahedral amine with isopropyl groups in ortho position.[26] Isopropyl groups are hydrophobic and their steric demand protects the imine groups from hydrolysis. The COFs are reported to be stable in acidic and strong alkaline solutions without a decrease in surface area and crystallinity. Such stability was also achieved by methoxy substitution of the aldehyde node.[177] In another study, Wang *et al.* reported enhanced BET surface areas for ortho methoxy substituted aldehyde nodes and meta methyl substituted amine linkers.[178]

COF stability is not only about the chemical stability of the functional groups involved, but also about the stability of the physical properties such as pore size, pore shape and surface area. It has been identified that the conditions for work-up and COF activation are crucial to get accessible pores and high surface areas. After synthesis, COFs are most commonly washed with several solvents to remove impurities and water from the pores prior to drying. Vacuum drying has often been used, but was identified to induce partial pore collapse due to capillary forces.[64] Capillary forces increase with decreasing pore size and COFs with typical pore sizes around a few nanometres are therefore subjected to strong capillary forces. To overcome pore collapse, milder activation methods such as supercritical CO_2 drying[64] or washing with ultra-low surface tension solvents prior to drying[65] were suggested to keep the framework intact upon activation. Feriante *et al.* and Zhu *et al.* both reported methoxy-functionalised, imine-based COFs which were less prone to pore collapse compared to the non-methoxylated equivalent.[64,65] In the current paper, we introduce methyl groups in the synthesis of imine based COFs as alternative to the bulky isopropyl and the smaller methoxy groups. Depending on the COF application, the use of this smaller — but still hydrophobic — group can be advantageous as it has less impact on the pore size.

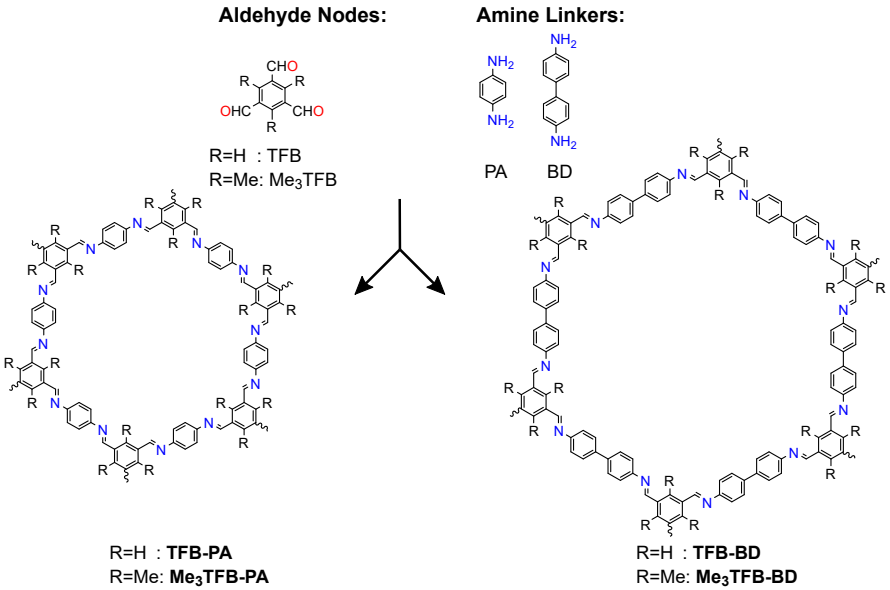

Scheme 2.1: Different aldehyde and amine building blocks used for introducing methyl groups in COFs and their resulting structures.

Herein, we present 2,4,6-trimethylbenzene-1,3,5-tricarbaldehyde (Me_3TFB) as building block for two novel COFs, namely Me_3TFB-PA and Me_3TFB-BD, which are compared with two reference COFs TFB-PA [6] and TFB-BD. [59,179] The methylation significantly increases the BET surface area by a factor of 1.8 and 1.4, respectively. The physical stability of the framework towards pore collapse during vacuum activation also profits from the methylation. This work shows a facile approach in stabilizing COFs by methylating the aldehyde. The novel COFs maintain their high surface area on the bench for at least four weeks. Finally, the effect of acid vapour on the optical and structural properties of the COFs was studied.

2.3 Results and discussion

2.3.1 Synthetic procedures

1,3,5-Benzenetricarbaldehyde (TFB) and 2,4,6-trimethyl-benzene-1,3,5-tricarbaldehyde (Me_3TFB) were condensed with two different amines, namely 1,4-phenylenediamine (PA) and benzidine (BD) (**Scheme 2.1**) to yield the novel 2D imine-linked COFs (Me_3TFB-PA and Me_3TFB-BD) and their non-methylated equivalents (TFB-PA and TFB-BD). Each COF has been synthesised and characterised thrice. We selected this set of COFs, because TFB-PA and TFB-BD have been widely studied in literature.[6,59,179,180] The synthesis was carried out at 70 °C and atmospheric pressure with acetic acid as catalyst and water to enhance dynamic covalent chemistry in a mixture of mesitylene:1,4-dioxane 1:4 v/v for three days.[30] A washing protocol from Vitaku *et al.* has been used for the work up.[31] Afterwards, half of the obtained powder was dried overnight in a vacuum oven at 120 °C and the other half at 120 °C in a regular, air ventilated oven before the COFs were characterised. The characterisation for the reference COFs can be found in the Supporting Information (**Section 2.S**).

2.3.2 Characterisation

FT-IR spectroscopy on the novel COFs confirmed the formation of imine bonds (**Figure 2.1A**). Me_3TFB-PA shows a characteristic imine stretch at 1623 cm^{-1}, demonstrating a successful reaction. A weak band at 1693 cm^{-1} indicates low fractions of aldehyde bonds. This IR characteristic has also been reported by others and may origin from unreacted side-groups at the outside of the 2D polymeric sheet.[60,64,65]

The formation of imine bonds was also confirmed by ^{13}C cross-polarisation magic angle spinning solid-state NMR (^{13}C CPMAS ssNMR) (**Figure 2.2A**) as the signal at 162 ppm is typical for imine carbons. The signal at 194 ppm points to aldehyde carbons, but compared to the starting compound this is strongly attenuated and just the above noise level.

Comparable FT-IR results can be found for Me_3TFB-BD COF with an imine band at 1627 cm^{-1} and a small carbonyl stretch at 1693 cm^{-1} (**Figure 2.1B**). Again, an ssNMR signal at 162 ppm confirms the formation of an imine (**Figure 2.2B**). All FT-IR spectra of the triplicates can be found in the Supporting Information.

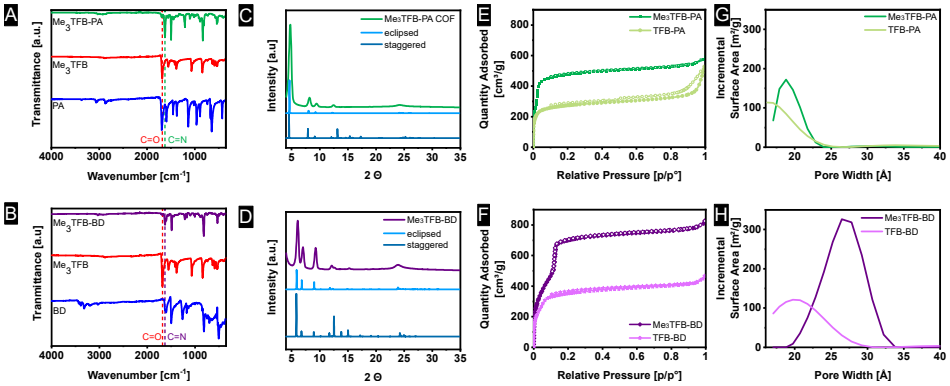

Figure 2.1: Characteristics of Me_3TFB-PA (top) and Me_3TFB-BD (bottom): FT-IR spectra of COFs and starting materials (A and B), PXRD spectra including simulated PXRD patterns (C and D), nitrogen sorption isotherms including their non-methylated references (E and F) and pore size distributions (G and H).

Thermogravimetric analysis (TGA) revealed that Me_3TFB-PA is thermally stable up to 355 °C and Me_3TFB-BD up to 390 °C (**Section 2.S**), which is in line with several previously reported imine linked COFs.[6,59,65,120]

Powder X-ray diffraction (PXRD) was performed on all samples to determine the crystallinity of the materials. The obtained spectra were compared to the simulated diffraction patterns of optimised crystal structures obtained from density functional theory (DFT) calculations (coordinates in Supporting Information). Me_3TFB-PA COF displays several diffraction peaks which are clearly baseline separated from each other at 4.8°, 8.2°, 9.4°, 12.5° and a broader signal around 24° (**Figure 2.1C**). Two different stacking structures have been computed for comparison: an eclipsed and a staggered structure. Comparing peak positions and relative intensities of the peaks, it can be concluded that Me_3TFB-PA COF crystallises in an eclipsed stacking conformation. For all three samples, Scherrer analysis was performed and gave an estimated average domain size of 15.1±1.5 nm. The PXRD diffractogram of Me_3TFB-BD COF also shows several narrow diffraction peaks, especially at low angles: 3.6°, 6.1°, 7.0°, 9.3°, 12.1°, 12.6°, 15.3° (**Figure 2.1D**). The peak at 3.6° was confirmed by a second low angle PXRD measurement with different settings which only scanned angles from 1.5-10° to be able to detect signals in this low-angle region without detecting the source. The diffractogram can be found in the Supporting Information (**Section 2.S**) as well as the low angle diffractogram of Me_3TFB-PA. Scherrer analysis for this sample results in an approximate domain size of 20.5±2.1 nm. Comparison with the computed PXRD diffraction patterns leads again to a preferred eclipsed stacking.

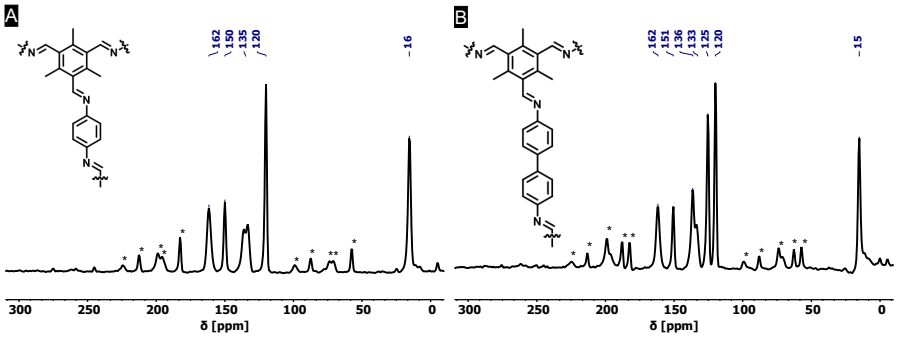

Figure 2.2: Solid-state NMR spectra of Me_3TFB-PA (A) and Me_3TFB-BD (B). The signal at 162 ppm can be assigned to the carbon of an imine-bound nitrogen, indicating the formation of imine bonds. Spinning side bands, here indicated with an asterisk, were determined by comparing different MAS frequencies.

2.3.3 BET surface area

Nitrogen sorption measurements were carried out to determine the surface area of the COFs (**Section 2.S**). For Me_3TFB-PA, the adsorption-desorption isotherm can be classified as a type I isotherm (**Figure 2.1E**).[1] This is characteristic for microporous materials of which most of the surface area is internal surface area within the framework. The micropores lead to rapid pore filling at low pressures and a nearly horizontal plateau with increasing relative pressures. Also TFB-PA yields a type I isotherm, including an H4 hysteresis loop, which is absent for Me_3TFB-PA. Hysteresis loops can be a result of capillary condensation and/or pore blocking.[181] The pore volume was determined in the adsorption branch at p/p^0 = 0.95, yielding a value of 0.88$\pm$0.04 cm^3/g. The BET surface area (S_{BET}) was calculated using the Rouquerol criteria[127] to apply the BET theory to microporous materials. For all samples of the same COF, the same pressure range was used for the linear regression. Afterwards, the obtained BET surface areas were averaged. For Me_3TFB PA S_{BET} was found to be 1877$\pm$20 m^2/g. To determine the pore size distribution, HS-2D-NLDFT analysis was carried out using the isotherm data and a model with cylindrical micropores for carbon surfaces with N_2. Me_3TFB-PA COF shows a narrow pore size distribution with a clear maximum at 1.9 nm (**Figure 2.1G**). The pore size is slightly larger compared to TFB-PA which exhibits a broader pore size distribution with only one maximum at 1.7 nm.

Me_3TFB-BD COF on the other hand, has a type IVb isotherm (**Figure 2.1F**). The microporosity is shown by a large adsorption of nitrogen in the low pressure range (p/p^0 < 0.1). The step in the isotherm at p/p^0 = 0.1 indicates capillary condensation. The lack of hysteresis is in line with

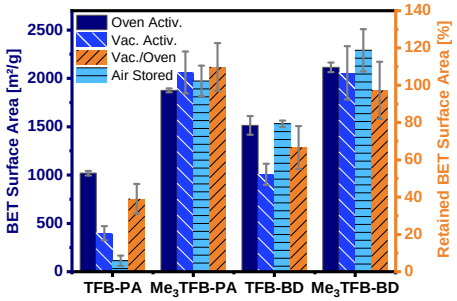

Figure 2.3: BET surface areas with different activation methods (oven-dried and vacuum-dried) and after four weeks stored on the bench. The retained BET surface area gives the ratio how much S_{BET} has been left after vacuum drying. The errors result from the analyses of three different batches.

the cylindrical shape of the pores.[1] The pore volume at p/p^0 = 0.95 and BET surface areas were measured to be 1.24±0.03 cm^3/g and 2115±50 m^2/g, respectively, while the pore size distribution has a narrow maximum at 2.7 nm (**Figure 2.1H**). With this analysis, where the Rouquerol criteria[127] were prioritised, R^2 values in the range of 0.996-0.997 were found for the benzidine COFs. The same HS-2D-NLDFT model has been used for the pore size distribution calculation. Comparing the pore size distribution of Me_3TFB-BD with the pore size distribution of the non-methylated TFB, which shows a pore size of 2.1 nm, results again in a larger pore size for the methylated COF.

By comparing the BET surface area of the methylated COFs with their non-methylated equivalents after oven activation, it can be clearly seen that the methylated aldehyde building block significantly increases the BET surface area (**Figure 2.3**). The methylated building block increases the BET surface area by a factor of 1.8 and 1.4 for TFB-PA and TFB-BD, respectively. We would have expected that two ortho methyl groups would sterically hinder the reaction which would have resulted in lower BET surface areas. Therefore, we used theoretical modelling to further study this increase in BET surface area. The crystal structures of DFT optimisation reveal the C_3 symmetric incorporation of the aldehyde building block into the framework (**Section 2.S**). Additionally, TFB and Me_3TFB were geometry optimised by DFT calculations and the rotational barriers for the rotation of the carbonyl groups were modelled (**Section 2.S**). It was found that the methyl groups hinder the full conjugation of the carbonyl groups with the π system of the aromatic Me_3TFB ring, leading to a non planar structure with lower symmetry compared to TFB. For methylated and non-methylated aldehydes, the resulting rotational energy profiles show two minima with a difference in energy of 4.2 kJ/mol, which means both conformations can be present in the system at 70 °C during the reaction. The rotational barrier,

which has to be overcome to change conformation, is lower for Me_3TFB compared to TFB. This is due to the enhanced conjugation and full symmetry in TFB while Me_3TFB does not have such a strong conjugation and symmetry. The rotational barrier is hence smaller and the reaction rate for the conformational change is magnitudes higher. This implies that, during COF condensation, favoured C_3 symmetric aldehyde conformations are re-formed faster from the C_S symmetric conformation for Me_3TFB, which is in line with the experimentally found larger domain sizes and higher BET surface areas. Furthermore, to evaluate the effect of methyl groups on the stability of the thus-formed Me_3TFB-BD and Me_3TFB-PA COF materials, the formation energies all for COFs were calculated according to the reaction formula shown in **Section 2.S**, based on the assumption that all aldehyde groups react with all amine groups to form the imine linked COF. The results (**Section 2.S**) indicate that formation of both Me_3TFB-BD and Me_3TFB-PA, *i.e.*, the COFs featured with methyl groups on the aldehyde node, are thermodynamically more favourable than their non-methylated counterparts, indicating a higher stability of the methylated COFs compared to the non methylated COFs.

To study whether the addition of methyl groups also results in a more stable framework, we studied the pore collapse by re-measuring the BET surface area of all COFs after vacuum activation (120℃, vacuum oven, overnight). To correct for the difference in BET surface area due to different pore sizes, the retained BET surface area has been calculated as the ratio of the vacuum activated S_{BET} over the oven activated S_{BET}, given in area in percentages. Both methylated COFs have a higher BET surface area compared to their non methylated equivalents (Me_3TFB-PA, S_{BET}=2061$\pm$218 m^2/g; Me_3TFB-BD, S_{BET}=2057$\pm$276 m^2/g; TFB-PA, S_{BET}=398$\pm$72 m^2/g; TFB-BD, S_{BET}=1008$\pm$109 m^2/g) after vacuum activation (**Figure 2.3**). The retained BET surface area for TFB-PA is only 39$\pm$8% which means the framework collapses when exposed to vacuum. A comparable trend, though less prominent, can be observed for TFB-BD with a retained S_{BET} of 67$\pm$12%. In the case of the methyl containing COFs, the vacuum activation is qualified as the better method for Me_3TFB-PA COF (retained S_{BET} 110$\pm$13%), while both activation processes are equally good for Me_3TFB-BD (retained S_{BET} 97$\pm$15%). In other words, the BET surface areas increase by a factor of 2.8 and 1.4 for Me_3TFB-PA and Me_3TFB-BD, respectively. The methylated COFs are hence less prone to pore collapse.

In addition, we noticed that the BET surface area of TFB-PA decreases already drastically to 113$\pm$53 m^2/g in the first four weeks which means only 11% of the original BET surface area are accessible after one month. Therefore, we investigated the air stability of the other three COFs as well,

by leaving the oven activated samples for four weeks in an open vial on the bench, before determining the BET surface area again. These three COFs did not show such a large drop in the S_{BET} values. Instead, on average a slight increase is observed (up to 8% for Me_3TFB-BD), although the differences are within the standard deviation. In any case, as no decrease is observed, we conclude that TFB-BD, Me_3TFB-PA, and Me_3TFB-BD are stable for the reported conditions. Again, this shows that the introduction of methyl groups stabilises the phenylenediamine COF.

2.3.4 Acid-vapour sensing

The optical properties of some COFs are reported to respond to change under acidic conditions and with different solvents, enabling them to be used as chemical sensors. In more detail, Ascherl *et al.* observed a solvatochromic effect, which has been visible in diffuse reflectance spectroscopy, before employing the pyrene containing COF for the development of a humidity sensor.[7] Several studies report on COF-based chemosensors for the detection of gaseous hydrochloric acid,[147,148] and a series of aqueous Brønsted acids.[148,149] Recently, Yang *et al.* have studied the effect of imine-protonation on the optical properties of three imine-linked COFs. It was found that all COFs showed a bathochromic shift after acid exposure due to the protonation of the imine bond.[182] Based on both findings, we looked into the absorption spectra of Me_3TFB-PA and Me_3TFB-BD and their response towards hydrochloric acid vapour. To this end, samples of the new COFs were pressed as a thin film between two glass plates. Absorption spectra were collected before treatment with acid by measuring the samples in an integrating sphere and collecting diffuse reflectance and diffuse transmission to calculate the absorbance. Both absorbance spectra have an inverse S curve shape, start absorbing between 400-450 nm, and have absorption edges around 378 nm for Me_3TFB-PA and 385 nm for Me_3TFB-BD (**Figure 2.4A,B**). To facilitate the comparison between the different samples, the inflection point was used and the first derivative was calculated in Origin to determine the minimum (**Figure 2.4C,D**), which were found to be similar for both COFs (414 nm for Me_3TFB-PA and 419 nm for Me_3TFB-BD COF).

As the two-plate configuration does not allow vapour exposure experiments, a new sample was taken from the same synthetic COF batch, which was subjected to hydrochloric acid vapour for 30 min. Within minutes, a colour change (paler powder for methylated COFs, red for non-methylated equivalents) was observed by the naked eye (**Figure 2.4**) which was confirmed by an absorbance measurement of the acid exposed COF sample. The original inverted S curve was blue shifted and

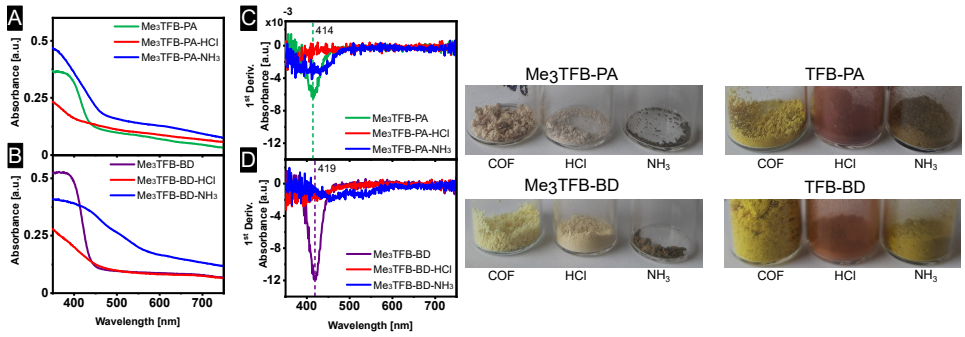

Figure 2.4: Absorbance spectra (A and B) and their first derivative (C and D) for a better comparison of Me_3TFB-PA and Me_3TFB-BD, as well as optical photographs of all stages in the sensing process.

additionally became more stretched for methylated COFs. In comparison, the spectra of the non methylated COFs were red shifted, but also stretched.

In order to study the applicability of this interesting property, we investigated whether the COF's response towards hydrochloric acid vapour is reversible by subjecting the acid exposed material towards ammonia vapour for 30 min. Within minutes, another colour change could be observed (**Figure 2.4**), back more towards the original yellow, but going even further to brown. This was the case for both methylated and non methylated COFs. To study this in more detail, the absorbance was once more measured. The absorbance curve resembles more its original shape for Me_3TFB-PA COF, although the first derivative indicates a wider range in which the absorbance changes and the absorption edge is red shifted with respect to the acid exposed sample. For Me_3TFB-BD COF, the spectrum also shifts back to higher wavelength, but even wider. The first derivative indicates two small minima with shifted positions that do not overlap with the original minimum, so the acid has an impact on the COF structure. The absorbance spectra for the non methylated COFs can be found in the Supporting Information (**Section 2.S**). No change in absorbance could be found for just exposing the samples to ammonia vapour (**Section 2.S**).

We speculate that the acid protonates the nitrogen atom (**Figure 2.5C**). In a second step, this protonation could lead to a bond cleavage, affecting the COF structure, which is expected to limit the sensor performance. In an attempt to gain insight into the sensing mechanism, FT-IR spectra were recorded in all stages of the sensing process (**Figure 2.5A,B**). Upon exposure to acid vapour the FT-IR spectra do not show any imine stretching vibration anymore. Instead, strongly increased

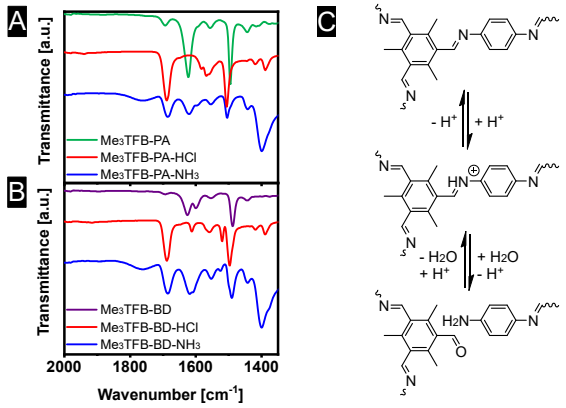

Figure 2.5: FT-IR spectra (A and B) to elucidate the sensing mechanism (C).

bands at 1688 cm^{-1} are observed, leading to the conclusion that the exposure of acid breaks down the framework, explaining the observed colour changes of the materials. After exposure towards ammonia, equally strong bands near 1621 cm^{-1} (imine stretching vibration) and 1685 cm^{-1} (carbonyl stretching vibration) are visible, indicating a partial recovery of the imine bonds.

2.4 Conclusions

In conclusion, a new methyl substituted aldehyde building block has been used for COF synthesis, resulting in two novel frameworks, namely Me_3TFB-PA and Me_3TFB-BD. They have been compared with non methylated reference COFs regarding their BET surface area, pore collapse and their applicability as optical acid sensors. With a facile synthetic approach, which does not require any specialised equipment, we found that methylation of the aldehyde node results in enhanced BET surface areas up to ca. 2000 m^2/g and high degrees of crystallinity compared to their non methylated equivalents. The obtained BET surface areas are comparable to the ones achieved by supercritical CO_2 activation. The higher surface areas and crystallinity are in line with DFT-calculated reaction rates. With respect to TFB, Me_3TFB loses symmetry and its full conjugation due to the ortho-substituted methyl groups. This leads to a smaller rotation barrier towards the favoured C_3 conformation for crystallisation and therefore to higher reaction rates. Additionally, the novel methylated COFs are less prone to pore collapse during vacuum activation and the BET surface area remains stable within at least four weeks.

The COFs can be used as an optical sensor to detect hydrochloric acid based on a change in colour. The sensing mechanism reveals that the colour change is likely attributed to the cleavage of the imine bond, which is partially restored after exposure to ammonia vapour. Even though this limits their applicability as a reusable sensor for hydrochloric acid, our approach enables the facile synthesis of high surface area COFs that are more robust compared to commonly known COFs. The effect of ortho-substituted methyl groups of the amine building block and systematically increasing the number of methyl groups on the resulting COF properties are currently under investigation.

2.S Supporting Information

The Supporting Information is available free of charge on the website of the Royal Chemical Society:

Or it can be accessed via the following link:
https://drive.google.com/file/d/1gRVaPBHOwPtisWFIVKEb7MtNDxxoZ4Sq/view?usp=sharing

3 Tuning UV absorption in imine-linked covalent organic frameworks (COFs) via methylation

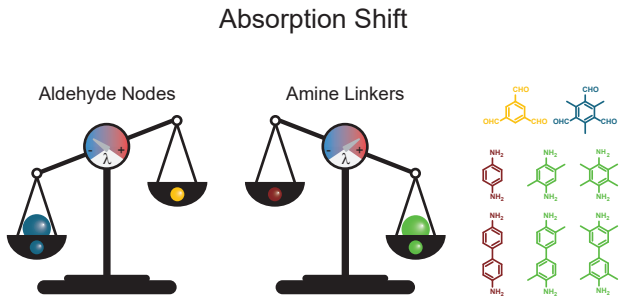

Ellen Dautzenberg, Milena Lam, Tatiana Nikolaeva, Wouter M. J. Franssen, Barend van Lagen, Ilse P. A. M. Gerrits-Benneheij, Nikolay Kosinov, Guanna Li, Louis C. P. M. de Smet

J Phys Chem C, **2022**, *126*, 21338-21347.

3.1 Abstract

Covalent organic frameworks (COFs) are porous materials with high surface areas, making them interesting for a large variety of applications including energy storage, gas separation, photocatalysis and chemical sensing. Structural variation plays an important role in tuning COF properties. Next to the type of the building block core, bonding directionality and linking chemistry, substitution of building blocks provides another level of synthetic control. Thorough characterisation and comparison of various substitution patterns is relevant for the molecular engineering of COFs via rational design. To this end, we have systematically synthesised and characterised multiple combinations of several methylated and non-methylated building blocks to obtain a series of imine-based COFs. This includes the experimental assignment of the COF structure by solid-state NMR. By comparing the properties of all COFs, the following trends were found: (1) upon methylation of the aldehyde nodes, COFs show increased Brunauer-Emmett-Teller (BET) surface areas, reduced pore collapse, blue-shifted absorbance spectra and 0.2 eV increases in their optical band gaps. (2) COFs with *N,N*-dimethylated amine linkers show a lower porosity. (3) In tetramethylated amine linkers the COF porosity even further decreases, the absorbance spectra are clearly red-shifted, and smaller optical band gaps were obtained. Our study shows that methyl substitution patterns on COF building blocks are a handle to control the UV absorbance of the resulting frameworks.

3.2 Introduction

Porous materials are a class of solids with pore sizes of a few to several hundred nanometres. These pores can be classified into macro- (> 50 nm), meso- (2-50 nm) and micropores (<2 nm).[1] Besides zeolites and metal organic frameworks (MOFs), crystalline covalent organic frameworks (COFs)[13] have gained increasing interest, and a huge variety of different materials and applications have been reported.[2,43] The permanent porosity and the channel-like structure of COFs lead to high surface areas, which are of interest for, amongst others, energy storage,[2,3] gas separation,[2,8] chemical sensing,[2,7] and photocatalysis.[2,4,5] In the last-mentioned example solar energy was used to split, for instance, water or CO_2 into H_2 and O_2 gas or hydrocarbons, respectively.[4] These gases can be used as energy sources or starting materials for other chemical processes. COFs have been reported as good photocatalysts for such clean and green transformations.[4] The first COFs were linked by boronic esters, which were susceptible to hydrolysis. This has been improved by using imine-linked COFs or even more stable β-ketoenamine COFs.[21] In the latter case, imine bonds are formed first,

which then tautomerise irreversibly into the β-ketoenamine linkages. The irreversible tautomerisation results in lower crystallinity and surface area compared to their imine equivalents, which is the reason why imine COFs are widely used.[43] Imine COFs can be synthesised in a condensation reaction from aldehyde and amine building blocks under acidic catalysis, which is also known as Schiff base chemistry.[2,31,41,42] Vacuum drying has often been used, but was identified to induce partial pore collapse due to capillary forces.[64] Capillary forces increase with decreasing pore sizes and COFs, which usually have pore sizes around a few nanometres, are therefore subjected to strong capillary forces. To overcome pore collapse, milder activation methods such as supercritical CO_2 drying[64] or washing with ultra-low surface tension solvents prior to drying[65] were suggested to keep the framework intact. Feriante *et al.*[64] and Zhu *et al.*[65] both reported an methoxy functionalised, imine-based COF, which was less prone to pore collapse compared to the initial unfunctionalised COF. Recently, we have found that COFs consisting of 2,4,6-trimethylbenzene-1,3,5-carbaldehyde (Me_3TFB) lead to more robust frameworks compared to non-methylated 1,3,5-benzenetricarbaldehyde (TFB).[183]

While COF stability is essential for virtually all applications, other properties, like selectivity and catalytical performance, require tailor-made approaches. Identification of structure property relationships of COFs would facilitate the process of controlling such properties. Karak *et al.* reported on how an acidic catalyst influences the porosity of obtained COF materials.[184] Namely, they studied the effect of amine substitution on β-ketoenamine-linked COF properties. They investigated the porosity based on differences in hydrogen-bonding in an intermediate to be able to predict the porosity of the resulting COFs. These β-ketoenamine-linked COFs were synthesised via a mechanochemical synthesis of 1,3,5-triformylphloroglucinol (Tp) with several functionalised phenylenediamine (PA) and benzidine (BD) linkers, catalysed by different toluenesulfonic acids or hydrogen chloride. During this process, the diamine first forms an acid-diamine salt with the toluenesulfonic acids, which then further reacts with Tp to the final COF. The hydrogen-bond distance of the acid-diamine salt was found to affect the COF porosity. While the hydrogen-bond distance was tuned by the choice of toluenesulfonic acid, no trend between the BET surface area and their methylated amine linker was observed. Additionally, the applied mechanochemical synthesis — especially the intermediate acid diamine salt — differs from COFs synthesised in solution. In another study, Singh *et al.* reported on the possibility to fine-tune the optical band gap by changing the number of hydroxyl groups on the TFB aldehyde node by varying

the push-pull electronic effect.[5] The authors found that a more pronounced push-pull effect leads to lower resulting band gaps.

Combined with the earlier reported increased stability of methyl-substituted COFs,[183] these two studies motivated us to systematically investigate the effect of methyl groups on the porosity and UV absorbance of imine-based COFs. To this end and given their pore stability and utilisation potential of their UV absorbance, we decided to introduce an increasing number of methyl groups, this time also in the amine linkers. Such thorough comparison of similar, yet different structures enables a fundamental understanding, which can be employed to rationally design COF materials with tailor made properties. By expanding our methylated imine-based COF library and by thoroughly characterising, including detailed solid-state NMR (ssNMR) measurements as well as experimental band gap analyses, we investigate the influence of methylation of aldehyde nodes and amine linkers on the resulting COF crystallinity, BET surface areas, the tendency for pore collapse and the UV absorbance of the COFs.

3.3 Results and discussion

We synthesised a full range of COFs with a) methylated (Me_3TFB) and non-methylated (TFB) aldehyde nodes and b) varying numbers of methyl groups on two different amine linkers (1,4-phenyleneamine derivatives: PA, Me_2PA, Me_4PA and benzidine derivatives: BD, Me_2BD, Me_4BD) whose structures are presented in **Figure 3.1**. Systematic combination of all building blocks leads to a series of twelve different COF materials of which five have not been reported in literature to the best of our knowledge (**Figure 3.1**). We successfully synthesised five novel COFs: Me_3TFB-Me_4PA, Me_3TFB-Me_2BD, Me_3TFB Me_4BD, TFB-Me_2PA, and TFB-Me_4BD. Keeping the synthetic and experimental conditions similar for all COFs within this and our previous study — in which we compared TFB-PA and TFB-BD to Me_3TFB-PA and Me_3TFB-BD for acid vapour sensing[183] — we also synthesised the COFs that have been published before (TFB-Me_2PA,[185] TFB-Me_4PA[186] and TFB-Me_2BD[187]), completing the matrix in **Figure 3.1** and facilitating a direct comparison.

3.3.1 Synthesis and Characterisation of COFs

In a classical Schiff base condensation reaction, two equivalents of aldehyde node and three equivalents of amine linker were reacted at 70 °C for three days in 1,4-dioxane:mesitylene 1:4 *v/v* at atmospheric pressure. While reactions with unmethylated amines were carried out with additional

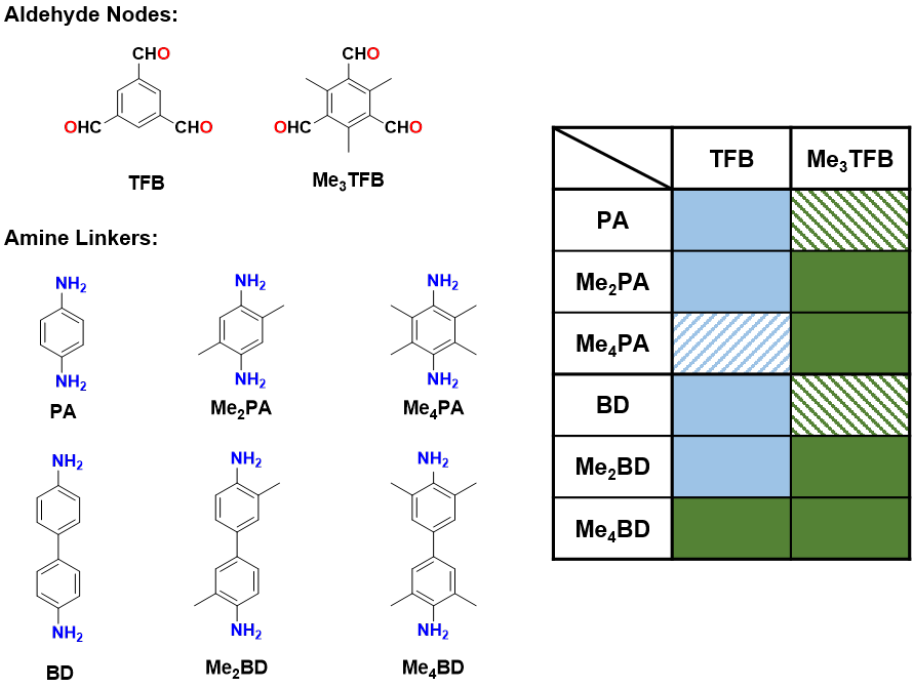

Figure 3.1: Structures of the aldehyde nodes (top left), amine linkers (bottom left) and matrix of the synthesised COFs (right) - plain blue: published in peer-reviewed literature before,[6,59,185,187] blue diagonal stripes upward: synthesis reported in a patent and characterisation data not shown,[186] plain green: novel COFs, green diagonal stripes downward: published by our group.[183]

water to enhance the dynamic covalent chemistry (DCC), methyl-containing amines were reacted only with acetic acid acting as catalyst. The additional water can not only enhance error-correction via DCC, but in the case of methylated amines, the equilibrium was also shifted towards the starting materials as indicated by fourier-transform infrared spectroscopy (FT-IR), which showed a higher intensity for the C=O stretch of the aldehyde around $\sim$1690 cm^{-1}. Furthermore, the BET surface area was found to be lower for COFs based on methyl-containing amines when additional water was added during the synthesis. After this reaction optimisation, all COFs have been synthesised and characterised in triplicate. The COFs were isolated by Büchner filtration and subjected to an extensive washing procedure developed by Dichtel and co-workers.[31] The material was then divided into two batches for different COF activations (drying). One batch was dried at 120 °C overnight in an air ventilated oven and the other one was dried at 120 °C overnight in a vacuum oven.

First, based on new bands that appeared near 1620 cm¹ (**Section 3.S**), FT-IR spectroscopy confirmed the successful formation of imine bonds. All COF spectra show an attenuated C=O stretch of the aldehyde around $\sim$1690 cm^{-1}, which is likely due to unreacted side groups at the outside of the 2D polymeric sheet.[60,65,188] These relative intensities vary, depending on the number of methyl groups attached to the amine linker. The more methyl groups are attached, the stronger is the residual aldehyde vibration in the spectrum. The repeatability for TFB-Me$_4$PA is less good compared to the other COFs of this series. To shed light on the full COF series, this sample was still included in the further analysis. The lower repeatability is expressed by the larger error margins.

The crystallinity of the COFs was confirmed by powder X-ray diffraction (PXRD) analysis. The crystallinity and the BET surface areas of COFs are typically closely related, so both measurements were taken into account together for the characterisation of the materials. All diffractograms, except for TFB-Me$_4$BD, show diffraction peaks (**Section 3.S**). Some diffraction peaks are low in intensity and broad, but together with the BET surface area determination, we concluded that the obtained structures are COFs. However, based on its PXRD and BET characteristics, TFB-Me$_4$BD is considered as COF-like porous organic polymer (POP).

Pawley refinement was performed in triplicate with the PXRD diffractogram using the space group *P6/m*, which corresponds to an eclipsed stacking structure. The unit cell dimensions and R_{wp} and R_p values are given in **Table 3.1**. For TFB-PA and TFB-BD, Pawley refinement was not performed, because the stacking conformations have been published previously.[6,59,179] For TFB-Me$_2$BD, compared to literature, a larger interlayer stacking distance (3.73$\pm$0.02 Å vs 3.4 Å) and lower R_{wp} and R_p values were obtained.[187] For TFB-Me$_4$PA, the refinement matched better to the space group *P1* with lattice parameters of *a*=22.80$\pm$0.46 Å, *b*=22.21$\pm$0.26 Å, *c*=6.74$\pm$0.24 Å, α=89.5$\pm$1.21°, β=91.1$\pm$3.82° and γ=59.1$\pm$1.10° with R_{wp}=3.42$\pm$1.24% and R_p=2.23$\pm$0.60%. For TFB-Me$_4$BD, no Pawley refinement was conducted, because of the non-existing crystallinity. The Pawley-refined PXRD patterns were compared to the simulated diffraction patterns of optimised crystal structures obtained from density functional theory (DFT) calculations. To compare experimental COF with simulated PXRD patterns, Zhang *et al.* suggested to use simulated patterns of statistical COF models, consisting of more than one single stacking order, to accurately model the PXRD diffractions of COFs.[189] To obtain insight in the effect of stacking on the characteristics of PXRD patterns, the two extreme models “eclipsed” and “staggered” were simulated. Small local disorders were neglected to reduce computational complexity. Such small deviations in peak position and peak broadening can also be observed in our materials. It

Table 3.1: Unit cell dimensions for all uncharacterised COFs within this manuscript with the space group *P6/m*, both as determined by Pawley refinement and as computed by DFT calculations.

COF	Pawley-refined unit cell dimensions				Computed unit cell dimensions	
	a=*b* [Å]	*c* [Å]	R_{wp} [%]	R_p [Å]	*a*=*b* [Å]	*c* [Å]
TFB-Me_2PA	23.54±0.66	3.76±0.06	2.13±0.81	11.48±0.55	22.69	3.78
Me_3TFB-PA	21.96±0.07	3.77±0.04	5.77±2.57	3.97±1.67	22.52	3.75
Me_3TFB-Me_2PA	21.87±.012	3.73±0.01	4.08±0.81	2.79±0.51	22.56	3.80
Me_3TFB-Me_4PA	23.17±0.21	3.73±0.02	2.92±3.16	2.09±2.13	22.69	3.78
TFB-Me_2BD	30.35±0.29	3.72±0.02	2.92±3.16	2.09±2.13	29.95	3.74
TFB-Me_4BD	not crystalline				30.24	3.80
Me_3TFB-BD	29.64±0.11	3.67±0.11	6.79±0.56	4.74±0.46	30.01	3.72
Me_3TFB-Me_2BD	29.86±0.55	3.65±0.08	2.04±1.33	1.51±0.90	30.02	3.72
Me_3TFB-Me_4BD	28.98±0.74	3.52±0.13	0.70±0.08	0.56±0.06	30.12	3.78

was therefore hypothesised that the small deviations in peak position between the experimental and the DFT-computed PXRD patterns are related to stacking disorder. All COFs — except for TFB-Me_4PA — crystallise predominantly in an eclipsed stacking conformation including some stacking disorder. The deviations between the computed unit cell dimensions and the Pawley-refined values is below 5%, which is within the expected accuracy of the DFT calculations, further supporting the formation of eclipsed COFs. Only the deviation in interlayer stackings of Me_3TFB-Me_4BD is slightly higher (6.8%). The diffraction patterns (**Section 3.S**) and unit cell dimensions of TFB-Me_4PA exhibit a better match with the staggered model as already indicated by the different space group.

Upon increasing the number of methyl groups in the amine linker, the crystallinity decreases. This can be rationalised by a less reactive tetramethyldiamine due to steric hinderance. The more unreacted aldehyde groups remain at the outside of the 2D polymeric sheets, the higher is the intensity of the C=O stretch in the FT-IR spectra. For aldehyde nodes, the crystallinity is larger when using methylated building blocks.

To study the COF stability in water, 1 M NaOH, 1 M hydrochloric acid, dichloromethane (DCM) and *N,N*-dimethylformamid (DMF), COFs were immersed for five days into the respective solvents and upon re-isolation and drying in a regular oven at 120 °C overnight, the PXRD patterns were recorded again. To investigate the chemical stability of the novel COFs, representative samples (methylated aldehyde, fully methylated amine, different amine) were chosen: Me_3TFB-PA, TFB-Me_4PA, Me_3TFB-Me_4PA and Me_3TFB-BD (**Section 3.S**). Wang et al.[174] and Daugherty et al.[18] studied already the

chemical stability of TFB-PA and TFB-BD, respectively. Me_3TFB-PA, TFB-Me_4PA, Me_3TFB-Me_4PA and Me_3TFB-BD were found to be stable in 1 M NaOH and DMF. All tested COFs are chemically stable in DCM except for Me_3TFB-BD, which is only partially stable in DCM. All COFs are stable in water, except for Me_3TFB-Me_4PA. The instability of Me_3TFB-Me_4PA in water is surprising, because the high number of hydrophobic methyl groups was anticipated to prevent water from a nucleophilic attack.

The thermal stability was determined by thermogravimetric analysis (TGA), Me_3TFB-Me_4PA and TFB-Me_4PA started to decompose at 363 °C and 412 °C, respectively (**Section 3.S**). This is comparable to the thermal stability of Me_3TFB-PA and Me_3TFB-BD.[183] It is anticipated that the stability of the other COFs in this series will be similar.

3.3.2 Solid-state NMR assignment

^{13}C cross-polarisation magic angle spinning solid-state NMR (^{13}C CPMAS ssNMR) spectra were recorded to investigate the structure of the COFs. We used two different spinning frequencies to distinguish COF signals from spinning side bands (**Section 3.S**). Compared to the spectra of the starting materials, the ^{13}C CPMAS NMR spectra of COFs show a strongly attenuated signal around 190-200 ppm, characteristic for aldehyde carbons, and a signal around 160 ppm, which can be assigned to the imine carbons, (**Figure 3.2A1-C1**). These observations lead to the conclusion that imine-linked COFs have indeed been formed. Based on the ^{13}C CPMAS NMR spectra, structural assignments for COFs have been proposed.[6,59]

As a next step, CP contact time-dependent CPMAS NMR analysis provides added value for an evidence-based assignment of such materials.[174] By varying the CP contact time and recording the respective spectra, the ssNMR signals of differently substituted carbon atoms show a different relative cross-polarisation build-up, which enables the assignment of the signals to the carbons present in the COF structure. This is a facile and straightforward strategy for structure elucidation of solid materials in general and was only recently employed in COF characterisation. Acquiring 2D HETCOR ssNMR spectra at two different CP contact times enabled Samori and co-workers to fully assign the ^{13}C spectrum of TFB-PA.[174] To acquire 2D HETCOR spectra, a ssNMR probe with a spinning rate as high as 60 kHz is required and such a special probe is not widely available. Recently, Zhu *et al.* assigned the ^{13}C spectrum of a methoxy-functionalised, imine-linked COF based on 15 different CP contact times by comparing the relative CP data, which was obtained at lower spinning rates.[33] We

built further on this approach, expanded it to a more complex COF structure, and also analysed the ssNMR spectra with the open source software ssNnake[190]18 to obtain the CP build-up curves. The advantage of CP build-up curves over measuring at two CP contact times is that they directly visualise the rate of each signal build-up. Based on these curves, the required CP contact times for structure elucidation can be identified and selected to save measurement time for future structural assignments of similar COFs.

The assignment of the NMR spectra of the starting materials in **Figure 3.2A1-C1** has been done by solution NMR measurements (^{13}C and ^{135}DEPT), before double-checking whether the signals appear at approximately the same chemical shifts in ssNMR. At first, we applied our CP contact time dependent analysis to assign TFB-PA with the help of Me_3TFB-PA and TFB-Me_4PA (**Section 3.S**). As the methylated COFs are derivatives of the unmethylated COFs and a methyl substituent typically has only a small effect on arylic chemical shifts, we expect comparable chemical shifts, enabling one to assign all NMR signals by comparing the spectra and CP build-up curves (**Figure 3.2A2-C2**). We found for both combinations (TFB-PA/Me_3TFB-PA and TFB-PA/TFB-Me_4PA) that the assignment matches the one measured with 2D HETCOR NMR.[137] We now implemented this method in its full potential to our extended series, including TFB-BD and its methyl derivatives. TFB-BD has also been assigned previously, though no experimental support was shown.[59] Hence, we measured the CP build-up for TFB-BD (**Figure 3.2A2**), Me_3TFB-BD (**Figure 3.2B2**) and Me_3TFB-Me_4BD (**Figure 3.2C2**). Each COF is symmetrical and in this sequence each COF has one quaternary carbon more than the previous one. It is noteworthy, that the crystallinity of the COF is also reflected by the width of the signal. The sterically demanding Me_3TFB-Me_4BD has a lower crystallinity and thus more signals that overlap in the spectrum. The best resolution was obtained for Me_3TFB-BD (**Figure 3.2B1**), which therefore was taken as a starting point for the assignment.

The eight different carbon atoms in Me_3TFB-BD — as labeled in the chemical structure depicted in (**Figure 3.2B1**) — yield seven separate signals, indicating that two carbons have an identical chemical shift. First, the methyl group could be assigned to the signal at 15 ppm and the imine-carbon to the signal at 160 ppm, both based on their chemical shift. For the next step in the assignment, it is our experience that it is best to first look at the spectrum of TFB-BD (**Figure 3.2A1**). It shows only one slow CP build-up (**Figure 3.2A2**), which means that out of the three quaternary carbons, two are overlapping with a tertiary carbon. Based on the chemical shift, the carbon is deshielded, indicating an electronegative atom in its surrounding. In addition, the quaternary carbon from the amine linker could

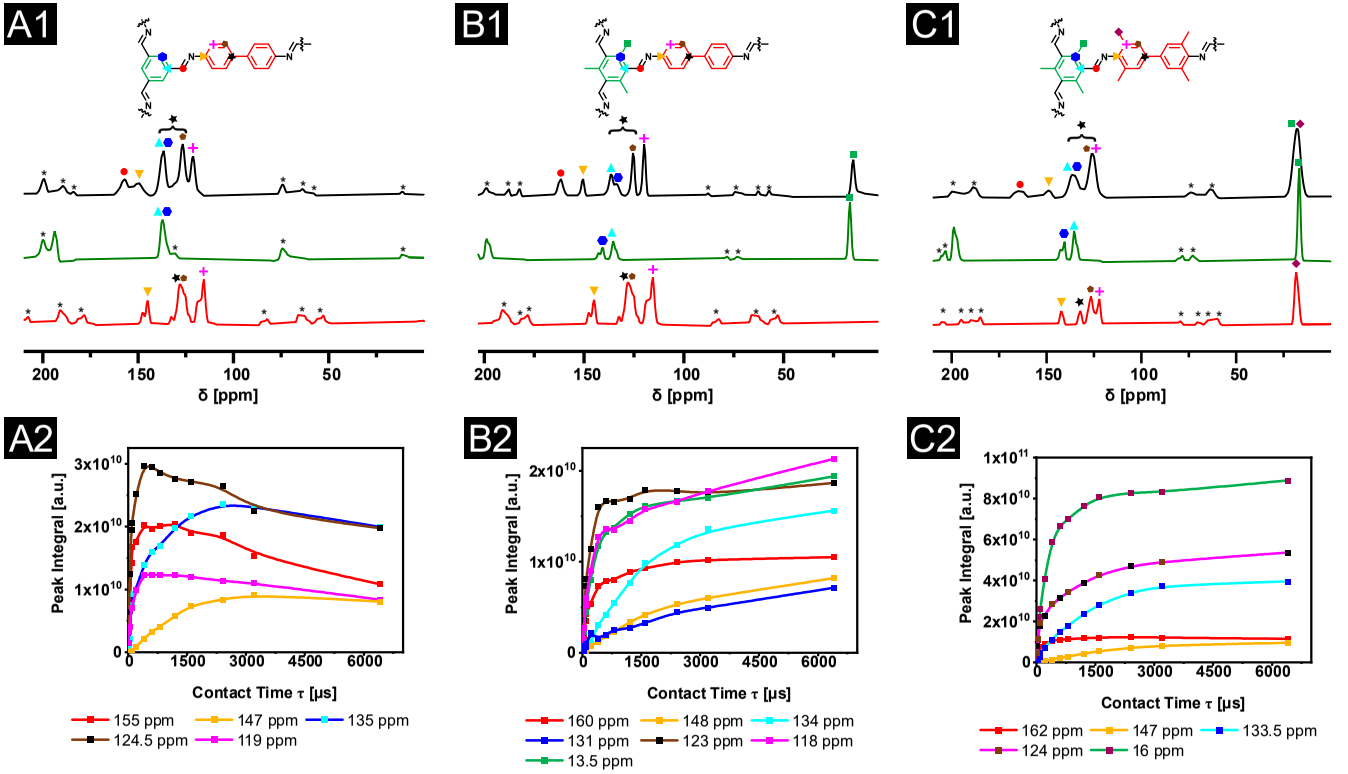

Figure 3.2: Solid-state ^{13}C CPMAS NMR spectra of respective COFs at 11 kHz spinning frequency at 3.2 ms CP contact time (black): TFB-BD (A), Me_3TFB-BD (B) and Me_3TFB-Me_4BD (C), aldehyde node at 3.0 ms CP contact time (green) and amine linker at 3.0 ms CP contact time (red) in the top (A1-C1) and CP build-up curves in the bottom (A2-C2). Spinning side bands are denoted with an asterisk.

be assigned to ∼148 ppm in the spectrum of TFB-PA, supporting the same assignment for TFB-BD, Me_3TFB-BD and Me_3TFB-Me_4BD. The signals at 134 ppm and at 131 ppm (**Figure 3.2B1**) can be assigned to the aryl carbons from the aldehyde node based on the chemical shifts of the starting materials. In the spectra of TFB-BD (**Figure 3.2A1**) and Me_3TFB-Me_4BD (**Figure 3.2C1**) these two signals overlap which is also supported by the relatively fast CP build-up for TFB-BD (**Figure 3.2A2**) due to the tertiary aryl carbon and the slow build-up after methylation when both aryl carbons are quaternary. We assume that the signal at 134 ppm belongs to the carbon next to the imine carbon based on the assignment found for TFB-PA. By now, only three carbon atoms are not assigned yet. Based on the starting material, we hypothesise the signal at 123 ppm belongs to the *meta* position and the signal at 118 ppm belong to the *ortho* position with respect to the former amine. The carbon atom, which links the two phenyl rings in benzidine, cannot be assigned to a specific signal. Its signal seems to overlap with other signals and based on the chemical shift in the starting material, it can either overlap with the carbons from the aldehyde node or with the carbons from the benzidine. The same order for the assignment was applied to TFB-BD and Me_3TFB-Me_4BD. The ssNMR spectra for different CP contact times and the spectra of the other COFs can be found in **Section 3.S**.

3.3.3 BET surface area dependencies

Nitrogen sorption experiments have been carried out to determine the porosity and BET surface area of all COFs. All samples were measured in triplicate to check the repeatability. The isotherms can be found in **Section 3.S**. The adsorption branches were used to calculate the BET surface area (S_{BET}). All samples are microporous, which means the original p/p^0 range from 0.05 to 0.3 is not applicable. Therefore, lower relative pressures have been used for the linear fit and the Rouquerol criteria[127] were applied. The same pressure range has been used for the linear fit of the same COF. The BET surface areas for all COFs and both activation methods are displayed in **Figure 3.3**. The BET surface areas vary over a very broad range from 28 to 2215 m^2/g. For TFB-PA,[18] TFB-Me_2PA,[185] TFB-BD,[191] and TFB Me_2BD,[187] S_{BET} has been reported before and the highest reported values are 1571 m^2/g, 144 m^2/g, 1948 m^2/g, and 821 m^2/g, for these COFs respectively. For TFB-Me_4PA, which is reported in a patent, we could not find any S_{BET} value. However, TFB-Me_2PA was measured to have a S_{BET} of 680±55 m^2/g and TFB-Me_2BD of 1026±168 m^2/g, which are, to the best of our knowledge, the highest reported values so far for these specific COFs. For TFB-BD, the BET surface area was found to be 1514±97 m^2/g. The reported value in literature is approximately 29 % higher,

which is likely due to the supercritical CO_2 drying. This is a mild activation method that prevents pore collapse. The exact values of all BET surface areas can be found in **3.S**.

We recently reported that the BET surface area increases due to methylation of the aldehyde for Me_3TFB-PA and Me_3TFB-BD.[183] **Figure 3.3** shows that methylation of the aldehyde leads to an increase in BET surface area for five out of the six pairs synthesised in this study. The only exception is TFB-Me_4PA/Me_3TFB-Me_4PA for which the BET surface areas are approximately the same. It must be noted that the synthesis of TFB-Me_4PA is challenging and shows low repeatability. The increase in S_{BET} for Me_3TFB COFs is in line with the crystallinity of the COFs. The magnitude of this increase varies for the different COFs. The expansion of this previous results implies an overall trend of increasing BET surface area by employing a methylated aldehyde node. It is, however, important which building block is methylated, because S_{BET} decreases when the amine linker is methylated. In **Figure 3.3** the BET surface area continuously decreases upon attaching more methyl groups *ortho* to the amine group. This trend is visible for all four COF series (TFB-PA, Me_3TFB-PA, TFB-BD and Me_3TFB-BD), in which we added increasingly more methyl groups. These findings are in line with a higher C=O aldehyde to C=N imine stretch ratio in FT-IR spectra for non-methylated COFs compared to their methylated counterparts. This leads us to the conclusion that the position of the methyl group is crucial for the porosity of the COFs. We hypothesise that the steric demand of the methyl group plays a role in the COF formation and that this affects the COF formation in two ways. As reported previously,[183] the methyl groups reduce the conjugation of the carbonyl groups with the π-system of the aromatic Me_3TFB ring, leading to a smaller rotational barrier after methylation. The smaller barrier enhances the reaction rate of the conformational change by several magnitudes and the preferred orientation of the aldehyde node for the framework formation is achieved faster, which results in a more regular framework. On the other hand, when the steric demand is present on the amine linker, the nucleophilic attack of the amine group at the carbonyl group can be already more difficult and is less likely to happen, which leads to the observed decrease in BET surface area. This line of thought fits with the restricted synthesis based on steric hinderance as discussed based on the FT-IR and PXRD patterns.

Not only the structure, but also the activation method plays a crucial role in the porosity of COFs. To investigate the stability of the COFs in this study, all COFs were activated at 120 °C in the two different ways as mentioned before: vacuum vs ambient pressure. Afterwards, the BET surface area was measured for all samples and to correct for the difference in BET surface area due to

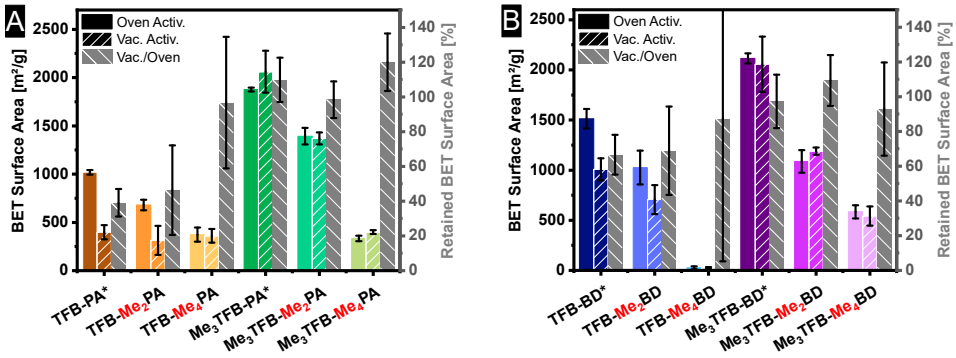

Figure 3.3: BET surface areas and retained BET surface areas for PA-COFs (A) and BD-COFs (B) after oven- and vacuum-activation. The retained BET surface area gives the ratio how much S_{BET} has been left after vacuum drying. The errors are based on the analyses of three batches. The asterisk indicates already published data which is shown to illustrate the trends better.

different pore sizes, the retained BET surface area has been calculated (**Section 3.S**). Again, the methylated aldehyde nodes lead to an increase in retained S_{BET}, meaning the frameworks are less prone to pore collapse. The magnitude of this effect varies from COF to COF, being the smallest for TFB-Me$_4$BD/Me$_3$TFB-Me$_4$BD with only 5% difference and the largest with 70% difference for TFB-PA/Me$_3$TFB-PA. For most methylated COFs also the standard deviations are lower than the ones for the non-methylated aldehyde COFs with the exception of TFB-PA/Me$_3$TFB-PA and TFB-BD/Me$_3$TFB-BD which have roughly the same standard deviations. Based on these findings, Me$_3$TFB can reduce pore collapse and lead to robust COFs.

3.3.4 UV absorbance

The UV absorbance of the COFs was determined with diffuse reflectance spectroscopy. In **Figure 3.4**, the absorbance spectra are displayed for the different COFs and the first derivatives of these plots are given in the insets. The absorption edges of all COFs are within 370 to 450 nm (**Table 3.2**), thus in the purple and blue region of the visible spectrum, explaining the yellow color of all samples. The intensity depends on the thickness of the sample film, but the shape of the curve does not change. However, it is observed that sometimes the plateau is reached relatively fast, whereas for other samples the curve changes only slowly before reaching the plateau. As the shape of the spectra does not depend on the amount of sample, we believe that the slope of the curve is also characteristic for a specific material, supporting the use of the inflection point as a new data analyses approach.

Table 3.2: Overview of absorption edges, inflection points and the calculated band gaps for all COFs.

COF	Estimated absorption edge [nm]	Derived inflection point [nm]	Derived optical band gap* [eV]
TFB-PA	429	449	2.70
TFB-Me_2PA	448	469	2.64
TFB-Me_4PA	438	484	2.52
Me_3TFB-PA	377	414	2.94
Me_3TFB-Me_2PA	380	427	2.83
Me_3TFB-Me_4PA	370	435	2.85
TFB-BD	435	447	2.70
TFB-Me_2BD	441	459	2.72
TFB-Me_4BD	432	482	2.54
Me_3TFB-BD	390	419	2.93
Me_3TFB-Me_2BD	410	444	2.80
Me_3TFB-Me_4BD	435	460	2.56

*Based on Tauc plot analysis

Hence, we used Origin to calculate the first derivative and used the inflection point for additional information. Data analysis with this approach shows, that for COFs with a methylated amine linker, the absorbance spectra red shifts whereas a blue shift is observed for methylated aldehyde nodes (**Figure 3.4**). Methylation therefore gives a handle to tune the UV absorbance of COFs. Methylation of both aldehyde node and amine linker results in an inflection point in between the COFs with only one methylated building block. By increasing the number of methyl groups on the amine linker, the bathochromic shift of the absorbance spectrum gradually becomes more pronounced (**Section 3.S**).

Traditional analysis of the absorption edge leads to the same findings with one exception: the trend in which the spectra red shifts based on the number of methyl groups does then not apply anymore. Additionally, from Me_3TFB-PA to Me_3TFB-Me_4PA the absorption edge does not increase, but for the other three COF series, this trend still applies. These findings further strengthen our mathematical approach to analyse diffuse reflectance spectra by comparing their inflection points.

All changes in absorbance are also visible by eye, because the isolated COF powders have different shades of yellow (**Section 3.S**). All the trends we found lead to the possibility of pre-designing the UV absorbance based on the choice of building blocks.

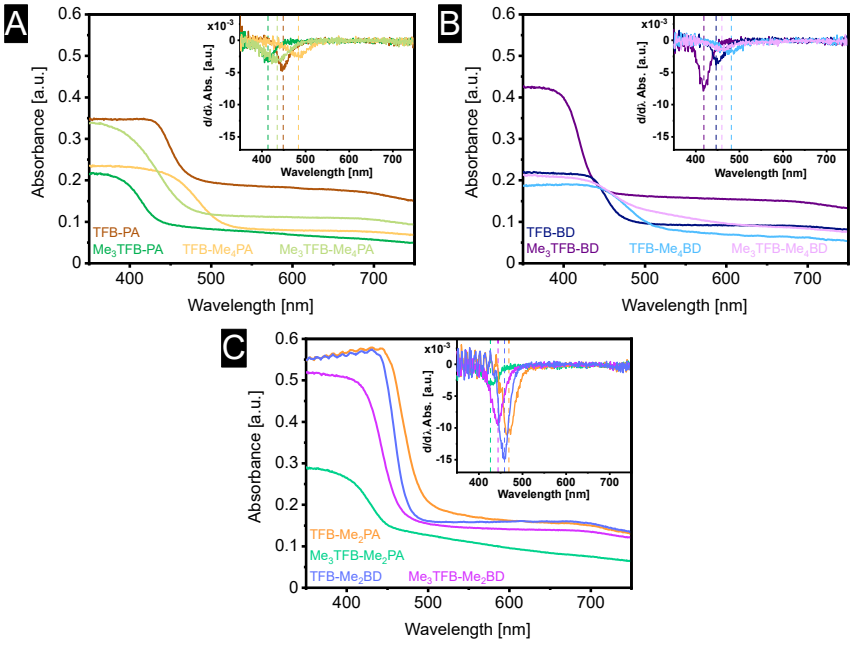

Figure 3.4: Absorbance spectra of TFB-PA, TFB-Me_4PA, Me_3TFB-PA and Me_3TFB-Me_4PA (A), TFB-BD, TFB-Me_4BD, Me_3TFB-BD and Me_3TFB-Me_4BD (B) and TFB-Me_2PA, Me_3TFB-Me_2PA, TFB-Me_2BD, Me_3TFB-Me_2BD (C) and their first derivatives as insets for a better comparison.

The bathochromic shift upon methylation of the amine linker can be explained by the inductive, electron-donating effect of methyl groups. The hypsochromic shift for methylated aldehydes can, however, not be explained by this effect. The DFT structure optimisation of the COF sheets (**Section 3.S**) shows that the Me_3TFB-COF structures are bended, while the TFB-COF structures are flat. Such a difference was not found upon the methylation of the amine linker. We hypothesise that the observed bending from the methylated aldehyde node decreases the delocalisation of the entire conjugated system, which would result in an increased excitation energy, leading to a blue shift.

Fundamental knowledge on how the UV absorbance and the optical band gap are influenced by its COF structure is of importance to further develop photocatalytic applications. To study the effect of methyl groups on the optical band gaps, we converted our absorbance spectra into the Kubelk-Munk function,[192] assuming a direct allowed transition. Plotting this data in an adapted Tauc plot,[193] enables one to obtain the optical band gap (**Section 3.S**). The optical band gaps for TFB-COFs are in a range of 2.72 to 2.52 eV and methylated aldehyde nodes result in slightly higher band gaps of 2.94 to 2.56 eV. This result matches with the observed blueshift upon methylation of the aldehyde node.

Upon tetramethylation of the amine linker, the optical band gap decreases. The energies of the band gaps as well as the observed trends show a better match with the analysis of the UV spectra via their inflection points compared to the traditional analysis via the absorption edge. This supports again that diffuse reflectance spectra with S shaped curves can be analysed by their inflection point. Overall, the band gaps do not change considerably, which means methylation can be used to fine-tune the UV absorbance towards the desired application while getting a predictable porosity.

3.4 Conclusions

Multiple combinations of non-methylated (TFB) and methylated (Me_3TFB) aldehyde nodes with either methylated or non-methylated *p*-phenylenediamine or benzidine linkers, have been synthesised and imine COF formation was proved by FT-IR, BET surface area analysis and PXRD measurements. Pawley refinement yielded the unit cell dimensions, which were compared to the computationally modelled structures. For the first time, the signals of the ssNMR spectra of TFB-BD, Me_3TFB-BD and Me_3TFB-Me_4BD could experimentally be assigned using contact time dependent CPMAS NMR and comparing the different COF derivatives. An in-depth study of the COF series revealed several trends in their properties based on the methyl substitution pattern of their corresponding building blocks. First, COFs with Me_3TFB show larger crystallinity and therefore increased BET surface areas up to approximately 2100 m^2/g. In addition, the COFs are less prone to pore collapse which was proven by comparing vacuum activation with drying in a regular oven. Second, it is of importance which building block is methylated (aldehyde vs amine), since — in contrast to their aldehyde counterparts — COFs with methylated amine linkers show a decrease in crystallinity and BET surface area. This is likely attributed to the higher steric demand of the methyl groups, which is supported by the third trend: the more methyl groups are attached to the amine linker, the stronger are the decreases in crystallinity and BET surface area. In addition to the steric influence on the conjugation of the carbonyl groups with the aromatic ring, we hypothesise that the methyl groups on the amine linker sterically hinder the COF formation. An amine methylation does not show a significant effect on the robustness of the COF against vacuum activation, which is again in contrast to their aldehyde counterparts. Therefore, the position of functionalisation within the COF building blocks is crucial.

Fourth, the absorbance spectra blue shifts if Me_3TFB is used as a building block, which leads to a small increase in the optical band gap compared to TFB-COFs. We hypothesise that this is caused by the decreased conjugation caused by the methyl groups. COFs with methyl groups on the amine

linkers show a red shift of the absorbance and smaller optical band gaps, which is in line with the bathochromic effect expected from methyl groups.

To conclude, the effect of methyl substitution patterns on high surface area COF properties can serve for an enhanced rational design of COFs. Furthermore, it allows one to fine-tune the optical band gaps, which can be relevant for photocatalytic applications of COFs.

3.S Supporting Information

The Supporting Information is available free of charge on the website of the American Chemical Society:

Or it can be accessed via the following link:
https://drive.google.com/file/d/1wjErpqvsa4qjE3kKERW11JKmuy_c4Zr7/view?usp=sharing

4 Functionalised modulators in imine-linked covalent organic frameworks (COFs)

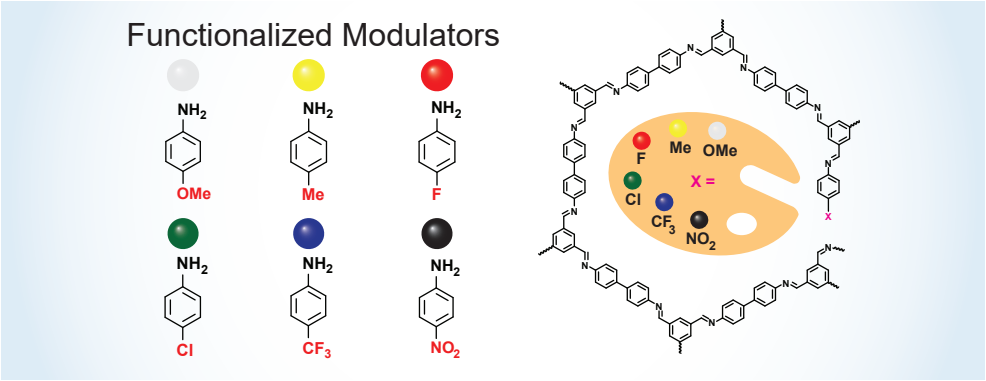

Ellen Dautzenberg, Frank Claassen, Louis C. P. M. de Smet

Microporous and Mesoporous Materials, **2023**, *350*, 112318.

4.1 Abstract

Covalent organic frameworks (COFs) are porous materials with high surface areas, making them interesting for a large variety of applications including energy storage, chemical sensing, and gas separation. In gas separation and sensing, functionalisation beyond the COF linkage can result in selective COF-gas interactions, tailoring the properties for the desired application. However, not all functional groups are compatible with the synthetic conditions needed for COF formation. Modulators, which are typically monovalent building blocks that would terminate the reaction, have been shown to maintain or even improve the COF porosity by slowing down the reaction kinetics. Herein, we report on a series of several *para*-functionalised (OMe, Me, F, Cl, CF_3, NO_2) amine modulators to introduce additional functionality into the framework to study the selective CO_2/N_2 gas separation under flue gas conditions. Thorough characterisation of the modulated COFs showed that the modulators are located on the outside of the polymeric sheet and get replaced by benzidine molecules, favouring a regular network formation over a homogeneous modulator distribution. The fractions of eventually incorporated modulator vary per functional group between 2.1 mol% (NO_2-modulated COF) and 8.9 mol% (Me-modulated COF) while maintaining high BET surface areas (> 1800 m^2/g). It was found that all modulated COFs adsorb moderate quantities of CO_2 and show comparable CO_2/N_2 IAST selectivity values under flue gas conditions. A higher number of functional groups in the framework was shown to enhance the IAST selectivity.

4.2 Introduction

Porous materials are solid materials, possessing permanent pores with pore sizes of a few to several hundred nanometres. These pores can be classified into macro- (> 50 nm), meso- (2-50 nm) and micropores (<2 nm).[1] In 2005, Yaghi and co-workers reported the first covalent organic framework (COF) as a new type of fully organic porous nanomaterial.[13] Since then, COFs have gained increasingly more interest and a huge variety of different materials and applications have been reported.[2,43] The permanent porosity and their channel-like structure lead to high surface areas, which are of interest for, amongst others, energy storage,[2,3] chemical sensing,[2,7] photocatalysis[2,4,5] and gas separation.[2,8] COFs are usually synthesised via polycondensation of two multivalent building blocks. The formed COF linkages are based on dynamic covalent chemistry (DCC).[14,15] DCC refers to reversible reactions carried out under thermodynamic reaction conditions, which enable error correction within the reaction. This leads to a crystalline framework with long-range order. Imines are

known for DCC, which makes them interesting for COFs. They can be synthesised in a condensation reaction from aldehyde and amine building blocks with an acidic catalyst, which is also known as Schiff base chemistry.[2,31,41,42]

In the context of gas separation applications, COFs are exposed to a mixture of gases of which one gas would — ideally — selectively adsorb onto the COF surface and inside the COF pores. Here, the porosity of COFs is advantageous to store large quantities of gas, which has, for instance, been used for carbon dioxide (CO_2) capture and storage. As the term 'gas separation' already states, it is important to have a selective adsorption of one gas over another, in order to achieve the desired separation. In fact, the development of new, more selective, porous materials for CO_2 capture crucially depends on the ability to determine this gas selectivity. Measuring mixed-gas adsorption requires specialised and expensive equipment.[194] The measuring principle relies on dynamic methods, in which the gas mixtures are constantly flowing over the sample and so-called breakthrough curves are recorded to determine how much of which gas is adsorbed. In contrast, measuring the adsorption isotherm of a pure component is far more straightforward and is possible with common physisorption instruments. Physisorption instruments measure the quantity of gas adsorbed at each pressure, leading to isotherms of the pure gases.

In order to determine gas separation selectivity values out of pure component isotherms, the so-called ideal adsorption solution theory (IAST) was developed by Myers and Prausnitz.[138] The basis of IAST is analogous to Raoult's law.[138] Both theories assume a linear dependence between gas pressure and the mole fraction of the gaseous component; in case of Raoult' s law the vapour pressure and in IAST the equilibrium gas-phase pressure.[138] The simplicity of these calculations makes IAST a widely used method for selectivity determination in gas separation. The IAST selectivity *S* of a binary gas mixture is defined as the ratio of the mole fractions in the adsorbed state (*q*) over the mole fractions of the bulk phase (*p*) of components 1 and 2 (**Equation 4.1**).[140]

$$S = \frac{q_1 \times p_2}{q_2 \times p_1} \tag{4.1}$$

The validity of IAST has been studied by comparing the IAST results with grand canonical Monte Carlo (GCMC) simulations for metal organic frameworks (MOFs).[195] Despite the development of more accurate GCMC simulations over the past decades, the obtained selectivity predictions, as well as experimentally obtained data, are still comparable to IAST predictions.[196–202] The comparable

results of IAST with GCMC simulations, its simplicity and general applicability are the reason why IAST is still the benchmark theory for mixed adsorption studies.

Being a primary greenhouse gas, CO_2 plays an important role in climate change. Strategies to mitigate global warming include the reduction of CO_2 emissions via carbon capture and storage. The separation of CO_2 from N_2 — and the associated CO_2/N_2 selectivity — play a crucial role in such strategies. In this context, the porosity of COFs is advantageous to store large quantities of gas.[173,203] Computational studies have shown that metal doping significantly increases the CO_2 uptake at 298 K and 1 bar.[204] Among the screened metals (Li, Na, K, Be, Mg, Ca, Sc, Ti), the CO_2-metal interaction is best in terms of adsorption and desorption for Li. The CO_2 uptake and CO_2/N_2 selectivity have been investigated under high pressure (> 1 bar) or flue gas (15% CO_2, 1 bar) conditions for example. It was found that the CO_2 adsorption increases with increasing pressure. At 5 bar pressure, triazine-based β-ketoenamine COF reached a CO_2 adsorption of 12.97 mmol/g and 3.64 mmol/g at 273 K and 298 K, respectively.[175] Flue gas conditions are relevant for the purification of industrial exhaust gases and several COFs have been investigated under those conditions. Covalent triazine frameworks (CTFs), a special type of COFs, are reported to have high CO_2/N_2 selectivity values. Mahato *et al.* reported the highest CO_2/N_2 IAST selectivity value for COFs under those chosen flue gas conditions so far of 185.8 at 273 K with an CO_2 adsorption of 3.50 mmol/g.[168] Among COF materials, imine COFs are most commonly used and Huang *et al.* synthesised an porphyrin COF, whose channel-walls were post-synthetically functionalised with carboxyl groups.[173] The selectivity under the above mentioned conditions was enhanced by more than ninefold compared to the pristine COF to S=77. Das *et al.* studied an imine network and determined CO_2/N_2 selectivity values of 211 at 273 K and 100 at 298 K.[172] These values were validated by breakthrough experiments, leading to a selectivity values of 125 at 298 K, which is even higher than predicted by IAST. Structure-performance studies of six different COFs, carried out by Wang *et al.*, have revealed that β-ketoenamine COFs outperform imine COFs with similar pore sizes.[174] They did not find a direct relation between the CO_2 uptake and the pore size.

Research has not been limited to CO_2 separation, but also sulfur dioxide (SO_2) removal from flue gas by COFs has been studied.[81] Imide-linked COFs were functionalised by incorporation of 4-[(dimethylamino)methyl]aniline and the SO_2 uptake was measured over time, leading to 6.30 mmol SO_2 g^{-1}, which is equivalent to 40 wt%.

Such monovalent amines or aldehydes can be used as modulators. Modulators would terminate the polymerisation. Due to the dynamic nature of imine chemistry, the imine bonds can react back to the starting materials and the modulator can be replaced by a diamine to continue polymerisation or the imine bonds can undergo metathesis. This dynamic behaviour enables two different possibilities how the modulator acts during polymerisation: (1) the modulator is homogenously distributed, leaving some pores unclosed and therefore disrupts the regular framework, resulting in a non-ideal honeycomb structure or (2) the modulator is heterogeneously distributed. In several studies, it has been shown that the mostly unfunctionalised modulator was mainly located on the outside of the 2D polymeric sheet, acting as a capping agent.[72–75] Calik *et al.* studied the position of the modulator by using a thiol-functionalised modulator to enable staining with iridium clusters.[76] High-angle annular dark-field scanning transmission electron microscopy showed that the stained modulators were mainly located at grain boundaries. Moreover, Lee *et al.* used a dimethylamine-functionalised modulator in imide COFs for SO_2 capture.[81] Since the polymerisation is dynamic, the modulator gets constantly replaced by diamine molecules. This exchange reaction slows down the framework polymerisation and leads to a more regular framework.[72,73,75–80] In general, such modulators can additionally contain different functional groups,[81] ranging from electron-withdrawing groups to electron-donating groups. The influence of such functional groups was studied by Hammett *et al.* who derived an equation that correlates the chemical structure with the corresponding reactivity.[205,206] Later Hansch *et al.* compiled extensive lists of Hammett parameters for a broad library of functional groups.[207,208] The applicability of the Hammett equations has been shown in several studies, amongst others the hydrolysis of *p*-nitrophenyl benzoate esters,[209] imine exchange in multistep metallo-organic transformations[210] or imine exchange in covalent adaptable networks.[211]

As shown by these examples, functional groups play an important role in tailoring the selectivity of COFs for gas adsorption and modulators have proven to form COFs with high porosity. Therefore, we decided to extend this approach by employing a series of functionalised modulators, which are even commercially available. The obtained materials were thoroughly characterised and the modulator concentrations within the framework were determined. Additionally, the impact of the different functional groups on CO_2/N_2 selectivity under flue gas conditions was systematically studied.

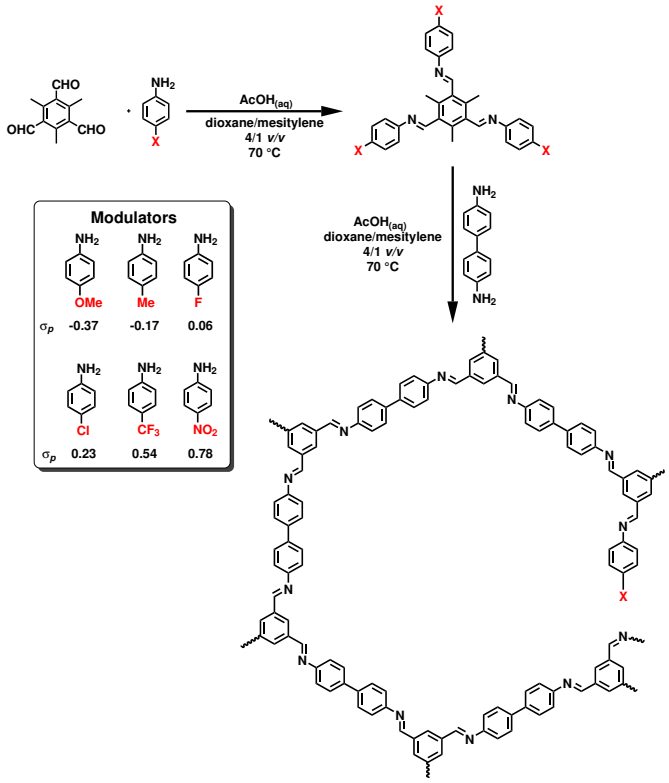

Scheme 4.1: Schematic showing the synthesis of modulated COFs in a two-step reaction. In the inset all *para*-substituted modulators used in this study, including their Hammett parameters, are given.

4.3 Results and discussion

In a first approach to introduce functional groups in our imine-linked COFs,[183] we have tried to react several *ortho*-substituted (OMe, OH, F, NO_2) benzidine building blocks with our recently reported methyl aldehyde building block.[183] While the methoxy-substituted benzidine resulted in a COF, the hydroxy-substitution led to an amorphous network, and fluoride- and nitro-substitution did not react at all (**Section 4.S**). The electron-withdrawing character of fluoride- and nitro-substitution leads likely to a decrease in reactivity and thus no reaction could be observed. We therefore looked into a different strategy to incorporate those functional groups in our COFs and decided to continue via *para*-substituted modulators (**Scheme 4.1**).

4.3.1 Synthesis, reaction optimisation and characterisation of COFs with modulators

In a classical Schiff base condensation reaction, two equivalents of aldehyde node and three equivalents of amine linker were reacted at 70 °C in 1,4-dioxane:mesitylene 1:4 *v*/*v* at atmospheric pressure. The three equivalents of amine linker consist together out of benzidine and the respective modulator. With the amount of modulator added, we were aiming for approximately 30 mol% of modulator of all amines in the framework. This will be abbreviated as “mol% modulator”. With the chosen building block, more than 30 mol% of modulator would decrease the number of functional groups for imine formation per monomer below two, which would interfere with the formation of a regular framework.

In a one pot synthesis of CF_3-modulated COF, only ∼3% modulator was found based on digestion ^{1}H-NMR. In order to get higher quantities of modulator incorporated into the framework, the reaction conditions were optimised. In a first step, the modulator was reacted quantitatively with all aldehyde groups of Me_3TFB, to which then 70 mol% benzidine was added *in situ*, and an immediate precipitation could be observed (**Scheme 4.1**). The precipitate was isolated after 6 h, 1 d, 2 d and 3 d and the BET surface area was determined to check the porosity. It was found that the BET surface area after 1 day of reaction time was 2028 m^2/g and did not change much anymore upon further increased reaction times (**Section 4.S**). Since a trade-off between the concentration of functional groups within the framework and porosity is needed, the COFs were also digested in DCl/D_2O, before ^{1}H-NMR analyses to calculate the fraction of modulator. The concentration of modulator decreases over time, which means that the reactivity of benzidine is higher compared to the reactivity of modulator. This indicates that it is thermodynamically advantageous to form a crystalline framework rather than incorporating all functional monomers into the polymers, as that would lead to interrupted networks.

The synthesis of methoxy-modulated COFs required different reaction conditions, because initially, before optimisation, no precipitate and thus no COF was formed. Instead, Me_3TFB and 30 mol% OMe modulator were reacted for one day before benzidine was added and allowing the reaction to proceed for another two days.

After this reaction optimisation, all modulator-functionalised COFs have been synthesised and characterised in triplicate. The COFs were isolated by Büchner filtration and subjected to Vitaku *et al.*'s extensive washing procedure.[31] The material was then dried at 120 °C overnight in an air-ventilated oven. The characterisation of modulated COFs is exemplarily demonstrated for CF_3-modulated COF,

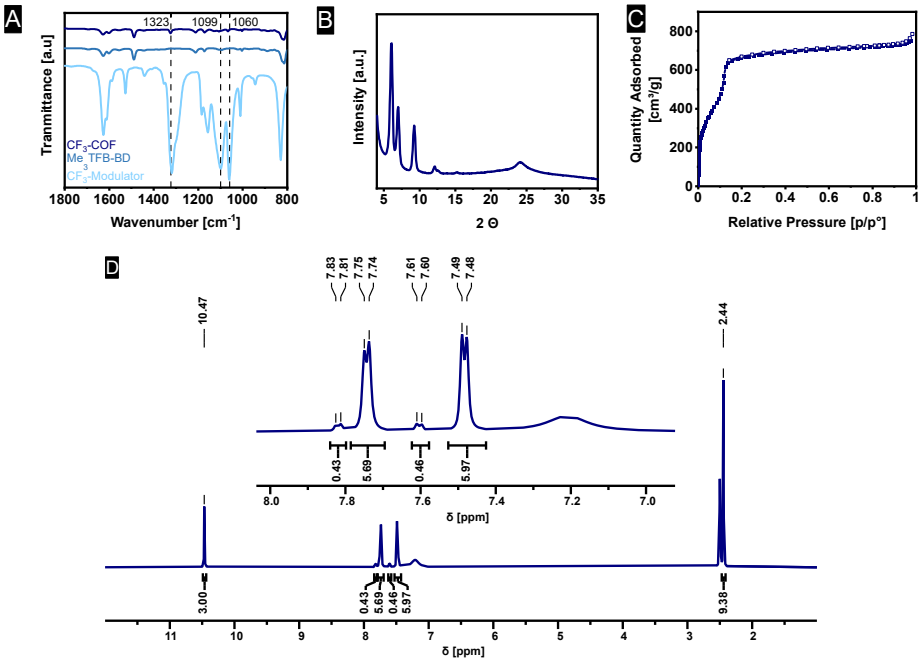

Figure 4.1: Characterisation of the CF_3-modulated Me_3TFB-BD COF: FT-IR spectrum (A), PXRD diffractogram (B), adsorption-desorption isotherm (C), and NMR digestion to quantify the modulator content (D).

because this modulator can easily be recognised by fourier-transform infrared spectroscopy (FT-IR). The characterisation for the other modulated COFs can be found in the **Section 4.S**.

As a first step, to confirm the successful COF formation, FT-IR was performed, yielding an almost identical spectrum as the spectrum of Me_3TFB-BD COF (**Figure 4.1A**). Additionally, characteristic bands of the modulator 4-trifluoromethylaniline can be identified, *i.e.*, the strong bands at 1319, 1099 and 1061 cm^{-1}, which are characteristic for CF_3 groups.[212] The absence of bands at 1319 cm^{-1} and 1061 cm^{-1} in the FT-IR spectrum of Me_3TFB-BD shows that the that modulator has been incorporated. The band at 1099 cm^{-1} overlaps with other COF related bands and is therefore not clearly visible. The incorporation of the other modulators is less visible in the FT-IR spectra (**Section 4.S**).

Powder X-ray diffraction (PXRD) analysis was carried out to study the crystallinity. The diffractogram of CF_3-modulated COF — as well as the diffractograms of all other modulated COFs (**Section 4.S**) — show the same diffraction peaks as Me_3TFB-BD (**Figure 4.1B**), confirming the crystallinity of all COFs. Pawley refinement was performed in triplicate with the PXRD diffractograms using space group *P6/m*,

which corresponds to an eclipsed stacking structure. The unit cell dimensions and R_{wp} and R_p values are given in **Section 4.S**. The unit cell parameters match with those of Me_3TFB-BD, confirming the same crystal structure.[213]

Nitrogen (N_2) sorption experiments have been carried out to determine the porosity and BET surface area of all COFs. The type IVb isotherm of Me_3TFB-BD with a pore size of 2.7 nm is retained in CF_3-modulated COF (**Figure 4.1C**). All other modulated COFs also have a type IVb isotherm with a pore size distribution centered at 2.7 nm (**Section 4.S**). A pore size of 2.7 nm is just in between micro- and mesoporosity and the microporosity is shown by a large adsorption of N_2 in the low pressure range (p/p^0<0.1). A step in the isotherms at p/p^0=0.1 indicates capillary condensation. The isotherms do not show a hysteresis during desorption. The comparable isotherm shape and pore size distribution of Me_3TFB-BD and all modulated COFs is in line with the comparable PXRD diffractograms and the low fractions of modulators in the COFs, pointing to the similarities in the structures of the functionalised, modulated COFs and Me_3TFB-BD. The adsorption branches were used to calculate the BET surface area (S_{BET}). All samples are microporous, which means the original p/p^0 range from 0.05 to 0.3 is not applicable. Therefore, lower relative pressures have been used for the linear fit and the Rouquerol criteria[127] were applied. The same pressure range has been used for the linear fit of the same COF. A BET surface area of 1966$\pm$54 m^2/g was found for CF_3-modulated COF.

Since the IR spectra could not unambiguously show the presence of the modulator inside the COF, it was proven and quantified by NMR digestion. In NMR digestion, the COF sample is cleaved into its monomers again for the purpose of COF analysis (**Section 4.S**). In more detail, the sample was exposed to DCl in D_2O solution in deuterated DMSO-d_6, and the ^{1}H-NMR spectrum was measured (**Figure 4.1D**). The resulting spectrum shows a signal at 10.47 ppm, which is a characteristic chemical shift for aldehyde protons, indicating that the COF is depolymerised. The four doublets between 7-8 ppm correspond to the arylic protons of the benzidine and the modulator. After phase and baseline correction, the signals were integrated and based on the integrals, the amount of modulator in mol% was calculated. For CF_3-modulated COFs, 7.4$\pm$0.4 mol% modulator is incorporated within the framework, which is significantly less than the 30 mol% feed. This shows that the polymerisation with benzidine is favourable compared to maintaining the modulator-aldehyde imine bonds. Since there is not enough benzidine to react with all aldehyde groups, the yield of COF precipitate would also reduce, which was confirmed by our experiments.

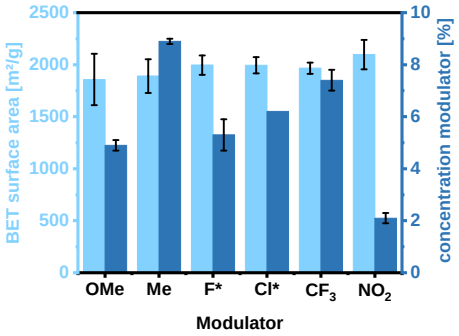

Figure 4.2: Average BET surface areas (left axis) of all modulated COFs and the concentration of modulator incorporated into the framework in mol% of amines (right axis). The errors bars result from the analyses of triplicates, apart from the modulator concentration of F-modulated COF, which were performed in duplicate (**Section 4.S**).

Comparing the entire range of modulated COFs, the BET surface areas are between 1857±247 m^2/g and 2097±141 m^2/g and do not vary much depending on the modulator used (**Figure 4.2**). Such high BET surface areas translate to a high number of adsorption sides for gases, which make these materials promising for gas applications. The amount of modulator that has been incorporated into the framework is repeatable for a specific modulator, which can be seen by the small error margins. The amount of modulator varies significantly depending on the modulator used and ranges from 2.1±0.2 mol% for NO_2-modulated COFs to 8.9±0.1 mol% for Me-modulated COFs **Figure 4.2**, **Section 4.S**). There is no trend from the Hammett parameter to the amount of modulator within the COF, which allows to synthesise COFs with varying functional groups to get comparable materials in terms of their BET surface area, crystallinity, and degree of functionalisation.

To investigate the spatial arrangement of the modulator, X-ray photoelectron spectroscopy (XPS) wide scans have been measured for the F-modulated COF in triplicate at two different spots for each sample (**Figure 4.3**). XPS is a technique to analyse the surface of a sample and it has a high sensitivity for fluorine.[214,215] Based on the F1s signal intensity, the fraction of modulator at the surface of the COF sample is estimated to be 22±8 mol% (**Table 4.1**). As this value is much higher compared to the 5.3±0.6 mol% determined by ^{1}H-NMR digestion of the bulk powder, the modulator is mostly located at the surface.

The diffraction pattern indicates a regular framework formation, which means that a Me_3TFB-BD framework is formed in the bulk, containing modulator units on the outside of the 2D polymeric sheets. This finding is in line with recent literature.[72–76]

Table 4.1: Atomic ratios and modulator concentration as determined by XPS. Two spots on each sample were measured and analysed. The modulator concentration is approximated based on the integration of the wide scan.

COF	Atomic ratios					Modulator concentration
	C1s	N1s	O1s	F1s	Cl2p	[mol%]
F-modulated Me_3TFB-BD	88.8	9.5	1.0	0.7	-	21±9
Cl-modulated Me_3TFB-BD	90.8	8.3	-	-	0.9	24±2

The thermal stability was studied by thermogravimetric analysis (TGA). Me_3TFB-OMeBD started to decompose at 366 °C and all modulated COFs started to decompose between 410-418 °C (**Section 4.S**). The type of functional group of the modulator therefore has no effect on the thermal stability of the COF. All thermal stabilities are comparable to the one of Me_3TFB-BD.[183]

To study the stability in water, all modulated COFs and Me_3TFB-OMeBD were immersed for five days into deionised water and upon re-isolation and drying at 120 °C overnight, the PXRD patterns were recorded again. All COFs could be isolated from the vials used for the water stability test, which allowed re-analysis by PXRD, showing that none of the harvested materials were completely amorphised. Except from Cl-modulated COF and Me_3TFB-OMeBD, all other COFs were found to be stable under the tested conditions, as indicated by the retained PXRD patterns (**Section 4.S**).

To investigate the morphology of the COFs, scanning electron microscopy (SEM) was carried out (**Section 4.S**). The samples do not have spherical particles with a certain particle size distribution, but the COF powder consists of aggregates of different sizes. Me_3TFB-BD and all modulated COFs consist of worm-like cylinders grown together in an irregular fashion. The diameter of the cylinders is in the range of a few hundred nanometres while their length is in the micrometre regime. In the

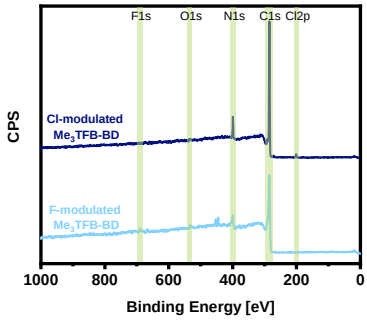

Figure 4.3: XPS survey scan of Cl-modulated and F-modulated COFs.

case of OMe-modulated COF, the porous surface of those cylinders was observed (**Section 4.S**). Me_3TFB-OMeBD shows a fluffy morphology as also observed for other benzidine-based COFs.[216]

4.3.2 Gas adsorption studies

In order to determine whether the modulated COFs are promising candidates for gas separation applications, N_2 and CO_2 sorption measurements have been conducted at 273 K and 295 K (**Section 4.S**). While the CF_3-modulated COF was a good example to demonstrate the characterisation, the gas adsorption and IAST selectivity is exemplary discussed based on the OMe-modulated COF. We have chosen the OMe-modulated COF because the directly synthesised Me_3TFB-OMeBD was the only COF that we could obtain for a comparison between the direct, *i.e.* modulator-free, condensation and the modulator approach. The adsorption isotherms at 273 K and 295 K of N_2 and CO_2 of OMe-modulated COF are linear (**Figure 4.4A**). The maximum quantity adsorbed of N_2 at 273 K was 0.14 mmol/g at 1.33 bar and for CO_2 0.84 mmol/g at 1.05 bar. The quantities adsorbed of N_2 and CO_2 for the other modulated COFs can be found in **Section 4.S**. At 273 K, many adsorption isotherms were not well resolved in the low pressure range due to the low adsorption quantities, which were most probably not well resolved anymore due to the accuracy of the pressure transducer. This inaccuracy became even more pronounced in the adsorption isotherms at 295 K. The same OMe-modulated COF adsorbed 0.08 mmol/g of N_2 and 0.64 mmol/g of CO_2 at 1.33 bar and 295 K. These values are significantly lower than those reported for various related systems. For example, for porous imine based networks the quantity of adsorbed CO_2 are reported to be $\sim$1.8-3.3 mmol/g at 273 K, and $\sim$1.2-2.5 mmol/g at 298 K.[171,172] Benzimidazole COFs are reported to have 2.68-3.45 mmol/g CO_2 adsorption at 273 K and 1.82-2.32 mmol/g at 298 K.[217] A carboxylic acid-functionalised imine-linked COF even showed CO_2 adsorptions of 3.95 and 1.73 mmol/g at 273 K and 298 K, respectively.[173] These differences can be rationalised by the relative low number of polarisable groups in our modulated COFs compared to those reported in literature.

These isotherms were then used to calculate the IAST selectivity with our recently developed GraphIAST[218] over pressures from 0.1-1.0 bar and mole fractions ranging from 0.05-0.95. The obtained three dimensional IAST selectivity plots at 273 K and 295 K are shown in **Figure 4.4B** and **Figure 4.4C**. At lower mole fractions or pressures, the selectivity drops below 10. Overall the IAST selectivity is lower compared to existing literature that reports selectivity values between 31 and 100 for imine networks[171,172] and benzimidazole, azine[203] or imine[173] COFs, and Mahato *et al.* studied

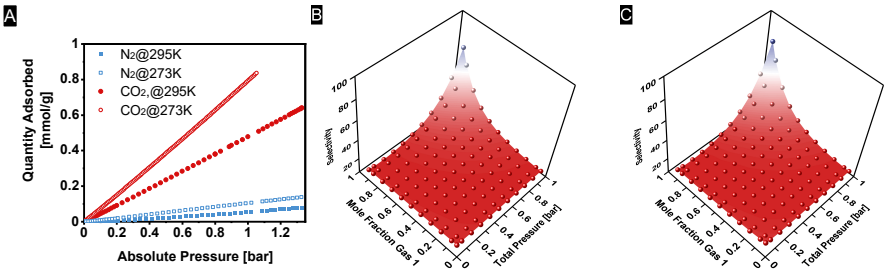

Figure 4.4: N_2 and CO_2 adsorption isotherms at 273 K and 295 K (A), CO_2/N_2 IAST selectivity of OMe-modulated COF at 273 K (B), and CO_2/N_2 IAST selectivity of OMe-modulated COF at 295 K (C).

a covalent triazine framework (CTF) with a CO_2/N_2 selectivity as high as 185.8 at a mole fraction of 0.15 CO_2, 1 bar and 273 K.[168]

The low quantities adsorbed and the low selectivity values of our modulated COFs are not high enough to compensate for the energy and resources needed to synthesise them. Therefore, the modulated COFs are not suitable for gas separation applications. From Figure 4B and Figure 4C, it also becomes apparent that the CO_2/N_2 IAST selectivity significantly increases at higher pressures and higher CO_2 mole fractions. Despite the good selectivity values of 37±23 (mole fraction 0.8 at 1 bar) to 70±50 (mole fraction 0.95 at 1 bar) at 273 K and 40±33 (mole fraction 0.8 at 1 bar) to 75±71 (mole fraction 0.95 at 1 bar) at 295 K, the error margins are currently still very high. Furthermore, to the best of our knowledge, all carbon capture applications require good selectivity values at lower mole fractions.

In industrial processes, the concentration of CO_2 is significantly higher compared to the atmosphere. Flue gas, for example, contains between 10-25 vol% CO_2.[219] Capturing the CO_2 and separate it from the other gases before the flue gas gets diluted by the atmosphere would be more efficient. Within this context a mole fraction 0.15 at 1 bar was chosen to study the performance of our modulated COFs (**Figure 4.5**). The corresponding CO_2/N_2 IAST selectivity values range from 6 to 24 at 273 K and 7 to 20 at 295 K (**Figure 4.5A**). Also the highest value is below selectivity values of channel-wall-functionalised COFs already reported in imine-linked literature,[171–173] and comparable to imine COFs with only backbone functionalisation.[169,170] However, the higher IAST selectivity values for CF_3- and Me-modulated COFs indicate at first a preferred adsorption of CO_2 in these two functional COFs. However, triplicate analysis revealed that the error margins for these selectivity calculations and their underlying isotherms are too large to draw this conclusion. Especially for Me-modulated

COFs, it was difficult to record N_2 isotherms. At 295 K, we were only able to measure an isotherm for one of the three Me-modulated COFs.

The different functional groups on the modulators range from electron-donating to electron-withdrawing groups, which could influence the CO_2/N_2 selectivity. To further analyse any relation between the type of functional group and the CO_2/N_2 selectivity, the CO_2/N_2 IAST selectivity was plotted against the Hammett parameters of the group under investigation (**Section 4.S**). However, no correlation between the Hammett parameter and the CO_2/N_2 IAST selectivity was found. We hypothesise that the low fraction of modulator within the samples is not enough to reveal the influence of electron-donating and electron-withdrawing groups on the CO_2/N_2 IAST selectivity.

To further analyse the data and normalise the IAST selectivity of all modulated COFs, the IAST selectivity of the modulator-free Me_3TFB-BD was also determined at 1.0 bar and a mole fraction of 0.15 (**Figure 4.5B**). This enabled us to investigate whether the modulators have an advantageous effect compared to COFs without functional groups on the resulting IAST selectivity. Based on this normalisation, the higher ratios for CF_3- and Me-modulated COFs are again not significant since the error margins are too large and the other modulated COFs have ratios of $\sim$1, indicating that they have a similar IAST selectivity than the one of Me_3TFB-BD.

Next, the relation between the IAST selectivity and the concentration of modulator within the framework was studied. Since each modulator is incorporated in different amounts, these amounts need to be taken into account. Therefore, we normalised the selectivity by the average of the modulator concentration (**Figure 4.5C**). As the functional groups of the modulators vary from electron-donating to electron-withdrawing, the normalised IAST selectivity was compared in line with the Hammett parameter. The results do not show a trend based on the electronic properties of the modulators and no functional group was outstanding. The interpretation of the data was mainly hampered again by the large error margins, which are related to the accuracy of the pressure transducer. Additionally, we hypothesise that these low quantities of adsorbed gases and the low IAST selectivity values are related to the concentration of modulator within the COF.

Thus, we synthesised and analysed Me_3TFB-OMeBD in triplicate to see whether the small quantities of functional groups in modulated COFs are simply not enough for a clear CO_2/N_2 IAST selectivity. By comparing the IAST selectivity of OMe-modulated COF to Me_3TFB-OMeBD, it can be seen that the IAST selectivity almost doubles when more functional groups are present in the framework

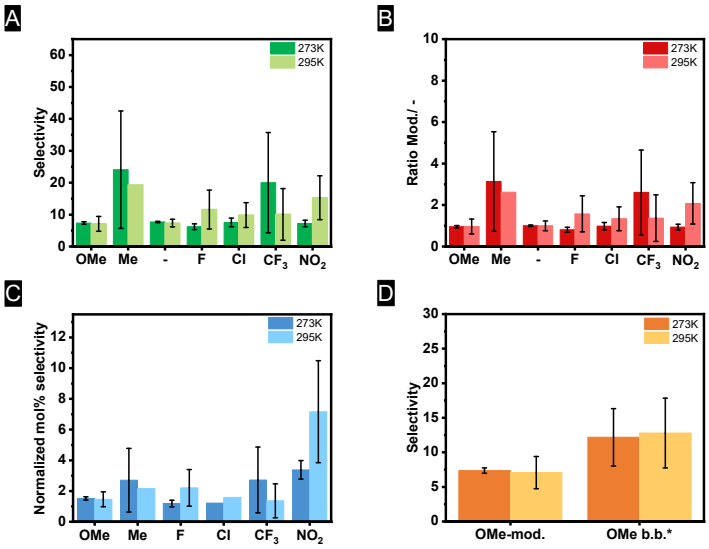

Figure 4.5: CO_2/N_2 IAST selectivity of (A) modulated COFs, normalised to unmodulated Me_3TFB-BD (B), normalised to the incorporated modulator concentration (C), and comparison of CO_2/N_2 IAST selectivity of OMe-modulated COF vs Me_3TFB-OMeBD (D). * Mod. stands for modulator (referred to as OMe-modulator) and b.b. stands for building block, here *o*-dianisidine.

(**Figure 4.5D**). Therefore, more functional groups seem to be advantageous for higher selective COF behaviour. As not all functional building blocks are always compatible with the formation of a crystalline COF, it is of importance to develop synthetic routes for such structural variation, which will enable controlled analysis of the structure-property relationships of COFs in gas separation.

4.4 Conclusions

In conclusion, we have incorporated a series of functionalised modulators in Me_3TFB-BD COF frameworks and studied their performance in CO_2/N_2 gas separation, also in comparison to the pristine Me_3TFB-BD COF. Next to the imine linkage, which can already provide interactions with CO_2, additional functional groups in the framework can tailor the COF towards improved COF-gas interactions. We have employed modulators, which are known to improve COF porosity, and additional functional groups in the *para* position (OMe, Me, F, Cl, CF_3, NO_2) were thought to enhance COF-CO_2 interactions. The higher reactivity of benzidine, compared to that of all modulators, leads to relatively lower modulator embedding than the 30 mol% of modulator present in the reaction mixtures, ranging from 2.1 mol% for the NO_2-modulated COF to 8.9 mol% for the Me-modulated COF. All BET

surface areas remain high (> 1800 m^2/g) and prove the high porosity of the modulated COFs. These modulated COFs adsorbed moderate quantities of CO_2 in gas separation experiments, while the CO_2/N_2 IAST selectivity values are comparable (*S*=6-24 for the different modulators at 273 K) to imine-COFs without channel-wall functionalisation under flue gas conditions. The low number of functional, polarisable groups within the COF hampered displaying any trends of favourable CO_2 interactions with a certain functional group, but for all it was found that an increase in functional group embedding leads to higher CO_2/N_2 IAST selectivity values.

4.S Supporting Information

The Supporting Information is available free of charge on the website of Elsevier:

Or it can be accessed via the following link:
https://drive.google.com/file/d/1OqvAy8YD-X3S7m3N6veYkiQj6fusmRHY/view?usp=sharing

5 Aromatic amine-functionalised covalent organic frameworks (COFs) for CO_2/N_2 separation

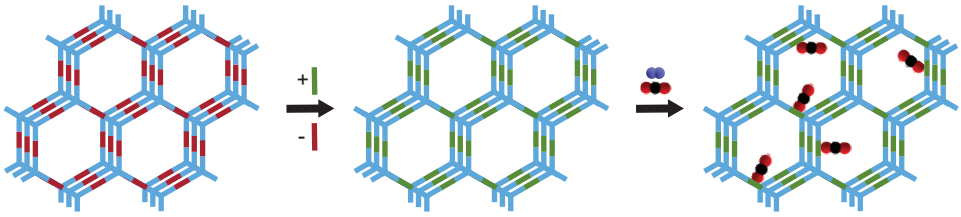

Me_3TFB-BD Me_3TFB-$(NH_2)_2BD$ CO_2-Me_3TFB-$(NH_2)_2BD$

Ellen Dautzenberg, Guanna Li, Louis C. P. M. de Smet

ACS Appl. Mater. Interfaces, **2023**, *15*, 5118-5127.

5.1 Abstract

CO_2 is a prominent example for an exhaust gas, and it is known for its high impact on global warming. Therefore, carbon capture from CO_2 emissions of industrial processes is increasingly important to halt and prevent the disruptive consequences of global warming. Covalent organic frameworks (COFs) as porous nanomaterials have been shown to selectively adsorb CO_2 in high quantities and with high CO_2/N_2 selectivity. Interactions with amines are recognised to selectively adsorb CO_2 and help capture it from exhaust emissions. Herein, a novel COF (Me_3TFB-$(NH_2)_2$BD), which was not accessible via a direct condensation reaction, was synthetised by dynamic linker exchange starting with Me_3TFB-BD. Despite the linker exchange, the porosity of the COF was largely maintained, resulting in a high BET surface area of 1624±89 m^2/g. The CO_2 and N_2 adsorption isotherms at 273 K and 295 K were studied to determine the performance in carbon capture at flue gas conditions. Me_3TFB-$(NH_2)_2$BD adsorbs 1.12±0.26 mmol/g and 0.72±0.07 mmol/g of CO_2 at 1 bar and 273 K and 295 K, respectively. The COF shows a high CO_2/N_2 IAST selectivity under flue gas conditions (273 K: 83±11, 295 K: 47±11). The interaction of the aromatic amine groups with CO_2 is based on physisorption, which is expected to make the regeneration of the material energy efficient.

5.2 Introduction

Porous materials are a class of solid, permanently porous materials with pore sizes of a few to several hundred nanometres. These pores can be classified into macro- (> 50 nm), meso- (2-50 nm) and micropores (<2 nm).[1] In 2005, Yaghi and co-workers[13] reported the first covalent organic framework (COF) as a new type of fully organic porous material. Since then, COFs have gained increasingly more interest and a huge variety of different materials and applications have been reported.[2,19,43] Their permanent porosity and channel-like structure lead to a high surface area, which is of interest for, amongst others, energy storage,[2,3] chemical sensing,[2,7] photocatalysis[2,4,5] and gas separation.[2,8] Usually, two multifunctional building blocks are linked by dynamic covalent chemistry (DCC).[14,15] DCC refers to reversible reactions carried out under thermodynamic reaction conditions, which enables error correction within the reaction, leading to crystalline frameworks with long-range order. Additionally, the exchange of building blocks (linker exchange) in already existing, crystalline frameworks opens the possibility to synthesise COFs with improved crystallinity[18] or make COFs accessible that were not accessible via condensation of the respective building blocks.[16,17] Qian *et al.* reported the first COF to COF linker exchange by replacing 1,4-phenylenediamine (PA) with benzidine (BD) in an imine linked

COF, which yielded an almost complete transformation.[110] The linker-exchange strategy was applied to achieve, amongst others, different COF linkages,[16,102,111,112,220] changes in the pore hierarchy and size by different linker symmetries,[113–115] the transformation of linear polymers into COFs[118,119] or 3D into 2D COFs,[221] and the introduction of functional groups into the framework.[116]

Being a primary greenhouse gas, CO_2 plays an important role in climate change. Strategies to mitigate global warming included the reduction of CO_2 emissions via carbon capture and storage. The separation of CO_2 from N_2 — and the associated CO_2/N_2 selectivity — play a crucial role in such strategies. In more detail, CO_2 capture is industrially performed by amine solutions that react with it.[163,222] However, in this case the CO_2 covalently binds, which means that the regeneration process requires a lot of energy. Alternatively, porous materials as outlined above are promising candidates for carbon capture, because their large surface area enables them to store large quantities of CO_2. To store CO_2, it must first be — ideally selectively — separated from a gas mixture, for example, from the atmosphere or flue gas. For direct air capture, 400 ppm of CO_2 in N_2 is relevant, because this is the current atmospheric CO_2 concentration.[161,162] Coal flue gas contains 10-25 vol% CO_2.[219] Capturing the CO_2 and separating it from the other gases before the flue gas gets diluted by the atmosphere could help to reduce CO_2 emissions into the atmosphere.[161,162] In this context, the porosity of COFs is advantageous to store large quantities of gas.[173,203]

The CO_2/N_2 selectivity can be calculated out of pure component isotherms based on the ideal adsorption solution theory (IAST), which was developed by Myers and Prausnitz.[138] To simulate the adsorption behaviour of gas mixtures, the pure component isotherms must be measured at the same temperature and on the same adsorbent. The basis of IAST is analogous to Raoult's law for vapour-liquid equilibrium.[138] For IAST, the adsorbed phase is assumed to behave like an ideal solution that is in an equilibrium with the bulk adsorptive. It is assumed that the adsorbent is thermodynamically inert, that the Gibbs definition of adsorption applies, and that the surface area is universally accessible and temperature invariant. It must be noted that IAST is only of limited validity for polar adsorptives or mixtures, in which one component strongly adsorbs and the other one weakly. Other limitations are heterogeneous adsorbents and low loadings as they can lead to poor predictions of mixture adsorption. In more detail, for example, low loadings can lead to inaccurate spreading pressures, falsifying the selectivity calculation. If the fitted isotherms do not accurately reproduce the Henry constant for the specific adsorbate, the IAST calculation will predict incorrect selectivity values.[139] Nevertheless, the simplicity of these calculations makes IAST a widely used method for

selectivity determination and provides good results for screening the applicability of porous materials in gas separation. The selectivity S of a binary gas mixture in IAST is defined as the ratio of the mole fractions in the adsorbed state (q) over the mole fractions of the bulk phase (p) of components 1 and 2 (**5.1**).[140]

$$S = \frac{q_1 \times p_2}{q_2 \times p_1} \tag{5.1}$$

Several different porous materials have been investigated for such CO_2/N_2 separations under flue gas conditions, amongst others benzimidazole linked porous organic polymers (POPs). They have been shown to store CO_2 in large quantities (up to 5.19 mmol/g at 273 K and 1 bar) with good CO_2/N_2 selectivity values (63 at 298 K and 1 bar in a 0.1/0.9 mixture).[165,166,217,223–227] Post-synthetic functionalisation can further enhance the selectivity.[166] The well-known amine-CO_2 interaction[163,222] makes the amine functionalised benzidine linker 3,3'-diaminobenzidine ($(NH_2)_2$BD) interesting for CO_2/N_2 separation. For example, this linker was employed to synthesise a benzimidazole-linked COF (IISERP-COF3),[228] a semi crystalline covalent organic polymer,[229] and benzimidazole POPs for CO_2 adsorption.[217,225] Besides benzimidazole linked porous materials, imine linked materials have also been investigated, which often have CO_2/N_2 IAST selectivity values in the range of 10-30 without additional pore-wall functionalisation that would then be present inside the pores.[169,170] To the best of our knowledge, the highest CO_2/N_2 IAST selectivity value so far (185.8 at 273 K for 15% CO_2) was reported by Mahato *et al.* for a covalent triazine framework.[168] Recently, Yaghi and co-workers studied the incorporation of aliphatic amine groups into a tetrahydroquinoline COF.[160] They found high CO_2 adsorptions of 0.304 mmol/g at 0.4 mbar and 25 °C, which are relevant conditions for direct air capture, and that 50% humidity even enhances the CO_2 uptake to 0.393 mmol/g at 298 K and 1 bar. Based on solid-state NMR (ssNMR), they showed that carbamates were formed during the adsorption, therefore confirming chemisorption interactions.

Thus, functional groups are important for the interaction of porous materials with CO_2 to achieve high adsorption quantities and high selectivity values for carbon capture. The nitrogen-CO_2 interaction — especially the one of amine-CO_2 — has shown to be beneficial in terms of adsorption and selectivity, and can be used for the rational design of novel materials for carbon capture. However, the chemical properties, *e.g.* the pKa value, are dependent on the nature of the nitrogen atom. Aliphatic amines, as used by Yaghi and co-workers,[160] can interact more strongly with CO_2 compared to aromatic

amines, leading to chemisorption. Since chemisorption requires higher energies for the regeneration of the material than physisorption, we decided to use aromatic amines, which are directly linked to the COF backbone. In a classical condensation reaction, these additional amine groups are expected to interfere with the framework formation, so we used the dynamic linker-exchange strategy to obtain Me_3TFB-$(NH_2)_2$BD). After the characterisation of the novel COF, we further studied the CO_2/N_2 adsorption and selectivity under flue gas conditions and direct air capture for gas separation.

5.3 Results and discussion

In an attempt to directly synthesise the amine-functionalised COF, 2,4,6-trimethylbenzene-1,3,5-tricarbaldehyde (Me_3TFB) and 3,3'-diaminobenzidine ($(NH_2)_2$BD) were reacted in a 1:4 *v*/*v* mixture of mesitylene:1,4-dioxane. Acetic acid was added as a catalyst for the reaction. The reaction mixture was heated to 70 °C for three days before the obtained precipitate was isolated by Büchner filtration and subjected to the extensive washing procedure from Dichtel and co-workers.[31] Afterwards, the obtained powder was dried at 120 °C overnight in a regular oven before the characterisation was carried out. The results of Fourier-transform IR spectroscopy (FT-IR), Powder X-ray diffraction (PXRD) and N_2 sorption analysis indicate the formation of an amorphous polymer without crystallinity and porosity (**Section 6.S**).

Then, the known Me_3TFB-BD COF was synthesised by condensation of Me_3TFB and benzidine (BD) according to a previously published procedure.[183] Afterwards, Me_3TFB-BD was dispersed in a 1:4 *v*/*v* mixture of mesitylene:1,4-dioxane together with acetic acid and water to achieve an equilibrium between formed and broken imine bonds. Additionally, $(NH_2)_2$BD was added, which can exchange with benzidine (**Scheme 5.1**). The reaction was carried out at 70 °C for three days, before the same work-up procedure as before was applied. Afterwards, the obtained powder was again dried at 120 °C overnight in a regular oven. Upon the linker-exchange reaction, the colour of the COF changed from light yellow to brown. The COF synthesis was repeated two more times to achieve independent triplicate analysis during characterisation of the material's properties. The COF synthesis was carried out at a 400 mg (2 mmol) scale of Me_3TFB and the linker exchange was carried out with up to 200 mg of pristine COF.

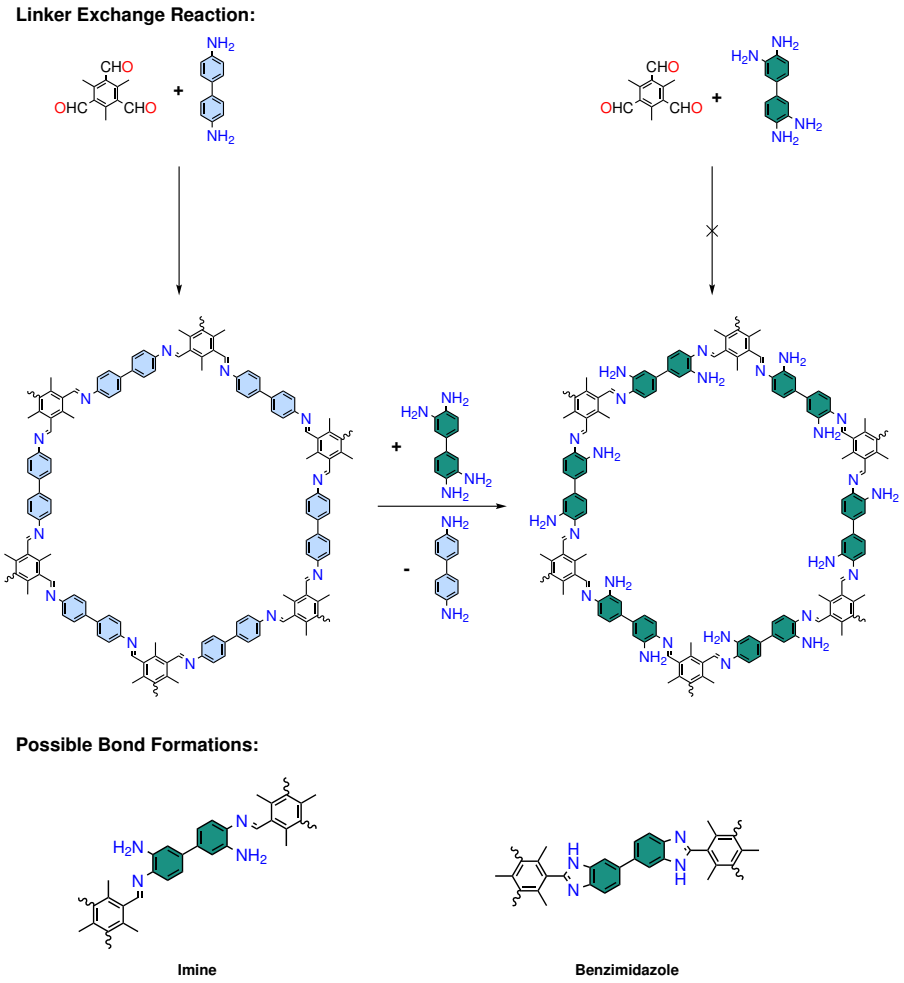

Scheme 5.1: Schematic overview of the Me_3TFB-BD COF reaction and the following linker-exchange with $(NH_2)_2$BD to Me_3TFB-$(NH_2)_2$BD (top). The direct condensation from the building blocks failed (top right). Here, the idealised structures are depicted. In theory two different bonds could be formed: imine bonds with primary amine substituents (bottom left) or benzimidazole bonds (bottom right).

Theoretically, the linker-exchange reaction can lead to two different bond formations, namely imine bonds with unreacted primary amines as *ortho* substituents or benzimidazole bonds (**Scheme 5.1**). Both bond formations are reported for porous materials.[223,228] Here, we thoroughly characterised the COF by ssNMR and FT-IR to determine which bond(s) has/have been formed.

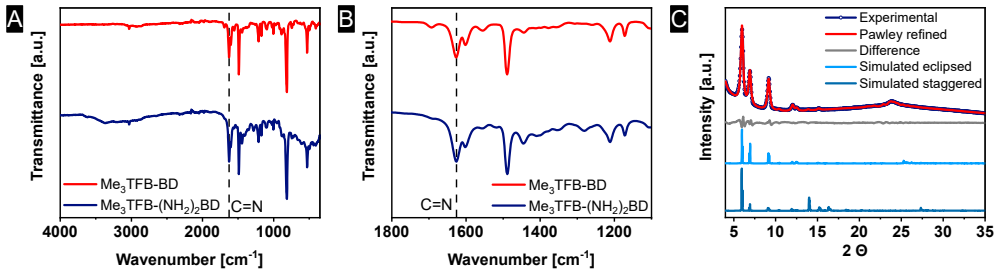

Figure 5.1: FT-IR spectra of Me_3TFB-$(NH_2)_2$BD and Me_3TFB-BD . The C=N stretching band at 1626 cm^{-1} and the N-H stretching band between 3600-3000 cm^{-1} indicate the formation of imine bonds and primary amines (A). Zoom-in into the relevant wavenumbers for C=O and C=N stretches. No leftover C=O stretching bands are visible, indicating the complete conversion of aldehydes into imine bonds (B). PXRD pattern of Me_3TFB-$(NH_2)_2$BD, including Pawley refinement, the difference between the experimental and Pawley-refined pattern, and simulated eclipsed and staggered PXRD patterns (C).

To study the linker-exchange, the FT-IR spectrum of Me_3TFB-$(NH_2)_2$BD was measured and compared to the one of Me_3TFB-BD. In short, the C=N imine band at 1627 cm^{-1} indicates the formation of imine bonds (**Figure 5.1A + B and Section 6.S**). A broad band is visible between 3600-3000 cm^{-1}, which can be assigned to the N-H stretch, confirming the linker exchange. The band at 1693 cm^{-1}, which can be assigned to C=O stretching, is significantly smaller, indicating a low amount of aldehyde groups likely present only at the periphery of the 2D sheets.[60,64,65] However, FT-IR cannot be used to unambiguously assign the bond formation, because the respective bands (imine: 1627 cm^{-1}, benzimidazole: 1610-1625 cm^{-1})[183,223,226] are too close to each other.

The PXRD patterns of Me_3TFB-$(NH_2)_2$BD display several diffraction peaks, which are clearly baseline separated from each other at 3.5°, 6.0°, 6.9°, 9.2°, 12.0°, 12.5°, 15.2°, and a broad peak at 24° (**Figure 5.1C**). The peak at 3.5° could only be detected with a special low-angle measurement (**Section 6.S**). Pawley refinement was performed in triplicate (**Section 6.S**), using the space group *P6/m*, which corresponds to a hexagonal, eclipsed stacking structure. The refined unit cell dimensions are *a*=29.58±0.05 Å and *c*=3.75±0.08 Å with R_{wp}=3.44±0.46% and R_{wp}=2.31±0.26%. The unit cell dimensions are close to those of Me_3TFB-BD COF.

To obtain insight in the stacking of the COF sheets, the structures of two extreme models referred to as “eclipsed” and “staggered” were optimised using DFT. The DFT optimisation was performed by using the Vienna ab initio simulation package (VASP); further details can be found in **Section 6.S**. Next, the PXRD diffractograms were modelled for both computed structures. The simulated PXRD diffractions of the eclipsed pattern (**Section 6.S**) match well with the experimental PXRD result,

indicating an eclipsed stacking conformation for Me_3TFB-$(NH_2)_2$BD (**Figure 5.1C**). The deviation between the computed unit cell dimensions and the Pawley-refined values is mostly below 5%, except for the interlayer distance *c*, which deviates by 6.5%. This is within the expected accuracy of the DFT calculations, further supporting the formation of eclipsed COFs.[230]

These PXRD results confirm the formation of a crystalline Me_3TFB-$(NH_2)_2$BD COF, which could not be obtained via the classical one-step condensation reaction. Thereby, the linker-exchange strategy provides a powerful tool to obtain previously inaccessible COFs with high crystallinity even if the functional group on the linker molecule can interfere with the bond formation.

To unambiguously assign the linkage, ^{13}C cross polarisation magic angle spinning solid-state NMR (^{13}C CPMAS ssNMR) was conducted. The spectrum of the newly obtained Me_3TFB-$(NH_2)_2$BD sample as well as its CP build-up curve were measured (**Section 6.S**). In comparison with spectra of the small model compound 2-phenylbenzimidazole (**Section 6.S**) and Me_3TFB-BD,[213] the linkage was found to consist of imine bonds (**Figure 5.2**). In more detail, the chemical shift of the benzimidazole carbon is at 152 ppm and the shift of the imine carbon at 162 ppm (**Figure 5.2A**). The ssNMR spectrum of Me_3TFB-$(NH_2)_2$BD shows a signal at 162 ppm, clearly indicating imine bond formation. Additionally, the CP build-up curve of the imine COF (Me_3TFB-BD) matches with the CP build-up curve of Me_3TFB-$(NH_2)_2$BD, while 2-phenylbenzimidazole shows a significant slower build-up (**Figure 5.2B**). This was expected, because a benzimidazole carbon atom is not directly bound to a proton, slowing the CP build-up down. Compared to the ssNMR spectrum of Me_3TFB-BD, the additional signal at 142 ppm appears due to the amine substituent on the benzidine, which shifts the signal downfield. The presence of the signals at 142 ppm (C-NH_2) as well as 120 ppm (C-H), indicates the formation of a partly exchanged material.

Digestion ^{1}H-NMR was attempted, but the COF was too stable to be completely broken down to monomers. In NMR digestion, it is aimed to depolymerise a material. Here, the COF is was attempted to depolymerised into its monomers by using DCl in D_2O in deuterated DMSO-d_6, before analysing the resulting solution by ^{1}H-NMR. Compared to Me_3TFB-BD, which could be digested under the same conditions,[231] no clear solution of digested Me_3TFB-$(NH_2)_2$BD could be obtained, but a dispersion was obtained. Thus, the post-synthetic linker exchange seems to enhance the chemical stability in acidic media. To further support this, Me_3TFB-$(NH_2)_2$BD was immersed in 1 M of HCl for five days and upon re-isolation and drying at 120 °C overnight, the PXRD pattern was recorded again. The COF could be isolated from the vial used for the stability test, showing that the material was not

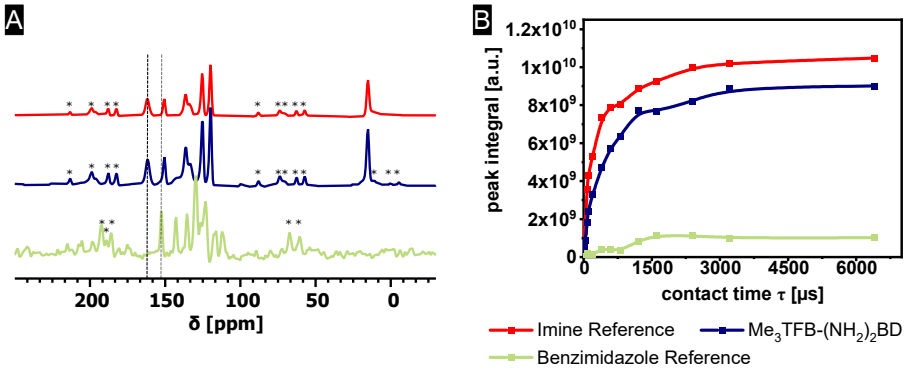

Figure 5.2: ^{13}C CPMAS ssNMR spectra of Me_3TFB-BD (red) as a reference imine COF, 2-phenylbenzimidazole (green) as benzimidazole model compound and Me_3TFB-$(NH_2)_2$BD (blue) at 11 kHz spinning frequency at 3.2 ms CP contact time (A). CP build up curves of the respective samples(B). Spinning side bands are denoted with an asterisk.

completely amorphised. The disappearance of the PXRD diffractions indicates that the crystallinity was not retained (**Section 6.S**). Therefore, Me_3TFB-$(NH_2)_2$BD shows an enhanced acid stability over Me_3TFB-BD, but cannot yet be considered as stable under these conditions.

The thermal stability was investigated using thermogravimetric analysis (TGA). The threshold for thermal stability was determined at the position where the COF lost maximum 5% of its initial weight. Me_3TFB-$(NH_2)_2$BD COF shows an excellent thermal stability up to 438 °C (**Section 6.S**).

As a next step, N_2 sorption measurements were carried out to determine the BET surface area. All three samples of Me_3TFB-$(NH_2)_2$BD show almost identical adsorption-desorption isotherms, confirming the good repeatability of the synthesis (**Figure 5.3A**). The isotherm can be classified as a type IVb isotherm. The large uptake of N_2 below $p/p^0 < 0.1$ indicates the microporosity of the sample even if the pore size distribution — as determined by an HS-2D-NLDFT model — is slightly exceeding the definition of micropores with 2.7 nm (**Figure 5.3B**). The fit of the HS-2D-NLDFT model can be found in **Section 6.S**. The average BET surface area was calculated using the Rouquerol criteria[127] to apply the BET theory to microporous materials. On average a BET surface area of 1624 ± 89 m^2/g was found (**Section 6.S**). The pore volume at $p/p^0 = 0.95$ was measured to be 0.90 ± 0.05 cm^3/g.

To study whether Me_3TFB-$(NH_2)_2$BD can potentially be used in CO_2 capture and storage, N_2 and CO_2 sorption experiments at 273 K and 295 K have been conducted (**Figure 5.4A**). The underlying data for each of the three experiments that compose this data set can be found in **Section 6.S**. The aromatic amine groups on the $(NH_2)_2$BD linker are expected to act as potential adsorption sides for

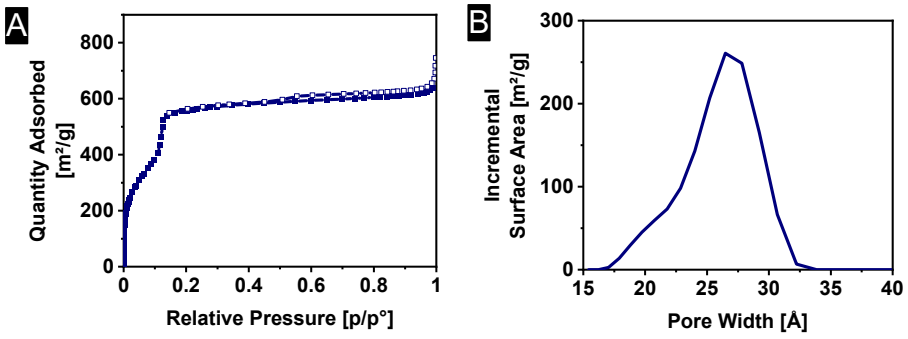

Figure 5.3: N_2 sorption isotherm of Me_3TFB-$(NH_2)_2$BD. Filled symbols represent the adsorption branch; empty symbols represent the desorption branch (A) and their respective pore size distributions (B).

CO_2, which should lead to higher adsorption quantities compared to the Me_3TFB-BD.[231] The N_2 adsorption isotherms of Me_3TFB-$(NH_2)_2$BD are linear, and the CO_2 isotherms show a significant increase at low pressures, and resemble a Langmuir isotherm without reaching the plateau up to 1 bar. At 1 bar, CO_2 adsorption capacities of 1.12±0.26 mmol/g at 273 K and 0.72±0.07 mmol/g at 295 K are found (**Table 5.1**). In comparison, Me_3TFB-BD adsorbs 0.76±0.03 mmol/g at 273 K and 0.41±0.01 mmol CO_2/g at 295 K at 1 bar.[231] The incorporation of aromatic amine groups leads therefore to an increase in CO_2 adsorption of 47±13% at 273 K and 77±10% at 295 K. In comparison to reported porous imine based networks and COFs, which have adsorption capacities of 1.05-4.70 mmol/g at 273 K and 1 bar and 0.70-2.613 mmol/g at 298 K and 1 bar,[170–173] Me_3TFB-$(NH_2)_2$BD has a modest adsorption capacity. As explained in **Section 5.2**, very recently, Yaghi and co-workers published COF-609, which contains aliphatic amine groups.[160] They reported on approximately 2.1 mmol/g CO_2 at 1 bar at 298 K. It is noted that the difference between COF-609 and Me_3TFB-$(NH_2)_2$BD is not only the type of amine, *i.e.*, aliphatic vs aromatic, but also the number of primary and secondary amine groups that can interact with CO_2. COF-609 consists of two primary, two secondary and one tertiary amine per repeating unit, while Me_3TFB-$(NH_2)_2$BD contains only two aromatic amine groups per repeating unit assuming a 100% conversion during linker-exchange. These differences are believed to contribute to the differences in CO_2 adsorption. Furthermore, Yaghi's COF-609 contains additional triazine moieties that can contribute to CO_2 adsorption[168] and their aliphatic amines form carbamates with CO_2, leading to chemisorbed gas. Chemisorption interactions, which cover covalent bond formation, are energetically stronger than physisorption interactions, which are mainly based on Van der Waals interactions.[1]

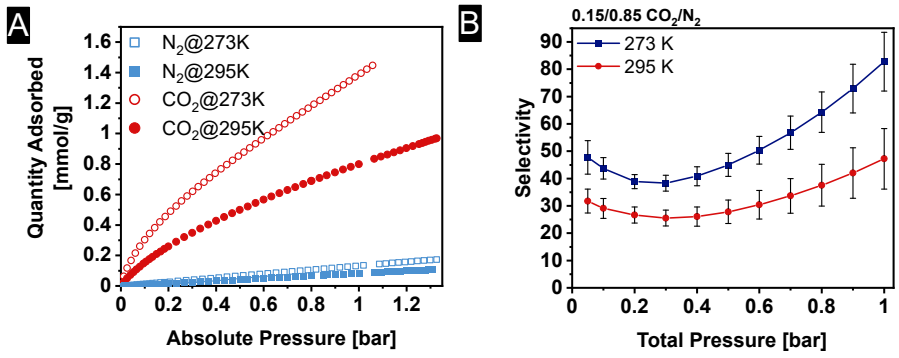

Figure 5.4: Adsorption isotherms of CO_2 and N_2 at 273 K and 295 K (A). IAST selectivity between 0.05-1 bar of a 0.15/0.85 CO_2/N_2 mixture (B).

Moreover, the quantity of adsorbed N_2 at 1 bar was measured to be 0.12±0.02 mmol/g at 273 K and 0.07±0.02 mmol/g at 295 K and thus much lower compared to CO_2 adsorption. For direct air capture, CO_2 adsorption at 0.04 mbar is relevant. Since the measured CO_2 isotherm is not recorded at such low pressures, the first data point at approximately 4 mbar was used to evaluate the material for direct air capture applications. At 4 mbar, Me_3TFB-$(NH_2)_2$BD adsorbed 0.0222±0.0004 mmol/g CO_2 at 273 K, which is less than the values reported by Das *et al.* (∼0.3 mmol/g at 273 K and 4 mbar).[172] Moreover, with 0.304 mmol/g at 273 K at an even lower partial pressure of 0.4 mbar, Yaghi and co-workers reported a higher adsorption capacity.[160] This shows that the material is not suitable for direct air capture.

Therefore, we looked into the adsorption capacity at 150 mbar, since this is relevant at coal flue gas conditions. At this pressure, the quantity of adsorbed CO_2 was measured to be 0.342±0.046 mmol/g at 273 K and 0.183±0.025 mmol/g at 295 K, respectively (**Table 5.1**). The quantities of adsorbed N_2 are 0.016±0.003 mmol/g at 150 mbar and 273 K and 0.009±0.002 mmol/g at 295 K and 150 mbar. In comparison with literature, the CO_2 adsorption capacity at 150 mbar is lower than the capacity of already reported imine-based porous polymers (0.8-1.36 mmol/g at 273 K and 0.4-0.9 mmol/g at 295 K).[170–173]

To study the interaction involved in Me_3TFB-$(NH_2)_2$BD, the reversibility of CO_2 adsorption was investigated over five adsorption-desorption cycles (**Section 6.S**). From the adsorption-desorption isotherm, it can be seen that the desorption occurred without hysteresis, except for the first run, indicating the reversibility of the isotherm. It was also shown that the adsorption-desorption cycles at

Table 5.1: Quantities of N_2 and CO_2 adsorption at different temperatures and pressures and the calculated IAST selectivity values.

COF	Pressure [bar]	Temperature [K]	Quantity adsorbed N_2 [mmol/g]	Quantity adsorbed CO_2 [mmol/g]	IAST Selectivity CO_2/N_2 0.15/0.85
Me_3TFB-$(NH_2)_2$BD	1 bar	273 K	0.12±0.02	1.12±0.26	83±11
		295 K	0.07±0.02	0.72±0.07	47±11
	150 mbar	273 K	0.016±0.003	0.342±0.046	-
		295 K	0.009±0.002	0.183±0.025	-
	4 mbar*	273 K	0.001±0.000	0.022±0.000	-
		295 K	0.001±0.000	0.007±0.001	-
Me_3TFB-BD**	1 bar	273 K	0.10±0.01	0.76±0.03	7.7±0.2
		295	0.05±0.00	0.41±0.01	7.4±1.2

* Data point closest to a partial pressure of CO_2 (0.4 mbar) for DAC.

** Data used from previous published work to facilitate a comparison.[231]

273 K have a comparable adsorption (1.4 mmol/g vs 1.3 mmol/g at 1 bar) during the first adsorption cycle compared to the other four cycles, which further supports the reversibility of adsorption. The reversibility of the adsorption-desorption isotherm is also given at 295 K (**Section 6.S**). To further study the COF-CO_2 interaction, the COF was subjected to CO_2 adsorption at 273 K. Without any additional treatment, the sample was then measured by FT-IR and ssNMR immediately afterwards to probe the formation of carbamates, which would indicate chemisorption of CO_2. Both the FT-IR spectrum and ssNMR spectrum (**Section 6.S**) did not show any difference compared to those of the as-synthesised Me_3TFB-$(NH_2)_2$BD and no carbamate bands or signals could be observed. In comparison to Yaghi's COF-609 where the aliphatic amines groups were found to chemisorb CO_2, the adsorption-desorption cycles and the lack of carbamate signals in the FT-IR and NMR spectra of Me_3TFB-$(NH_2)_2$BD after exposure to CO_2 indicate that the CO_2-COF interaction is based on physisorption, and that the CO_2 adsorption-desorption is reversible. In terms of applications, these results suggest that the material can be regenerated at relatively low cost in an energy-efficient way.

The isotherms were used to calculate the IAST selectivity with our recently developed GraphIAST[218] software at coal flue gas conditions. First, the entire selectivity value range was scanned between 0.05-1.0 bar and mole fractions ranging from 0.05-0.95. The mole fraction of 0.15 CO_2/N_2 was used to investigate the CO_2/N_2 IAST selectivity for flue gas separation. IAST selectivity values of 83±11 at 273 K and 47±11 at 295 K were found in a mixture of 0.15/0.85 CO_2/N_2 at 1 bar (**Table 5.1**).

These high selectivity values display that the approach taken in the design of Me_3TFB-$(NH_2)_2$BD is promising for gas separation applications. Here, it is useful to compare our results with that of recent literature. Das *et al.* studied an imine-based network and determined IAST CO_2/N_2 selectivities of 211 at 273 K and 100 at 298 K.[172] These values were validated by breakthrough experiments, leading to a selectivity of 125 at 298 K, which is even higher than predicted by IAST. The quantities of adsorbed CO_2 are 3.3 mmol/g at 273 K, and 2.4 mmol/g at 298 K. Another porous imine based network, studied by Popp *et al.*, adsorbs 1.8 mmol/g and 1.2 mmol/g CO_2 at 273 K and 298 K, respectively with an IAST selectivity value of 31 at 298 K and 1 bar.[171] Huang *et al.* synthesised an imine-linked porphyrin COF, of which the channel walls were post-synthetically functionalised with carboxyl groups to enhance selectivity.[173] The CO_2 adsorption was reported to be 3.95 and 1.73 mmol/g at 273 K and 298 K, respectively, and the CO_2/N_2 selectivity of a 15% mixture of CO_2/N_2 at 298 K and 1 bar was 77, an enhancement of more than a factor of nine compared to the non-functionalised pristine COF. These examples show that channel-wall postfunctionalisation[169,170] can significantly enhance the CO_2/N_2 selectivity, while our current approach using post-functionalisation via linker exchange can lead to comparably good results. The adsorbed quantities significantly increased from Me_3TFB-BD to Me_3TFB-$(NH_2)_2$BD not only indicating the successful linker exchange, but also showing that the aromatic amine groups of the $(NH_2)_2$BD linker interacts with CO_2.

5.4 Conclusions

A novel COF Me_3TFB-$(NH_2)_2$BD, which is not accessible with classical direct condensation reactions, was synthesised by the linker-exchange strategy in a facile two-step synthesis. The linkage could unambiguously be assigned to imine bonds based on the chemical shift and CP build-up curves in ssNMR, and the crystallinity and porosity were confirmed by PXRD and physisorption experiments. Upon the exchange of Me_3TFB-BD to Me_3TFB-$(NH_2)_2$BD, a BET surface area of 162 ± 89 m^2/g was found, which shows that the linker-exchange maintains most of the COF porosity. Furthermore, Me_3TFB-$(NH_2)_2$BD was studied for gas separation applications of CO_2 and N_2. We found modest CO_2 adsorption quantities and high CO_2/N_2 selectivity values based on IAST calculations under coal flue gas conditions (83 ± 11 at 273 K and 1 bar and 47 ± 11 at 295 K and 1 bar). The enhanced CO_2 uptake in comparison with the pristine Me_3TFB-BD COF is caused by the aromatic amine groups of the COF linker. While aliphatic amine groups bind CO_2 by chemisorption as shown by Yaghi and co-workers, the adsorption-desorption cycles of Me_3TFB-$(NH_2)_2$BD have shown that

the interaction of aromatic amine groups with CO_2 are based on physisorption. As physisorption is mainly based on weak Van der Waals interactions, we therefore anticipate that the regeneration of Me_3TFB-$(NH_2)_2$BD would require less energy, making it an interesting candidate for carbon capture.

5.S Supporting Information

The Supporting Information is available free of charge on the website of the American Chemical Society:

Or it can be accessed via the following link:
https://drive.google.com/file/d/1NSgTmUyHc5EyAj_jliV1mHlUd0kfZL9Z/view?usp=sharing

6 GraphIAST: A graphical user interface software for ideal adsorption solution theory (IAST) calculations

Ellen Dautzenberg*, Simon van Hurne*, Maarten M. J. Smulders, Louis C. P. M. de Smet

Comput. Phys. Commun, **2022**, *280*, 108494.

* contributed equally

6.1 Abstract

Industrial exhaust gasses have a strong environmental impact, including on global warming. Carbon dioxide (CO_2) is a prominent example of such an exhaust gas. Therefore, CO_2 capture and storage in industrial processes is becoming increasingly important. Preferably, these emitted gasses are separated before their release into the environment. Such applications require selective gas separation to isolate the harmful gasses or to allow recycling of industrially relevant gasses. Porous materials are promising candidates to achieve gas separation, since their large surface area enables them to adsorb large quantities while their selectivity can be tuned by controlling their chemical composition. Modelling adsorption behaviour and calculating corresponding selectivities in multicomponent gas mixtures of such porous materials, which is essential to quantify their gas separation performance, can be achieved through the ideal adsorption solution theory (IAST), which can be challenging to perform. The current available softwares for IAST calculations demand programming knowledge that not every materials scientist has or has access to, limiting the development of new porous materials for gas separation purposes. In this paper, we present a simple, user-friendly program for IAST loading and selectivity predictions for binary gas mixtures based on the Python module pyIAST. We have developed a graphical user interface resembling commonly known software and made three-dimensional selectivity predictions easily accessible within just a few clicks. The input and output data structure relies on the widely used *.csv format and isotherm data can be fitted with various established models. Therefore, our software provides a platform for IAST calculations for non-programming researchers, which is expected to enable more materials scientists to screen their porous materials for desired gas separation properties.

6.2 Program Summary

Program Title: GraphIAST

CPC Library link to program files: https://doi.org/10.17632/ytc64xwcr5.1

Developer's repository link: https://github.com/ORC-WUR/GraphIAST

Licensing provisions: MIT

Distribution format: exe

Programming language: Python

Operation systems: Linux, Windows

External routines: Math, Matplotlib, Numpy, Pandas, PIL, pyIAST, Tkinter

Supplementary material: User Manual, Case studies

Nature of problem: Using IAST to predict the selectivity in binary gas mixtures based on their pure component isotherms.

Solution method: Employing the pyIAST package and incorporating this into a GUI surrounding for a facilitated use of IAST analysis. Additionally, the selectivity predictions have been extended to multiple selectivities at different mole fractions and pressures.

6.3 Introduction

Many industrial processes lead to exhaust gasses, which can have an environmental impact by either being harmful/toxic to the environment or by contributing to global warming. Carbon dioxide (CO_2), for example, is known for its contribution to global warming. Based on the global industrial emission of carbon dioxide of approximately 20 Gt/yr in 2020,[232] it is becoming increasingly important to decrease the CO_2 emissions and prevent the disruptive consequences of global warming. In more detail, the atmospheric carbon dioxide level has risen by approximately 50% in the last 250 years to a current level of 0.042 vol% in 2021, which is about 40% higher than the previously highest reported atmospheric CO_2 concentration 300.000 years ago.[161,162] The concentration of CO_2 in flue gas is significantly higher (10-25 vol%) than the atmospheric concentration, which makes it advantageous to remove carbon dioxide from flue gas before it actually enters the atmosphere. Such gas separation is called carbon capture and storage (CCS).[163] Based on the Linde process, which involves liquifying gasses, cryogenic carbon dioxide capture has been studied, which is attractive for liquified CO_2, since it gets more cost effective at higher concentrations.[163] Alternatively, membrane technology has reached the demonstration scale, which refers to the last scale-up step before commercial use.

Membranes need to have high-temperature tolerance and selectivity in order to separate gasses.[163] Already industrially used are amine solutions that react with carbon dioxide and therefore removing it from the gas mixture. However, in this case, the CO_2 becomes covalently bound to the amines, which means the regeneration process requires a lot of energy.[163,222] Alternatively, porous solids have been studied for gas separation and gas capture.[140,233,234] The large surface area of porous materials, such as zeolites, activated carbon, metal organic frameworks (MOFs) or covalent organic frameworks (COFs), allows for high physisorbed gas quantities, which are beneficial for gas separation applications. Additionally, physisorption relies on adsorption by weaker forces and needs thus less energy for the regeneration of the porous solid.[163]

As the term gas separation already states, it is important to have a selective adsorption of one gas over another, in order to achieve the desired separation. In fact, the development of new, more selective, porous materials for carbon dioxide capturing crucially depends on the ability to determine this gas selectivity. Measuring mixed-gas adsorption experimentally requires specialised and expensive equipment.[194] The measuring principle relies on dynamic methods, in which the gas mixtures are constantly flowing over the sample and so-called breakthrough curves are recorded to determine, how much of which gas is adsorbed. In contrast, measuring the adsorption isotherm of a pure component is far more straightforward and is possible with common physisorption instruments. Physisorption instruments measure the quantity of gas adsorbed at each pressure, leading to isotherms of the pure gasses.

In order to determine gas separation selectivities out of pure component isotherms, the so-called ideal adsorption solution theory (IAST) was developed by Myers and Prausnitz.[138] The basis of IAST is analogous to Raoult's law.[138] Both theories assume a linear dependence between gas pressure and the mole fraction of the gaseous component; in case of Raoult's law the vapour pressure and in IAST the equilibrium gas-phase pressure.[138] The simplicity of these calculations makes IAST a widely used method for selectivity determination in gas separation. In order to simulate the adsorption behaviour of gas mixtures, the pure component isotherms have to be measured at the same temperature and on the same adsorbent. The selectivity of a binary gas mixture in IAST is then defined as the ratio of the mole fractions in the adsorbed state (q) over the mole fractions of the bulk phase (p) of components 1 and 2 (**Equation 6.1**).[140]

$$S = \frac{q_1/q_2}{p_1/p_2} \tag{6.1}$$

The validity of IAST has been studied by comparing the IAST results with grand canonical Monte Carlo (GCMC) simulations for metal organic frameworks (MOFs).[195] It was shown that the deviation between IAST and GCMC simulations was usually less than 10%. This shows that, compared to more computational-intensive GCMC simulations, IAST is a fast and reliable tool to predict gas adsorption selectivities of MOFs. Despite the development of more accurate GCMC simulations over the past decades, the obtained selectivity predictions, as well as experimentally obtained data, are still comparable to IAST predictions.[196–202] Therefore, IAST is still the benchmark theory for mixed adsorption studies, because of its simplicity and general applicability. However, researchers still need to rely on programming skills when working on multicomponent adsorption studies.[139]

6.4 State of the Art

There are several softwares for the analysis of pure component isotherms with the ideal adsorption solution theory reported in literature that have different levels of flexibility and accessibility. Simon *et al.* developed a powerful open source python package, called pyIAST, which allows one to fit a set of pure component isotherms, which can be more than two, by several different thermodynamic models or by numerical quadrature.[235] These fitted isotherms can then be used for IAST or reversed IAST calculations. The result of the calculations can be used to determine the selectivity of one gas being adsorbed over the other gasses. Two- (2D) or three-dimensional (3D) selectivity data are obtainable. However, users have to write a python script for the IAST calculations themselves based on the offered python package. In more detail, this requires users to first write an entire script to analyze the data, which has to be continuously adapted for future experiments or different parameters. Notably, programming knowledge is required for 2D or 3D selectivity data.

Iacomi *et al.* have written the software package pyGAPS to facilitate high-throughput data analysis and data visualisation.[236] In pyGAPS many types of common adsorption isotherm analyses (such as BET and Langmuir surface area, *t* and a_s plots, pore size distribution analysis, isosteric enthalpy calculations and IAST calculations) are combined to allow fast data analysis. For IAST calculation, pyGAPS relies on the pyIAST package and has therefore the same possibilities (arbitrary number of components, 1D/2D/3D selectivity) and limitations as pyIAST. PyGAPS works independently of the

Table 6.1: Overview of selected characteristics of the published softwares for IAST calculations.

Software	GUI	# gas components	default output dimension	ease-of-use
pyIAST	✗	n	1D	∼
pyGAPS	✗	n	1D	∼
IAST++	✓	n	unspecified	✗
GraphIAST	✓	2	3D	✓

data origin and can create plots, which can facilitate the routine data analysis of adsorption isotherms. However, also for pyGAPS, users have to write the script themselves.

Lee *et al.* have developed a graphical user interface (GUI) software (IAST++) for users without any programming experiences, which would help them to analyze their data with the IAST calculation in a straightforward way.[237] The pure component isotherms can again be fitted in the *Modeler* section with various thermodynamic models or pure mathematical function and are plotted directly in the window. After fitting, the *IAST* section can be used for IAST calculations. When operating the software, it is, however, not clear what is calculated in the IAST module and based on which data, with which fits and in which units. Unfortunately, the only available user manual is an instruction video that is recorded on a computer screen in Korean language, making the software less accessible.

Herein, we present a GUI software based on pyIAST to facilitate the prediction of binary gas mixtures for non-programming researchers (**Table 6.1**). Users have control over the data selection, fitting procedure and conditions to predict the selectivity. We have expanded the pyIAST package to calculate the selectivity within a binary mixture for multiple pressures and mole fractions without the need to run the software multiple times. Selectivity predictions are mostly carried out for binary gas mixtures and the need for more gas components is rather small. The then obtained data can be exported into a *.csv file and used to obtain a three-dimensional plot of the selectivity against mole fractions and operational pressures.

6.5 GraphIAST

The most important aspects of a software are its functionality, how much it fulfills the need of a market, and the usability. Usability in software engineering is defined in ISO 9241-11[238] as the degree to which a software can be used by the customers to achieve the desired tasks in an effective

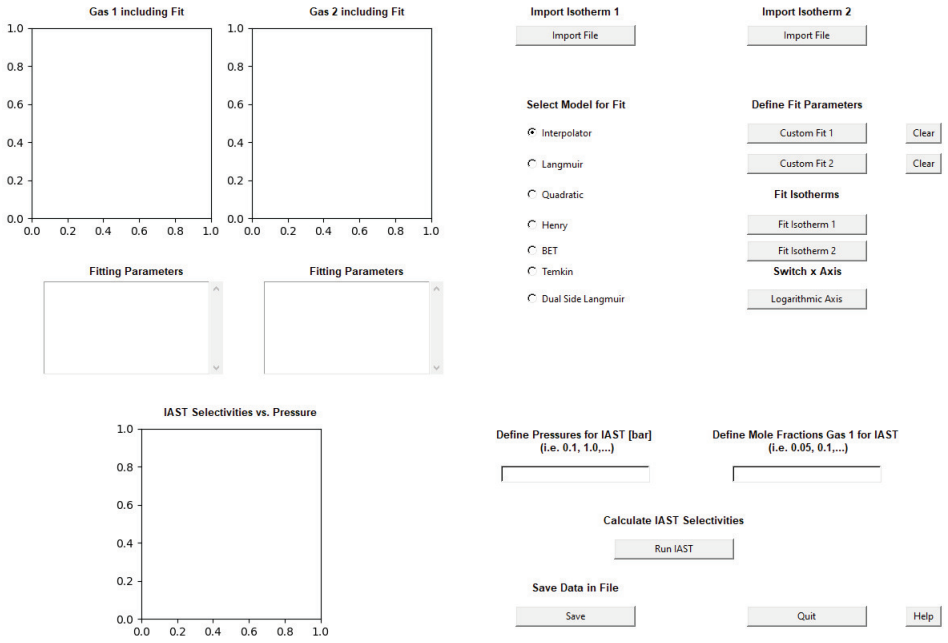

Figure 6.1: The interface users will see when starting the GraphIAST software. The left side visualises the data. The mathematical operations and all conditions can be selected on the right side and applied via the corresponding buttons.

manner while being satisfied with the context of use. At this point GUIs come into play. They enable the users to perform the tasks by seeing a visual interface and by clicking on specific icons instead of console-based programming the desired task. Today, most used software consists of GUIs to enable a wide-spread, effective and easy use.

Therefore, we decided to use the pyIAST package[235] to design a new GUI-based software for IAST predictions with ease-of-use and accessibility in mind. The software is an executable file that works on Windows and the python code can be easily made executable on Linux computers. Our goal is to enable more researchers to perform IAST calculations, by making the need for programming skills to perform these calculations obsolete. The mathematical and computational details for IAST calculations can be found in the documentation of pyIAST,[235] while we here focus on the GUI operation and how we expanded the selectivity calculations. The underlying aim for our software is to be able to fit pure adsorption isotherms with a set of physical models or general mathematical functions and to perform IAST selectivity calculations. For the user interface, we used the *tkinter* package in python. The software can be started in Windows via a double-click on the executable file and in

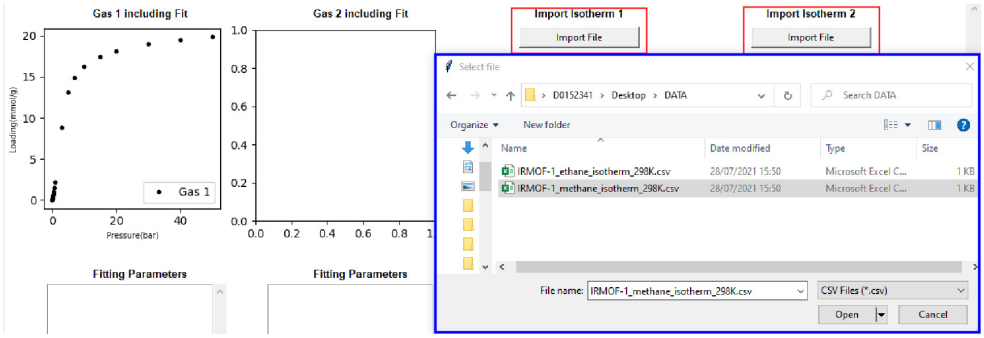

Figure 6.2: Screenshot of a pop-up window (highlighted by the blue box) importing the data into the software, which appears after pressing the buttons, here highlighted by the red boxes.

Linux users have to make the file executable first and then start via the command shell with *python3 ~/PATH/to/GraphIAST.py*. **Figure 6.1** displays the general appearance once our software after it has been started.

We used the case study of Simon *et al.* to demonstrate how GraphIAST is working.[235] In this example, adsorption isotherms of methane and ethane on a MOF were measured at 298 K. In their case study, they already proved that IAST gives valid results by comparing their IAST calculation to GCMC simulations.[235] The same test data can be found in the \test folder of our GitHub repository. It is important to note that the pressures are given in bar and the adsorbed quantities need to be given in mmol/g.

The data is then imported, which can be done by clicking on the *Import file* buttons. Here, it is important to decide which gas should be *Gas 1* and which *Gas 2* as the order will later influence the selectivity parameter. In this case study, ethane is *Gas 1* and methane is *Gas 2*. Even though IAST would allow multi-component isotherm calculations, we focused on binary mixtures for our software, because binary mixtures are usually used as model system. Such model systems are most commonly used to screen for promising gas separation in materials. For the data import, we use the common file explorer that most people know from their operating systems. The imported data will be automatically plotted in the figures on the left top side of the window (**Figure 6.2**).

Next, the data has to be fitted. For this, we included a list of radio buttons with the available models in pyIAST (**Figure 6.3**, green dashed box). The *Interpolator* function solves the fit numerically, while the other options in this list are thermodynamic models for adsorption processes.[235] After selecting

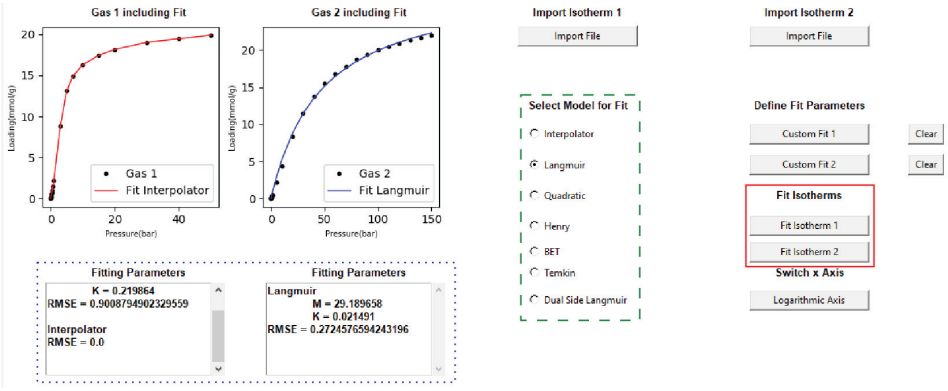

Figure 6.3: Visualisation how the imported data can be fitted.

the desired fit, both isotherms can be fitted individually by both *Fit Isotherm* buttons (**Figure 6.3**, red box). The two buttons ensure that both plots can be fitted with different models, if desired.

If the automated fit does not work, it is possible to define the starting fit parameters for the Residual Sum of Squares optimisation manually by the *Custom Fit* buttons. Those will open new windows in which the values of choice can be entered (**Figure 6.4**) for the specific model that users have selected to fit the isotherm. The field for the parameters for the remaining models can be left empty. With the *Clear* buttons the custom parameters can be deleted so that the software would set initial default parameters for the fit optimisation by itself again.

The custom parameters can also be cleared manually by deleting them in the *Custom Fit* menu. After every fit, the figures on the left side will update to also show the most recent selected fit. For

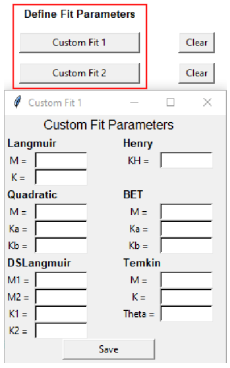

Figure 6.4: Pop-up window with buttons to access the separate windows to enter custom fit values as starting point for the Residual Sum of Squares optimisation.

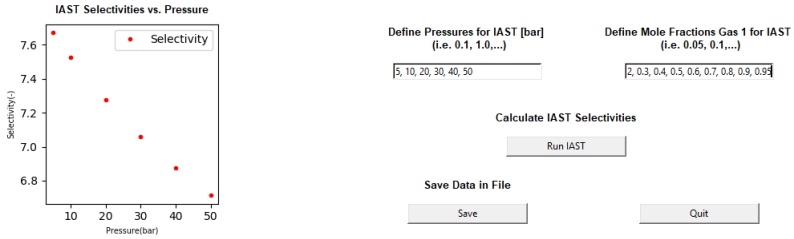

Figure 6.5: Example definition of pressures and mole fractions as input parameters o run the IAST calculations (right) and the resulting selectivity plot for the first mole fraction (left).

every successful fit the obtained fitting parameters as well as the root mean squared error will be displayed below the graphs (**Figure 6.3**, blue dashed box). A new fit does not overwrite the output. The users can scroll through the history of all the fitting done on the pure isotherm in the *Fitting Parameters* box underneath the plot. This way fits can be compared with each other by scrolling through the text output. When GraphIAST is used, it should be realised that IAST is only of limited validity for polar adsorbates or mixtures in which one component adsorbs strongly and the other one weakly. Henry's law covers adsorption at low pressures. If those fitted isotherms do not accurately reproduce the Henry constant for the specific adsorbate, the IAST calculation will predict incorrect selectivities. The button *Logarithmic Axis* switches the scale of the x-axis of the graphs from linear to logarithmic. When the x-axis has been changed to a logarithmic scale the button changes to *Linear Axis* which can be used to change the x-axis back to a linear scale.

In the next step both isotherms were fitted with the Langmuir model. To perform the IAST calculation, users need to define a pressure and a mole fraction at which the selectivity should be calculated (**Figure 6.5**). The original pyIAST package can only calculate the selectivity of one pressure and one mole fraction. However, in our case, a list with several pressures (for example 5, 10, 20, 30, 40, 50) and several mole fractions (for example 0.05, 0.1, 0.2, 0.3, 0.4, 0.5, 0.6, 0.7, 0.8, 0.9, 0.95) that can be freely defined by users (comma separated) and the selectivity of each combination will be calculated. This results in an output file (as shown in **Table 6.2**) from which a three-dimensional selectivity plot can be easily derived (**Figure 6.6**). IAST is limited by the maximum pressure that was measured in the single-component isotherms and the mole fractions have to be in the range between 0 and 1. We have implemented warnings that will prompt the users in case of wrongly entered parameters and data. The calculation can be performed by clicking on the *Run IAST* button.

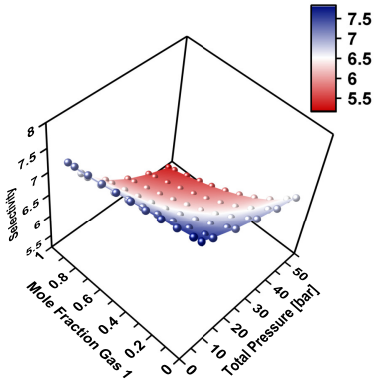

Figure 6.6: Exemplary 3D data plot of selectivity against pressure and mole fraction for the selected case study.

The successful calculation will be indicated by the graph in the bottom left corner. This will show all the selectivity values for the first mole fraction entered. All calculated values and all steps in between (partial pressures, loadings, and selectivities) can be exported and saved in a *.csv or text file (*Save* button).

Table 6.2: Example of the *.csv output of the first 15 lines of an IAST calculation performed using GraphIAST. The software calculates more digits, for readability reasons the output here has been rounded.

Total Pressure [bar]	Mole Fraction Gas 1	Mole Fraction Gas 2	Partial Pressure Gas 1	Partial Pressure Gas 2	Loading Gas 1 [mmol/g]	Loading Gas 2 [mmol/g]	Selectivity Gas 1 / Gas 2
5	0.05	0.95	0.25	4.75	1.05	2.59	7.67
5	0.10	0.90	0.50	4.50	2.01	2.37	7.63
5	0.20	0.80	1.00	4.00	3.72	1.97	7.56
5	0.30	0.70	1.50	3.50	5.19	1.62	7.50
5	0.40	0.60	2.00	3.00	6.48	1.31	7.43
5	0.50	0.50	2.50	2.50	7.61	1.03	7.37
5	0.60	0.40	3.00	2.00	8.61	0.79	7.32
5	0.70	0.30	3.50	1.50	9.51	0.56	7.26
5	0.80	0.20	4.00	1.00	10.32	0.36	7.21
5	0.90	0.10	4.50	0.50	11.04	0.17	7.16
5	0.95	0.05	4.75	0.25	11.38	0.08	7.14
10	0.05	0.95	0.50	9.50	1.82	4.59	7.53
10	0.10	0.90	1.00	9.00	3.39	4.09	7.46
10	0.20	0.80	2.00	8.00	5.97	3.25	7.34
10	0.30	0.70	3.00	7.00	8.00	2.58	7.23

6.6 Conclusions

Here we have presented a GUI software based on the pyIAST package that can calculate gas adsorption loadings and selectivities for binary gas mixtures. GraphIAST allows researchers without programming experience to use IAST calculations for multiple pressures and mole fractions in one go, since no programming is required to run the program. This enables the users to get the correlations of pressure, mole fraction and selectivity. We anticipate that by lowering the required programming skills for IAST calculations, it becomes more accessible for researchers to use IAST gas adsorption predictions in their research, which will spur development of more tailor-made tailor-made porous materials with selective gas separation or more efficient carbon capture.

6.S Supporting Information

The Software is available free of charge on the Github website:

Or it can be accessed via the following link:
https://github.com/ORC-WUR/GraphIAST

7 General discussion and future prospects

7.1 General discussion

The discovery of 2D or 3D covalent organic frameworks (COFs) in 2005 led to the development of a large variety of framework materials, which were explored for many different applications.[2,43] The rational design of COFs for a specific application requires fundamental knowledge on structure-property relationships. The aim of the work described in this thesis is to study the impact of functionalisation on the COF properties and to study their applicability in sensors and CO_2/N_2 separations. It was aimed to explore whether the type and degree of functionalisation would be a handle to tune the COF properties for the specific application, leading to tailor-made materials.

We have chosen imine COFs due to their well-known chemistry and their large diversity of building blocks that are easily commercially accessible or can be synthesised within a few steps. We studied the effect of methyl substituents on the stability of COFs and explored the use of the methylated COFs for acid vapour sensing (**Chapter 2** and **3**). Furthermore, we selected a range of electron-donating and electron-withdrawing substituents, which were attempted to be incorporated into the COF as modulators (**Chapter 4**), via direct condensation (**Chapter 4**) or linker-exchange (**Chapter 5**). The resulting COFs were explored for their use in CO_2/N_2 separation. In the following sections, the respective results will be discussed in a broader context, and future prospects are presented as well.

7.2 Structure-property relationships

Most COFs are synthesised via the solvothermal synthesis method (**Chapter 1.2** and careful reaction optimisation is carried out to obtain high quality COFs.[64,65,123] As this synthetic approach requires special equipment, we have used a facile reflux setup to synthesise all imine-linked COFs that are discussed in this thesis, which highlights the wide scope of this approach. These reaction conditions led to highly porous COFs with BET surface areas of up to $\sim$ 2100 m^2/g. Moreover, it was not needed to tune the solvent mixture for each COF. Instead, our reaction optimisations were focussed on the amount of water that is added during the synthesis (**Chapter 3**).[239] Furthermore, we found the work-up and activiation processes to be crucial for obtaining high quality COFs. As such, recent literature on COFs identifies the reduction of porosity and surface area due to pore collapse as one of the main challenges to be met during COF activation.[64,65] Most activation techniques apply vacuum to remove solvent residues from the pores. The surface tension of the solvents, the small pore sizes, and the vacuum lead to high capillary forces that can distort the pores, which leads to a decrease

in porosity and crystallinity. Moreover, in the early stages of this project, we found that TFB-PA, an imine COF synthesised from 1,3,5-triformylbenzene (TFB) and 1,4-phenylenediamine (PA), lost more than half of its porosity over time on a bench, as shown by a decrease of Brunauer-Emmett-Teller (BET) surface area. Therefore, we decided to study the activation and bench stability of COFs and to investigate whether the presence of methyl substituents on the building blocks enhances the stability. We have chosen methyl substituents due to the commercial availability of methylated amine building blocks and the straightforward synthesis of Me_3TFB. Furthermore, isopropyl substituents were found to enhance the chemical stability of two 3D COFs due to their hydrophobicity.[26] The methyl substituents were expected to act as a smaller alternative to the bulky isopropyl groups. As shown in **Chapter 2** and **3**, the use of Me_3TFB as a node in COF formation enhances the crystallinity and porosity of all COFs with respect to the unmethylated TFB and it reduces pore collapse. The BET surface areas of these COFs were comparable to those activated by supercritical CO_2 drying, an approach that requires specialised equipment. Density functional theory (DFT) calculations revealed that the loss of symmetry in Me_3TFB leads to a smaller rotational barrier of the carbonyl group compared to TFB. This allows a faster incorporation of Me_3TFB into the regular framework with respect to TFB. Additionally, the loss in porosity over four weeks could be overcome by using Me_3TFB as building block. In contrast to this, methylated amine building blocks, here used as a linker, lead to a decrease in porosity (**Chapters 3**), which illustrates the importance of a careful and thorough characterisation of COFs. The position of the functional group is crucial for COF properties. While the loss of symmetry and thus the reduced π-conjugation lead to higher reaction rates during COF synthesis, the methyl groups on the amines induce a higher steric hinderance, which is disadvantageous for COF porosity.

The effect of pore collapse is expected to become more prominent with decreasing pore size, *i.e.*, increasing strength of capillary forces. On the other hand, with smaller pore sizes the rigidity of the framework increases, which would prevent the pores from collapsing. Therefore, we decided to study the impact of the pore size on pore collapse in 2020. In total six different building blocks (**Scheme 7.1**) were used to synthesise six different COFs (TFB-TAPB, TFB-PA, TFPB-TAPB, TFB-BD, TAPB-PDA, TFPB-BD) and the resulting COFs were exposed to two different activation methods (activation in a regular oven or in a vacuum oven).[239]

Our findings suggest that each COF reacts differently to the two applied activation methods, yielding differences in porosity. This means that the activation method must be optimised for each individual COF. Alternatively, supercritical CO_2 drying is reported to yield the best result for activation.[64] With

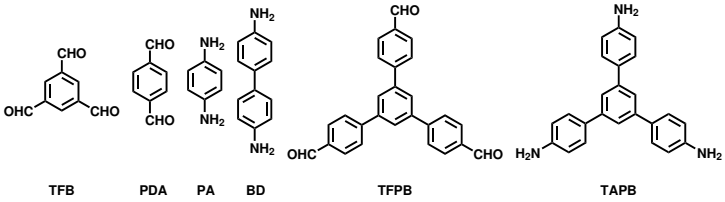

Scheme 7.1: Overview of the building blocks used to synthesise the five COFs for the pore collapse study.

respect to hexane, supercritical CO_2 reduces the capillary forces even more, which is advantageous for maintaining the porosity during activation. However, not every lab has access to the required advanced equipment.

Mid-2022, Zhu *et al.* systematically studied the impact of pore size, pore substituents and pore topology on the activation stability.[240] They synthesised rhombic and hexagonal COFs with varied pore sizes from 0.9-3.3 nm and with different substituents (F, OH, Cl, Br, OMe). The solvent exchange during COF work-up was finished with solvents with different surface tensions (methanol, THF, perfluorohexane) and the BET surface areas were compared. They found that COFs with smaller pore sizes are more robust, and that the activation stability decreases for larger pore sizes. Additionally, bulky and polar substituents are beneficial for the robustness. COFs with smaller pore sizes are expected to have larger BET surface areas, which makes it hard to compare absolute BET surface areas with each other. The strength of the study is the relative comparison of different activation solvents for the same COF. However, all activation methods use vacuum, and it is not clear whether supercritical CO_2 activation or other methods, for instance drying in a regular oven or in nitrogen flow, would yield higher BET surface areas for the respective COFs. In an earlier study of the same research group, it was shown that hexane yields similar activation stability as perfluorohexane.[65] Based on that, we decided to use hexane in our work as last solvent for the activation step as a greener alternative to perfluorohexane. Additionally, further research is needed to better understand the substituent effect in terms of the influence of the size of the functional group, its polarity and/or from other effects. To this end, a larger variety of functional groups could be studied, *e.g.*, a series in which similar sizes have different polarities or different electronic properties and vice versa to understand the underlying effect of the functional group on the COF properties.

The tuneability of COFs based on methyl substitution was further shown to not only enhance the stability and porosity, but also to shift the UV/vis absorption (**Chapter 3**). Based on diffuse reflectance

spectroscopy measurements, it was shown that the absorbance spectra blue shifted for Me_3TFB COFs compared to TFB COFs and red shifted upon the use of methylated amines with respect to unmethylated amines. These effects resulted in a shift in optical band gaps, showing that methyl substitution patterns are a handle to tune COF properties.

We took the functionalisation a step further by introducing a range of functional groups (OMe, Me, F, Cl, CF_3, NO_2) into COFs. As a first strategy, functionalised benzidine building blocks were purchased and reacted with Me_3TFB. However, the presence of electron-withdrawing groups in the benzidine derivatives reduced their reactivity, which hampered the formation of imine bonds, and no COFs were obtained (**Chapter 4**). Therefore, monovalent modulators that include those functional groups were used to synthesise COFs. The modulators were first reacted stoichiometrically with Me_3TFB and then benzidine was added to form the COF framework. The more reactive benzidine could exchange with the modulators, and the low fractions of modulators (2.1-8.9%) incorporated in the resulting COFs indicate again the importance of building block reactivity. While it was not possible to obtain imine COFs with electron-withdrawing groups, Banerjee and co-workers reported on the synthesis of β-ketoenamine COFs with similar electron-withdrawing groups.[71,184] Since we attempted to synthesise imine COFs instead of β-ketoenamine COFs, such small deviations in the pair of building blocks, *i.e.*, which monomers are combined to attempt a COF synthesis, seem to have a bigger influence on the COF synthesis and the resulting COF properties than initially expected. This finding is further supported by a recent study on structural COF isomers, *i.e.*, the position of the imine bond (C=N vs N=C), that have different macroscopic (crystallinity, UV-vis absorption, fluorescence) properties.[241,242] Therefore, we advise to take the pair of building blocks into account when designing a COF. Furthermore, additional studies on the reason why structural isomers result in different properties could be of interest.

Lastly, in **Chapter 5**, a post-synthetic linker-exchange strategy was used to incorporate building blocks into COFs that could not be obtained via direct condensation. Since hydroxy or amino groups can react with aldehydes, those groups can interfere with the formation of COFs by providing unwanted nucleophiles, leading to non-crystalline and non-porous materials. However, hydroxy groups are interesting for follow up reactions and amino groups are interesting for the interaction with CO_2. Post-synthetic functionalisation offers a possibility to obtain high surface areas COFs containing those functional groups. The amine building block of a highly porous non-functionalised COF can be exchanged with functionalised amine building blocks, yielding new, functionalised COFs. It must be

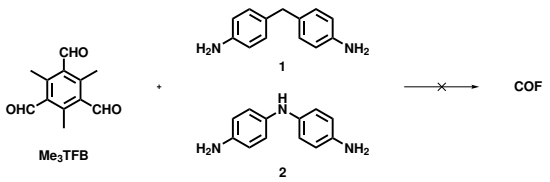

Scheme 7.2: Schematic showing the explored synthesis of Me_3TFB with two different non-conjugated diamines, which did not yield a COF.

noted that the porosity of the COFs decreases but remains high (2115±50 vs 1624±89 m^2/g), and that digestion NMR experiments could not be conducted to determine the ratio of different building blocks after linker-exchange, because the COF could not be cleaved into its monomers again.

This leads to the conclusion that post-synthetic functionalisation provides an important tool to synthesise COFs that are otherwise inaccessible, but the resulting materials are less well-defined in terms of their chemical composition and the characterisation and quantification are challenging due to the insolubility of COFs.

In an attempt to further guide future research on using functionalised building blocks in the synthesis of COFs, different amine building blocks were investigated. In a first approach, two different, not fully conjugated and flat divalent amine building blocks were tested for COF synthesis with Me_3TFB as aldehyde building block (**Scheme 7.2**). Unfortunately, the attempted COF synthesis did not yield any crystalline material.

Therefore, we designed divalent building blocks similar to 1,3,5-tris(4-aminophenyl)benzene (TAPB), in which one of the previous amino groups is replaced by an ether group containing the functional group of choice (**Figure 7.1**). This type of building block has been used for the formation of imine macrocycles with terephthalaldehyde.[243] We anticipated that the reaction with a trivalent aldehyde, such as TFB, Me_3TFB or TFPB, would yield crystalline COFs. However, in a few preliminary experiments, we obtained materials that were not crystalline. Further optimisation of the reaction conditions, for instance the composition of solvent mixtures, different temperatures, and different reaction times, will be required to further explore whether crystalline COFs could be obtained. Furthermore, theoretical calculations regarding the reactivity of the building block and the stability of the expected COF can shed light onto the feasibility of this approach.

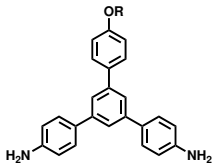

Figure 7.1: Structure of the divalent amine building block that could contain different functional groups without affecting the reactivity of the amines.

The different parameters related to the COF trilemma (**Chapter 1.2.1**) — stability, crystallinity, functionalisation — cannot be obtained all at the same time. Therefore, all possible functionalisation strategies are important to expand the scope of COF synthesis and applicability. The different advantages and disadvantages of each functionalisation strategy must be considered in an early stage to obtain the desired material's quality.

7.3 Solid-state nuclear magnetic resonance spectroscopy

Solid-state nuclear magnetic resonance (ssNMR) is one of the standard characterisation techniques to elucidate the chemical structure of COFs.[19] Next to ssNMR, also FT-IR is widely used to confirm the formation of COF linkages. The relevant regimes for the vibration bands of imine COFs are, however, overlapping with those of C=O and C=C, making it difficult to unambiguously assign the COF linkage. In ssNMR, the relevant chemical shifts are different enough to allow an unambiguous determination and learn which type of COF linkage has been formed or whether starting materials are left. However, the assignment of all atoms to their corresponding signals remains challenging, because 2D ssNMR is only available with specialised probes with magic angle spinning (MAS) frequencies of around 60 kHz. The highest spinning frequency that could be used during the work of this thesis was 14 kHz. Therefore, model compounds have frequently been used or the assignment was based on rational interpretation of the spectra.[6,21,59]

Recently, time-dependent ssNMR has turned out to provide additional information on the structural characterisation of COFs (**Chapter 1.3.3**). In parallel to our independent work described in **Chapter 3**, the relative CP build-up of each atom was used by Samori and co-workers and Zhu *et al.* to assign the ssNMR spectrum to their COFs.[33,137] In this thesis, we have shown the potential of CP build-up curves by showing, first, the proof-of-concept with TFB-PA, Me_3TFB-PA and TFB-Me_4PA and then assigning the ssNMR spectra of TFB-BD, Me_3TFB-BD and Me_3TFB-Me_4BD (**Chapter 3**). In more detail, we have measured the full CP build-up curves from 10-6000 μs and used solution NMR of the

starting materials, *i.e.*, the COF building blocks, to assign the signals. It was found that the signal of the quaternary carbon atom of the aldehyde node appears at approximately 137 ppm, which differs from the chemical shift of 130 ppm reported in literature.[6,59] This shows that the use of CP build-up curves provides a powerful way to assign NMR signals of COFs correctly.

The CP build-up strategy was applied in **Chapter 5** to elucidate the linkage formation of Me_3TFB-$(NH_2)_2$BD. In more detail, the formation of both imine and benzimidazole linkages was theoretically possible during linker-exchange. Comparison of the ssNMR signals of Me_3TFB-$(NH_2)_2$BD with a reference imine COF (Me_3TFB-BD) and a model benzimidazole compound, and the comparison of the full CP build-up curves enabled us to unambiguously assign Me_3TFB-$(NH_2)_2$BD as an imine-linked COF. For such intermolecular comparisons, it is important to record the full CP build-up curves, because the signal intensity can vary among different samples. Knowledge about the number of atoms within the sample (based on mass) is beneficial to compare the intensities of the signals. Nonetheless, the slope of the CP build-up curve can still provide additional information on the chemical environment and therefore on the chemical structure.

7.4 Optimisation of CO_2/N_2 separation

CO_2 capture and separation are of importance due to the large contribution of CO_2 to global warming. While the most abundant atmospheric gases N_2 and O_2 (about 79 vol% and 21 vol%, respectively) are no greenhouse gases, CO_2 effectively heats up the atmosphere, despite its low concentration (0.042 vol% in 2021). In comparison, flue gas exhausts contain significant larger concentrations of CO_2 (10-25 vol%), which makes the CO_2/N_2 separation more applicable before CO_2 enters the atmosphere.[161–163] Due to their large surface areas and tuneability, COFs are potential candidates for such CO_2/N_2 separations.

To study the CO_2/N_2 selectivity values of all COFs, ideal absorpion solution theory (IAST) calculations were performed. These calculations require programming knowledge to write a script to facilitate the analysis of the data. Since not every researcher has programming knowledge or access to it, we implemented the IAST script into a graphical user interface (**Chapter 6**). Additionally, we expanded the data presentation of these IAST calculations to 3D selectivity plots, in which the mole fraction and pressure can be varied simultaneously.

Then, we studied the CO_2/N_2 separation of Me_3TFB-BD and several modulated COFs to see whether a specific functional group has an impact on the CO_2/N_2 selectivity (**Chapter 4**). However, the low fractions of modulators that were incorporated into the framework did not yield an increase in CO_2/N_2 adsorption and selectivity. In comparison with Me_3TFB-OMeBD, which was obtained from direct condensation, it was shown that the number of functional groups within the COF plays an important role in the CO_2-COF interaction, as it affects the quantity of absorbed CO_2 as well as the CO_2/N_2 selectivity. In **Chapter 5**, the amine-CO_2 interaction was used to pre-design Me_3TFB-$(NH_2)_2$BD, which showed an improved CO_2/N_2 separation compared to the non-functionalised Me_3TFB-BD. In general, it is important to obtain high quantities of adsorbed CO_2 and high CO_2/N_2 selectivity values. It is, however, difficult to obtain both simultaneously, because high quantities of adsorbed CO_2 often also lead to higher quantities of adsorbed N_2, which does not increase or even decrease the CO_2/N_2 selectivity. Therefore, specific interactions between the COF and CO_2 are important to optimise the gas separation further.

Literature indicates that β-ketoenamine COFs lead to higher quantities of adsorbed CO_2 and to higher CO_2/N_2 selectivity values. Therefore, the linker-exchange strategy was taken one step further and Me_3TFB-$(NH_2)_2$BD was reacted with triformylphloroglucinol to yield TFP-$(NH_2)_2$BD. As a proof-of-concept, the sample was synthesised, characterised and tested for gas separation once.

For TFP–$(NH_2)_2$BD, the quantities of adsorbed nitrogen at 1 bar remained comparable to those of Me_3TFB-$(NH_2)_2$BD, while the quantities of adsorbed CO_2 almost doubled (**Table 7.1**). These results point to a significantly higher CO_2/N_2 IAST selectivity of approximately 2300 at 273 K and 374 at 295 K under flue gas conditions (0.15/0.85 CO_2/N_2). It must be noted that the selectivity value of 2300 is likely due to limits in the IAST theory. While triplicate analysis would be needed for the validation of these results, the preliminary data suggest that TFP-$(NH_2)_2$BD might be a promising candidate for gas separation because it adsorbs higher quantities of CO_2 while it does not adsorb more N_2, leading to high selectivity values. As micropores are advantageous for large CO_2 adsorption capacities, this approach could be taken a step further with TFP-(NH_2)2PA, which would have smaller pore sizes than the benzidine COF.[244]

In comparison with a recently published COF from Yaghi and co-workers, our Me_3TFB-$(NH_2)_2$BD contains less amino groups, which could explain the higher quantity of adsorbed CO_2 of their COF. Moreover, β-ketoenamine COFs contain one secondary amine per COF linkage, which results in a high number of functional groups within one COF structure. Therefore, we hypothesise that the

Table 7.1: Quantities of adsorbed N_2 and CO_2 of Me_3TFB-$(NH_2)_2$BD and TFP-$(NH_2)_2$BD after linker exchange at 1 bar and different temperatures and IAST selectivity under flue gas conditions.

COF	Temperature [K]	Quantity adsorbed N_2 [mmol/g]	Quantity adsorbed CO_2 [mmol/g]	CO_2/N_2 Selectivity 0.15/0.85
Me_3TFB-$(NH_2)_2$BD	273 K	0.12±0.02	1.12±0.26	83±11
	295 K	0.07±0.02	0.72±0.07	47±11
TFP-$(NH_2)_2$BD	273 K	0.13	2.04	2317
	295 K	0.08	1.33	374

higher CO_2 adsorption and higher CO_2/N_2 selectivity can be attributed to the increased number of amine groups within the COF. To elucidate the correlation between the CO_2 adsorption and the number of amino groups, acid-base titrations could be carried out. Another interesting aspect is the type of functional group that is involved in nitrogen-CO_2 interactions. Besides amino groups, COFs can contain triazine, azine, ketoenamine or imine groups and even the amino group itself can be subclassified into primary, secondary, and tertiary amines or into aliphatic vs aromatic amines. Knowledge about the interaction of a specific group with CO_2 can help to tailor COFs for CO_2/N_2 separation. For such studies, different COFs must be pre-designed and carefully analysed. In addition, computational support could be beneficial in this regard. Research along these lines is expected to result in more information on the interaction between CO_2 and N-containing COFs, further paving the way to rationally design COFs for CO_2/N_2 separation.

Next to structure-property relationships, CO_2/N_2 selectivity in gas mixtures and in flow are relevant, which can be studied by breakthrough experiments.[172] Instead of calculating the gas mixture from its pure component isotherms, the use of a Breakthrough analyser allows one to study the COF-gas interactions and selectivities of a gas mixture. This instrument can be configured with more than two gases, enabling the inclusion of water vapour in a controlled way to study the effect of humidity on the separation and selectivity performance of the COFs under process-relevant conditions.

7.5 COFs as sensors

The porosity and large surface area of COFs make them potential candidates for sensing applications, because the analyte can adsorb in the pores and onto the surface, thus contributing to a sensor response. This can be a change in the optical properties of a COF, such as UV/vis absorbance or fluorescence. Alternatively, when applied in a coating onto an electrical sensor, the response of gas

exposure to the COFs can, depending on the type of sensor platform, be recorded by measuring the resistance, electrical current, voltage or capacitance.[117,142,145,146]

The colour of COFs is reported to respond to the exposure of Brønsted acids,[147–149] solvents,[7] metals[151] or nitroaromatic compounds.[152] Within this context, Me_3TFB-PA and Me_3TFB-BD were exposed to hydrochloric acid and ammonia vapours and their change in absorption was compared to the ones of TFB-PA and TFB-BD (**Chapter 2**). Within minutes, the change in absorbance could already be detected by the naked eye through a colour change of the material. The absorbance spectra were blue shifted for Me_3TFB COFs and red shifted for Me_xBD/Me_xPA COFs with respect to unmethylated building blocks. The colour change was found to be reversible upon exposure to ammonia vapour. However, the absorbance spectra and FT-IR analysis revealed that the change was not fully reversible. It was not only shown that ammonia vapour recovered the COF, but also that the COF itself does not react to ammonia vapour. We hypothesised that, in line with literature,[117,142,145,146] the colour change could be attributed to a protonation of the imine nitrogen. Furthermore, FT-IR spectroscopy revealed that after protonation of the imine bonds, the bonds cleave into aldehydes and amines. Upon ammonia exposure, the imine bonds were only partially reformed.

Sensors often require affinity coatings to combine the analyte-sensor interaction with a processable device. However, COFs are usually obtained as fine powders, which are difficult to handle for sensor applications, at least not 'as is'. To this end, methods have been explored to apply the COF to a sensor surface.[154,156,157,245] There are different ways to achieve this: by drop-casting of a COF dispersion onto the surface, by in-situ growth of the COF on the surface or by depositing polymer-COF hybrid membranes (mixed matrix membranes, MMM). Drop-casting of a COF dispersion has the advantage that no hybrid materials are needed, which could weaken — or interfere with — the sensor response. However, the COF particles need to interact with the surface to remain adsorbed as a stable coating. Moreover, the challenge of this approach is to obtain a homogeneous layers, which is important for a reliable sensor response.[142] In-situ growth of COFs on a surface could link COFs covalently to the surface to overcome this stability problem, an approach that has been explored for MOFs on *e.g.*, copper electrodes[246] and very recently on capacitive sensors with micropatterned gold electrodes.[247] COFs can be anchored by using a primer layer on the surface. In the case of gold surfaces, we considered thiol amines as attractive candidates to form such a layer. In such an approach, the thiol moiety binds to the gold surface,[248] while the free, primary amine can act as an anchor for the build-up of a framework in a 'grafting from' fashion.

Two molecules that could be used to prepare such a primer layer are 4-aminothiophenol (ATP) and cysteamine. ATP is structurally comparable with the COF building blocks, while cysteamine is smaller and could potentially lead to a higher grafting density. Preliminary work on this approach showed that the cysteamine layer remained intact, while the ATP layer got removed from the surface when the primer layers were exposed to synthetic conditions that we typically used to prepare imine-based COFs.

Next, the COF can be polymerised in a second step on the primer layer. As a reference, also a bare gold surface was exposed to the polymerisation and it was found that the surface without primer layer also contained a layer of COFs. Therefore, it was not possible to distinguish between COFs grown from the primer layer (Au-Cysteamine-COF) and COFs that precipitated from the solution (Au + COF). Based on these preliminary findings, it is concluded that more research is needed to further explore possibilities for the covalent attachment of COFs onto a surface.

Another strategy to obtain COF-modified surfaces is to immobilise COFs on a thin polydopamine film. This approach would not be limited to gold surfaces, but is compatible with a large variety of different surfaces.[249] In the specific case of gold surfaces, the interaction of the gold surface with polydopamine most likely yields planar polydopamine layers[249–251] of which the carbonyl and amine groups can in principle be used as anchors for a COF layer. The orientation of the COF could be studied by scanning tunnelling microscopy.[252,253]

Alternatively, MMMs can be used to embed the porous COF in a polymer matrix. This way, the overall porosity of the affinity layer decreases, but the processability is facilitated. To form the membrane, the polymer-COF solution can be deposited by various means on the surface depending on the desired thickness of the coating.[142]

Banerjee and co-workers have developed an interfacial polymerisation that yields crystalline β-ketoenamine COFs as thin films.[254] In more detail, one building block is dissolved in one phase and the other building block and catalyst are dissolved in another phase that is immiscible with the first. Therefore, the reaction can only take place at the liquid-liquid interface, which leads to the formation of a thin film. The film was taken out from the interface and transferred onto various substrates. The membrane thickness can be tailored by the concentration of the building block solutions. To use these membranes for, for instance, separation applications, the obtained membranes need to be

mechanically stable. We suggest extending this approach to COFs with other linkages and to further optimise the interfacial synthesis to obtain COFs with improved processability.

Once a working protocol is established to deposit COFs on a model surface in a reproducible and homogeneous way, it will have to be transferred to sensor platforms before they can be studied as an affinity layer. Since many gases and vapours are smaller than the pore size of a COF, the affinity of an analyte towards a sensor cannot be based on size-exclusion but must originate from physicochemical interactions. As the number and diversity of functional groups in gas and vapour molecules are usually limited, a unique selectivity between one functionalised COF and a certain target analyte will be hard, if not impossible, to obtain. It might, however, be possible to reveal interactions between specific functional groups within the COF and the target gas or vapour. Therefore, these interactions could be studied, and combined in sensor arrays.[142] In a sensor array, several sensors with different affinities to various analytes are combined into one device and the overall sensor response can help to detect the analyte. Such sensor arrays could also be beneficial to deal with cross sensitivity arising from complex mixtures of gases or vapours that occur in real-life applications.

Summaries

7.1 Summary English

Covalent organic frameworks (COFs) are a class of thermally and chemically stable and crystalline materials with micro- and mesopores, *i.e.*, pores < 2 nm and not larger than 50 nm, respectively. Depending on the types of building blocks used, COFs can adopt 2D or 3D architectures with highly ordered structures. Due to their high surface area, and their large diversity in linkage chemistry and building blocks and control over the pore architectures, COFs are promising candidates for a large variety of applications, including energy storage, heterogeneous catalysis, chemical sensing and gas separation. Since their discovery in 2005, research has mainly focussed on synthesising novel materials and their applicability. To enhance the rational design of COFs for the application in mind, it is of vital importance to gain more knowledge on structure-property relationships. Next to the chemical structure, *i.e.*, the type of linkage and the degree and type of functionalisation, also the stability of COFs during their work-up, activation and functional performance are important to achieve high-quality materials. The main aim of this thesis is to explore facile synthesis strategies for COFs with different functional groups for tuneable gas and vapour interactions. In more detail, the impact of the functional groups on the crystallinity, porosity, and stability of COFs was studied on a fundamental level, aiming to tune the material properties via functionalisation in a controlled way. Some of the COFs were also studied on a more applied level by exploiting them as chemical sensors and investigating their performance in CO_2/N_2 separations.

In **Chapter 2** a new trimethylated aldehyde building block (2,4,6-trimethyl-1,3,5-triformylbenzene, Me_3TFB) was used together with phenylenediamine (PA) and benzidine (BD) to synthesise novel imine-linked COFs, which were compared to the unmethylated (1,3,5-triformylbenzene,TFB) reference COFs. The use of Me_3TFB led to an increase in porosity compared to TFB COFs, yielding high Brunauer-Emmett-Teller (BET) surface areas of up to ca. 2000 m^2/g. Density functional theory (DFT) calculations revealed that the loss in symmetry of Me_3TFB leads to a smaller rotation barrier towards the favoured C_3 conformation in the COF framework. This results in higher reaction rates and therefore to enhanced crystallinity and porosity. Moreover, it was found that Me_3TFB COFs were more stable during vacuum activation and the bench stability was significantly enhanced. As a proof-of-applicability, a colour change upon acid vapour exposure was shown.

The approach of employing methylated building blocks was expanded to a wider scope of COFs in **Chapter 3** by studying systematically COF combinations of methylated and unmethylated TFB, PA and

BD building blocks. The enhanced porosity and crystallinity upon use of Me_3TFB (**Chapter 2**) were also found within the full set of methylated building blocks that are part of **Chapter 3**. Additionally, it was found that the position of methyl groups is crucial for the COF properties. COFs with methylated amines show decreased porosity and crystallinity with respect to those made with unmethylated amines, which is attributed to the steric hinderance of the methyl group during the framework formation. The more methyl groups attached to the amine linker, the more pronounced the decrease in porosity and crystallinity becomes. Furthermore, with respect to TFB, the UV absorbance of Me_3TFB COFs blue shifts. It is hypothesised that the blue shift is due to a decrease in conjugation. On the other hand, for methylated phenylenediamines (Me_xPA) and methylated benzidines (Me_xBD) a red shift of the UV absorbance was observed with respect to PA/BD, which can be explained by the inductive, electron-donating effect of methyl groups.

Functionalisation beyond methyl groups was investigated in the study reported in **Chapter 4**. In more detail, a series of *para*-functionalised modulators (OMe, Me, F, Cl, CF_3, NO_2) was incorporated into Me_3TFB-BD. The higher reactivity of BD leads to lower fractions of modulators in the resulting COFs (2.1-8.9 mol%) than the 30 mol% modulator present in the reaction mixtures. As monovalent modulators inhibit framework formation, their incorporation may negatively impact the BET surface areas and crystallinity of the COFs. However, upon the use of modulators all COFs remained crystalline, and the BET surface areas remained high (> 1800 m^2/g). Based on digestion nuclear magnetic resonance spectroscopy (NMR) and X-ray photoelectron spectroscopy (XPS) analyses, the modulator could be located on the outside of the COF sheets, explaining the crystallinity and high porosity of the modulated COFs. The modulated COFs were then applied in CO_2/N_2 gas separation to investigate the effect of the functional groups on the separation selectivity under flue gas conditions. Moderate quantities of adsorbed CO_2 were found together with selectivity values between 6 and 24 for the different modulators at 273 K. Due to the low number of functional, polarisable groups within the COF, the selectivity remained similar for the non-functionalised Me_3TFB-BD COF and the functionalised, modulated COFs. Interestingly, Me_3FTFB-OMeBD — which is synthesised from methoxy-substituted benzidine and has more methoxy groups per pore compared to OMe-modulated COF (4.9 mol% modulator) — has a higher CO_2/N_2 selectivity than the modulated COFs. This shows that increasing the fraction of functional groups in the COF can lead to higher CO_2/N_2 ideal adsorption solution theory (IAST) selectivity values.

In **Chapter 5**, the CO_2-amine interaction was used to pre-design a COF for high CO_2/N_2 selectivity and high CO_2 adsorption quantity. As Me_3FTB-$(NH_2)_2$BD was not accessible via direct synthesis and, moreover, the use of modulators did not lead to high fractions of functional groups inside the COF, a post-synthetic linker-exchange was employed. The imine-linkage was unambiguously assigned by solid-state NMR and cross-polarisation (CP) build-up curves. BET surface area analysis indicated that most of the porosity of the pristine Me_3TFB-BD was retained during post-synthetic modification. As hypothesised, we found high CO_2/N_2 selectivity values (83 ± 11 at 273 K and 47 ± 11 at 295 K) under flue gas conditions together with moderate CO_2 adsorption quantities. The CO_2-amine interaction is based on weak Van der Waals interactions, which are expected to require little energy for the regeneration of the COF. The CO_2 adsorption quantities and the high CO_2/N_2 selectivity of Me_3FTB-$(NH_2)_2$BD indicate the promise of this approach for gas separation.

IAST calculations, which are useful to model mixed gas isotherms out of the pure component isotherms, require programming knowledge to use the existing python packages. This can restrict their use, since not every researcher has programming skills. Therefore, in **Chapter 6** a graphical user interface (GUI) software for IAST calculations is presented to predict the selectivity of binary gas mixtures. Additionally, the IAST selectivity can be calculated for multiple pressures and mixture compositions at the same time. The software is available on the open-source, software development platform GitHub, uses the *.csv file format, and allows isotherm fitting with various established models to provide a platform for non-programming material scientists. The software was used in **Chapter 4** and **5**.

Chapter 7 discusses the results obtained in **Chapter 2-6** in a broader context and outlines future research suggestions, which are partly supported by preliminary data on improved CO_2/N_2 separations, including enhanced quantities of adsorbed CO_2, and on depositing COFs on surfaces.

7.2 Summary Dutch — Samenvatting

Covalente organische raamwerken (COFs) zijn chemisch en thermisch stabiele, kristallijne materialen met micro- (< 2nm) en mesoporiën (2-50 nm). Afhankelijk van de gekozen monomeren vormen COFs twee- of driedimensionale netwerken. De monomeren van COFs kunnen op veel verschillende manieren worden gestructureerd in een netwerk hetgeen ook de structuur van de poriën kan beïnvloeden. De variatie wordt bovendien nog groter door de grote verscheidenheid aan beschikbare monomeren. De grote variatie in structuren en het grote interne oppervlak maken COFs interessante materialen voor diverse toepassingen zoals energieopslag, heterogene katalyse, chemische sensoren en gasscheidingen. Sinds de ontdekking van COFs in 2005 is onderzoek aan dergelijke raamwerken vooral gericht op de synthese van nieuwe materialen en hun applicatie. Om de eigenschappen van een COF al in de ontwerpfase mee te nemen, is het essentieel om kennis te hebben over structuur-eigenschap relaties. Behalve de chemische structuur is de stabiliteit van COFs tijdens het verwerken, het activeren en ook tijdens de applicatie van cruciaal belang om materialen van hoge kwaliteit te krijgen. Het hoofddoel van dit proefschrift is het verkennen van eenvoudige syntheseroutes voor COFs met verschillende functionele groepen. Dit proefschrift beschrijft onderzoek naar de invloed van dergelijke groepen op de kristalliniteit, de porositeit en de stabiliteit van COFs, met als doel om op basis van deze inzichten de materiaaleigenschappen te verbeteren. Ter illustratie van de toepasbaarheid is een aantal COFs bestudeerd als chemische sensor en/of is hun vermogen op het gebied van gasscheidingen getest.

In **Hoofdstuk 2** is een nieuw getrimethyleerd monomeer (2,4,6-trimethyl-1,3,5-triformylbenzeen, Me_3TFB) met fenyleendiamine (PA) of benzidine (BD) gebruikt om nieuwe COFs te synthetiseren op basis van imine-bindingen. De verkregen COFs zijn vervolgens vergeleken met de niet-gemethyleerede (1,3,5-triformylbenzeen, TFB) referentiematerialen. Ten opzichte van TFB COFs leidde het gebruik van Me_3TFB tot een verbetering van de porositeit. Dit resulteerde in Brunauer-Emmett-Teller (BET) oppervlakken met waardes tot 2000 m^2/g. Dichtheidsfunctionaaltheorie (DFT) berekeningen toonden aan dat het verlies van symmetrie in Me_3TFB leidde tot een kleinere rotatiebarrière. Dit resulteerde in een hogere reactiesnelheid, waardoor de carbonylgroep sneller in de gewenste C_3 conformatie kan roteren, welke binnen het COF-raamwerk gevormd wordt. Hieruit volgt een hogere kristalliniteit en porositeit. Verder zijn Me_3TFB COFs tijdens de vacuümactivering stabieler bevonden en was de opslagstabiliteit significant hoger. Ter illustratie van de toepasbaarheid als chemische

sensor zijn de COFs blootgesteld aan zure dampen, hetgeen leidde tot een kleurverandering van het materiaal.

De methode om gemethyleerde monomeren te gebruiken, is in **Hoofdstuk 3** verder uitgebreid door COF combinaties van gemethyleerde en niet-gemethyleerde TFB, PA en BD-monomeren systematisch te onderzoeken. De verbeterde kristalliniteit en porositeit bij gebruik van Me_3TFB (**Hoofdstuk 2**) werden ook gevonden bij COFs met alle andere amine-monomeren uit **Hoofdstuk 3**. Bovendien werd vastgesteld dat de positie van de methylgroep van cruciaal belang is; COFs met gemethyleerde amines hebben een lagere kristalliniteit en porositeit in vergelijking met COFs die uit niet-gemethyleerde amines bestaan. Dit komt door de sterische hindering van de methylgroepen tijdens de formatie van het netwerk. Hoe meer methylgroepen het amine-monomeer heeft, des te sterker de afname van kristalliniteit en porositeit. Verder leidde het gebruik van Me_3TFB COFs tot een blauwverschuiving van de UV-absorptie. Deze blauwverschuiving treedt vermoedelijk op vanwege de afname van de conjugatie van het π-systeem. Bij gebruik van gemethyleerd fenyleendiamine (Me_xPA) en gemethyleerd benzidine (Me_xBD) leidde tot een roodverschuiving in de UV-absorptie van de COFs ten opzichte de absorptie van PA/BD COFs. Dit kan uitgelegd worden door het inductieve, elektronenstuwende effect van de methylgroep.

Het functionaliseren van COFs met andere groepen is in **Hoofdstuk 4** onderzocht. Preciezer gezegd, werd een serie van para-gefunctionaliseerde modulatoren (OMe, Me, F, Cl, CF_3, NO_2) in Me_3TFB-BD ingebouwd. Hoewel 30 mol% modulator aanwezig was tijdens de synthese, werden lagere percentages modulator (2.1-8.9 mol%) in de gesynthetiseerde COFs gevonden. Dit verschil kan worden toegeschreven aan de hogere reactiviteit van benzidine. Aangezien modulatoren de netwerkformatie kunnen verstoren, kan hun inbouw in COFs een negatief effect hebben op het BET oppervlak en de kristalliniteit. Echter, bij gebruik van de modulatoren bleek dat de materialen kristallijn bleven en hoge BET oppervlakken (> 1800 m^2/g) zijn gevonden. Met behulp van kernspinresonantiespectroscopie (NMR) metingen aan gedepolymeriseerde monsters en röntgenfotoelektronenspectroscopie (XPS) van de COFs werd de modulator aan de buitenzijde van de COF laag gelokaliseerd, wat de hoge kristalliniteit en porositeit van de gemoduleerde COFs verklaart. Daarna werden de gemoduleerde COFs gebruikt in CO_2/N_2 scheidingen om het effect van functionele groepen op de selectiviteit van de scheiding van CO_2 van rookgas te onderzoeken. Voor verschillende modulatoren werden bij 273 K gematigde hoeveelheden van geadsorbeerd CO_2 vastgesteld met selectiviteitswaarden tussen 6 en 24. De selectiviteit van de gemoduleerde COFs bleef vergelijkbaar

met die van het niet-gefunctionaliseerde Me_3TFB-BD, wat verklaard kan worden door het geringe aantal functionele polariseerbare groepen binnen het COF. Interessant is dat Me_3TFB-OMeBD, dat werd gesynthetiseerd uit methoxy-gesubstitueerd benzidine en dus meer methoxygroepen per porie heeft dan het OMe-gemoduleerde COF (4.9 mol% modulator), een hogere CO_2/N_2-selectiviteit heeft dan het gemoduleerde COF. Uit dit resultaat blijkt dat een hoger aantal functionele groepen tot een hogere CO_2/N_2-selectiviteit leidt.

Met de bekende CO_2-amine interactie in het achterhoofd is in **Hoofdstuk 5** een amine-gefunctionaliseerd COF ontworpen met een hoge CO_2/N_2-selectiviteit en grote hoeveelheden geadsorbeerd CO_2 als inzet. Aangezien Me_3TFB-$(NH_2)_2$BD niet direct uit de monomeren gesynthetiseerd kan worden en het functionaliseren met behulp van modulatoren tot slechts kleine hoeveelheden aan functionele groepen in de COFs resulteerde, werd een post-synthetische uitwisselingsstrategie gebruikt. Vaste stof NMR en het gebruik van tijdsafhankelijke *cross-polarisation* curves bewezen de vorming van de imine-groepen. Op basis van de BET analyses kan worden geconcludeerd dat de meeste porositeit van de oorspronkelijke Me_3TFB-BD tijdens de post-synthetische uitwisseling werd behouden. Zoals verwacht, werdenj hoge CO_2/N_2-selectiviteitswaarden (83 ± 11 bij 273 K en 47 ± 11 bij 295 K) en grote hoeveelheden geadsorbeerde CO_2 onder rookgascondities gevonden. De CO_2-amine interactie is gebaseerd op zwakke vanderwaalskrachten, zodat alleen kleine hoeveelheden energie worden verwacht om de COF te regenereren. De hoeveelheid geadsorbeerde CO_2 en de hoge CO_2/N_2-selectiviteiten van Me_3TFB-$(NH_2)_2$BD duiden erop dat deze strategie veelbelovend is voor gasscheiding.

Ideale adsorptie-oplossingstheorie (IAST) berekeningen, die behulpzaam zijn het gedrag van gasmengsels uit de isothermen van hun individuele componenten te bepalen, kunnen met bestaande Python-pakketten uitgevoerd worden. Echter, hiervoor is programmeerkennis noodzakelijk. Aangezien niet elke onderzoeker over goede programmeervaardigheden beschikt, kan dit het gebruik van de IAST-pakketten beperken. Daarom is in **Hoofdstuk 6** zelf-ontwikkelde software met een grafische gebruikersinterface voor IAST-berekeningen gepresenteerd, waarmee de selectiviteit van binaire gasmengsels berekend kan worden. Verder kan met de IAST-selectiviteit voor verschillende drukken en molfracties tegelijk berekend worden. De software is beschikbaar op het open-source software-ontwikkelingsplatform GitHub, gebruikt het *.csv-bestandsformaat en maakt de fitting van isothermen met verschillende bekende fysische en numerieke modellen mogelijk. De software biedt dus een

platform om IAST-berekeningen uit te voeren zonder zelf te hoeven programmeren. De software is gebruikt in **Hoofdstukken 4** en **5**.

In **Hoofdstuk 7** zijn de resultaten van **Hoofdstukken 2-6** in een bredere context geplaatst en worden suggesties voor toekomstige onderzoek gedaan. De suggesties worden gedeeltelijk ondersteund door voorlopige resultaten op het gebied van verbeterde CO_2/N_2-separatie en grotere hoeveelheden geadsorbeerd CO_2, en ook het opbrengen van COFs op een oppervlak.

7.3 Summary German — Zusammenfassung

Covalent organic frameworks (COFs) sind chemisch und thermisch stabile, kristalline Materialien mit Mikro- (< 2 nm) und Mesoporen (2-50 nm). Abhängig von den Monomeren können COFs zwei- oder dreidimensionale Netzwerke ausbilden. Die Monomere von COFs können auf viele verschiedene Arten miteinander vernetzt werden und die Porenstruktur kann durch die Wahl der Monomere gesteuert werden. Gleichzeitig stehen viele verschiedene Monomere zur Verfügung, wodurch die Variabilität zusätzlich erhöht wird. Durch diese große Vielfalt sowie die hohen Oberflächen sind COFs vielversprechende Materialien für eine große Anzahl an Anwendungen, beispielsweise Energiespeicherung, heterogene Katalyse, chemische Sensoren und Gastrennung. Seit ihrer Entdeckung im Jahr 2005 hat sich die Forschung vor allem auf die Synthese neuer Materialien und deren Anwendung konzentriert. Um bereits in der Planungsphase der gewünschten Anwendung ein COF designen zu können ist es unabdingbar, mehr Wissen über die Struktur-Eigenschafts-Beziehungen zu erlangen. Neben ihrer chemischen Struktur ist die Stabilität der COFs während der Aufarbeitung, der Aktivierung und auch während der Anwendung von entscheidender Bedeutung, um qualitativ hochwertige Materialien zu erhalten. Das Ziel dieser Dissertation ist es, simple Synthesewege für COFs mit verschiedenen funktionellen Gruppen zu erforschen und ihr Potential in Bezug auf Wechselwirkungen mit Gasen und Dämpfen zu untersuchen. Die verschiedenen funktionellen Gruppen sollen dabei eine Möglichkeit zur Anpassung und Optimierung der COFs für die COF-Gas Wechselwirkung darstellen. Genauer gesagt wird der Einfluss der funktionellen Gruppen auf Kristallinität, Porosität und Stabilität untersucht, um basierend auf diesen Erkenntnissen die Materialeigenschaften zu verbessern. Einige COFs wurden, zur Verdeutlichung des Andwendungsbezugs, als chemischer Sensor verwendet und/oder ihr Potential im Bereich der Gastrennung untersucht.

In **Kapitel 2** wurde ein neuartiges trimethyliertes Monomer (2,4,6-Trimethyl-1,3,5-triformylbenzol, Me_3TFB) zusammen mit Phenylendiamin (PA) und Benzidin (BD) verwendet, um neue imin-vernetzte COFs zu synthetisieren. Diese wurde dann mit den nicht-methylierten (1,3,5-Triformylbenzol, TFB) Referenzmaterialien verglichen. Die Verwendung von Me_3TFB führte zu einer Verbesserung der Porosität verglichen mit den TFB COFs, was in Brunauer-Emmett-Teller (BET) Oberflächen von bis zu 2000 m^2/g resultierte. Dichtefunktionaltheorieberechnungen (DFT) zeigten, dass der Verlust der Symmetrie in Me_3TFB zu einer kleineren Rotationsbarriere führt. Diese verringerte Rotationsbarriere führt zu höheren Reaktionsraten, wodurch die Carbonylgruppe häufiger in der bevorzugten C_3 Konformation vorliegt, welche zur Bildung des COF-Netzwerks benötigt wird. Hierdurch wird eine höhere

Kristallinität und Porosität erzielt. Zusätzlich waren während der Vakuumaktivierung Me_3TFB COFs stabiler und die Lagerstabilität war signifikant erhöht. Zur Verdeutlichung des Anwendungspotentials als chemischer Sensor wurden die COFs Säuredämpfen ausgesetzt, woraufhin eine Farbänderung des Materials beobachtet werden konnte.

Der Ansatz methylierte Monomere zu verwenden wurde in **Kapitel 3** vertieft, indem COF-Kombinationen aus methylierten und nicht-methylierten TFB-, PA- und BD-Monomeren systematisch untersucht wurden. Die verbesserte Kristallinität und Porosität bei Verwendung von Me_3TFB (**Kapitel 2**) wurden auch bei COFs mit allen anderen getesteten Amin-Monomeren **Kapitel 3** beobachtet. Zusätzlich zeigte sich, dass die Position der Methylgruppe von entscheidender Bedeutung ist. COFs mit methylierten Aminen weisen eine niedrigere Porosität und Kristallinität im Vergleich zu COFs, welche aus nicht-methylierten Amin-Monomeren bestehen, auf. Dies ist auf den sterischen Anspruch der Methylgruppen während der Netzwerkbildung zurückzuführen. Je mehr Methylgruppen das Amin-Monomer trägt, desto stärker ist die Abnahme der Kristallinität und Porosität ausgeprägt. Des Weiteren kommt es durch die Nutzung von Me_3TFB COFs zu einer Blauverschiebung der UV-Absorption. Die Blauverschiebung tritt vermutlich auf, da die Konjugation des π-Systems abnimmt. Bei Verwendung von methylierten Phenylendiaminen (Me_xPA) und methylierten Benzidinen (Me_xBD) in COFs kommt es zu einer Rotverschiebung der UV-Absorption im Vergleich zur Absorption der PA/BD-COFs. Dies kann durch den induktiven, elektronenschiebenden Effekt der Methylgruppe erklärt werden.

Die Funktionalisierung von COFs neben der Methylgruppe wurde in **Kapitel 4** untersucht. Hierzu wurde eine Serie von *para*-funktionalisierten Modulatoren (OMe, Me, F, Cl, CF_3, NO_2) in Me_3TFB-BD eingebaut. Obwohl 30 mol% Modulator in der Reaktionsmischung vorhanden war, wurden nur geringere Anteile Modulator (2.1-8.9 mol%) in den synthetisierten COFs gefunden, was auf die höhere Reaktivität von Benzidin zurückzuführen ist. Da Modulatoren die Netzwerkbildung verhindern können, kann sich ihr Einbau in das COF negativ auf die BET Oberfläche und die Kristallinität auswirken. Trotzdem blieben bei Verwendung der Modulatoren alle COFs kristallin und es wurden zudem hohe BET Oberflächen (> 1800 m^2/g) gemessen. Basierend auf Kernspinresonanzspektroskopiemessungen (NMR) von aufgeschlossenen Proben und Photoelektronenspektroskopiemessungen (XPS) der COFs konnte der Modulator an der Außenkante der COF-Schicht lokalisiert werden, was die Kristallinität und hohe Porosität der modulierten COFs erklärt. Anschließend wurden die modulierten COFs in der CO_2/N_2 Trennung verwendet, um den Effekt der funktionellen Gruppen auf die Trennungsselektivität unter Prozessbedingungen von industriellem Abgas zu untersuchen. Die Selektivitäten wurden mittels

idealer Adsorptions-Lösungs Theorie (IAST) ermittelt. Für die verschiedenen Modulatoren wurden bei 273 K moderate Mengen an adsorbiertem CO_2 sowie CO_2/N_2 Selektivitäten zwischen 6 und 24 ermittelt. Die Selektivität der modulierten COFs blieb, aufgrund der geringen Zahl funktioneller, polarisierbarer Gruppen innerhalb des COFs, vergleichbar mit der des nicht-funktionalisierten Me_3TFB-BD. Interessanterweise hat Me_3TFB-OMeBD, welches aus methoxy-substituiertem Benzidin synthetisiert wurde und somit mehr Methoxygruppen pro Pore als OMe-moduliertes COF (4.9 mol% Modulator) aufweist, eine höhere CO_2/N_2 Selektivität als das modulierte COF. Dieses Ergebnis zeigt, dass eine zunehmende Zahl funktioneller Gruppen im COF zu höherer CO_2/N_2 Selektivität führt.

Die bekannte CO_2-Amin-Wechselwirkung wurde in **Kapitel 5** verwendet, um ein COF zu designen, welches eine hohe CO_2/N_2 Selektivität und hohes CO_2-Adsorptionsverögen aufweist. Da Me_3TFB-$(NH_2)_2$BD nicht direkt aus den Monomeren synthetisiert werden konnte und die Funktionalisierung mittels Modulatoren nicht zu hohen Anteilen an funktionellen Gruppen im COF geführt hat, wurde eine post-synthetische Austauschstrategie verwendet. Mittels Feststoff-NMR Spektroskopie und Verwendung von zeitabhängingen Cross-Polarisationskurven konnte die Bildung der Imin-Gruppen eindeutig belegt werden. BET-Oberflächenanalysen ließen darauf schließen, dass der Großteil der Porosität des originalen Me_3TFB-BD während der post-synthetischen Austauschreaktion erhalten wurde. Wie erwartet konnten unter Prozessbedingungen industrieller Abgase hohe CO_2/N_2 Selektivitäswerte (83 ± 11 bei 273 K und 47 ± 11 bei 295 K) und hohe CO_2-Adsorptionsvermögen gemessen werden. Die CO_2-Amin-Wechselwirkung basiert auf schwachen Van-der-Waals-Kräften, wodurch vermutlich nur geringe Energiemengen zur Regenerierung der COFs benötigt werden. Die Menge an adsorbiertem CO_2 sowie die hohen CO_2/N_2 Selektivitäten von Me_3TFB-$(NH_2)_2$BD deuten an, dass dieser Ansatz im Bereich der Gastrennung vielversprechend ist.

IAST-Berechnungen, welche verwendet werden um das Verhalten von Gasmischungen aus den Isothermen ihrer Einzelkomponenten zu berechnen, können mit existierenden Python-Paketen durchgeführt werden, jedoch sind vertiefte Programmierkenntnisse erforderlich. Da nicht jeder Wissenschaftler Programmierkenntnisse besitzt, kann dies die Verwendung der IAST-Pakete einschränken. Daher wird in **Kapitel 6** eine selbstentwickelte Software mit graphischer Benutzeroberfläche für IAST-Berechnungen vorgestellt, welche die Selektivität von binären Mischungen berechnen kann. Zusätzlich kann die IAST-Selektivität für verschiedene Drücke und Molenbrüche gleichzeitig berechnet werden. Die Software ist auf der open-source Softwarenentwicklungsplatform GitHub verfügbar, nutzt das *.csv Dateiformat und erlaubt ein Fitting der Isothermen mit verschiedenen etablierten physikalischen und

numerischen Modellen. Damit liefert sie eine Platform für Materialwissenschaftler, IAST-Berechnungen durchzuführen, ohne selbst programmieren zu müssen.

In **Kapitel 7** werden die Ergebnisse der **Kapitel 2-6** in einem breiteren Kontext diskutiert und zukünftige Forschungsansätze vorgeschlagen. Letztere werden teilweise durch vorläufige Daten in Bezug auf verbesserte CO_2/N_2-Trennung und verbesserte Mengen adsorbiertes CO_2 sowie in Bezug der Abscheidung von COFs auf Oberflächen unterstützt.

References

[1] Thommes, M.; Kaneko, K.; Neimark, A. V.; Olivier, J. P.; Rodriguez-Reinoso, F.; Rouquerol, J.; Sing, K. S. *Pure Appl. Chem.* **2015**, *87*, 1051–1069.
[2] Segura, J. L.; Mancheño, M. J.; Zamora, F. *Chem. Soc. Rev.* **2016**, *45*, 5635–5671.
[3] Deblase, C. R.; Silberstein, K. E.; Truong, T. T.; Abruña, H. D.; Dichtel, W. R. *J. Am. Chem. Soc.* **2013**, *135*, 16821–16824.
[4] Wang, H.; Wang, H.; Wang, Z.; Tang, L.; Zeng, G.; Xu, P.; Chen, M.; Xiong, T.; Zhou, C.; Li, X. *et al. Chem. Soc. Rev.* **2020**, *49*, 4135–4165.
[5] Singh, N.; Yadav, D.; Mulay, S. V.; Kim, J. Y.; Park, N. J.; Baeg, J. O. *ACS Appl. Mater. Interfaces* **2021**, *13*, 14122–14131.
[6] Ding, S.-Y.; Gao, J.; Wang, Q.; Zhang, Y.; Song, W.-G.; Su, C.-Y.; Wang, W. *J. Am. Chem. Soc.* **2011**, *133*, 19816–19822.
[7] Ascherl, L.; Evans, E. W.; Hennemann, M.; Nuzzo, D. D.; Hufnagel, A. G.; Beetz, M.; Friend, R. H.; Clark, T.; Bein, T.; Auras, F. *Nat. Commun.* **2018**, *9*, 3802.
[8] Fan, H.; Peng, M.; Strauss, I.; Mundstock, A.; Meng, H.; Caro, J. *J. Am. Chem. Soc.* **2020**, *142*, 2–7.
[9] Nick, S.; Chomicz, Z. *CHEMKON* **2013**, *20*, 14–20.
[10] Fujita, M.; Washizu, S.; Ogura, K.; Kwon, Y. J. *J. Am. Chem. Soc.* **1994**, *116*, 1151–1152.
[11] Li, H.; Eddaoudi, M.; O'Keeffe, M.; Yaghi, O. M. *Nature* **1999**, *402*, 276–279.
[12] James, S. L. *Chem. Soc. Rev.* **2003**, *32*, 276–288.
[13] Côté, A. P.; Benin, A. I.; Ockwig, N. W.; O'Keeffe, M.; Matzger, A. J.; Yaghi, O. M. *Science* **2005**, *310*, 1166–70.
[14] Rowan, S. J.; Cantrill, S. J.; Cousins, G. R.; Sanders, J. K.; Stoddart, J. F. *Angew. Chem., Int. Ed.* **2002**, *41*, 898–952.
[15] Hu, J.; Gupta, S. K.; Ozdemir, J.; Beyzavi, M. H. *ACS Appl. Nano Mater.* **2020**, *3*, 6239–6269.
[16] Maschita, J.; Banerjee, T.; Lotsch, B. V. *Chem. Mater.* **2022**, *34*, 2249–2258.
[17] Qian, H. L.; Li, Y.; Yan, X. P. *J. Mater. Chem. A* **2018**, *6*, 17307–17311.
[18] Daugherty, M. C.; Vitaku, E.; Li, R. L.; Evans, A. M.; Chavez, A. D.; Dichtel, W. R. *Chem. Commun.* **2019**, *55*, 2680–2683.
[19] Evans, A. M.; Strauss, M. J.; Corcos, A. R.; Hirani, Z.; Ji, W.; Hamachi, L. S.; Aguilar-Enriquez, X.; Chavez, A. D.; Smith, B. J.; Dichtel, W. R. *Chem. Rev.* **2022**, *122*, 442–564.
[20] Haase, F.; Troschke, E.; Savasci, G.; Banerjee, T.; Duppel, V.; Dörfler, S.; Grundei, M. M.; Burow, A. M.; Ochsenfeld, C.; Kaskel, S. *et al. Nat. Commun. 2018 91* **2018**, *9*, 1–10.
[21] Kandambeth, S.; Mallick, A.; Lukose, B.; Mane, M. V.; Heine, T.; Banerjee, R. *J. Am. Chem. Soc.* **2012**, *134*, 19524–19527.
[22] Li, Z.; Huang, N.; Lee, K. H.; Feng, Y.; Tao, S.; Jiang, Q.; Nagao, Y.; Irle, S.; Jiang, D. *J. Am. Chem. Soc.* **2018**, *140*, 12374–12377.
[23] Yang, Y.; Yu, L.; Chu, T.; Niu, H.; Wang, J.; Cai, Y. *Nat. Commun. 2022 131* **2022**, *13*, 1–9.
[24] Jiang, G.; Zou, W.; Ou, Z.; Zhang, L.; Zhang, W.; Wang, X.; Song, H.; Cui, Z.; Liang, Z.; Du, L. *Angew. Chemie Int. Ed.* **2022**, *61*, e202208086.
[25] Uribe-Romo, F. J.; Hunt, J. R.; Furukawa, H.; Klöck, C.; O'Keeffe, M.; Yaghi, O. M. *J. Am. Chem. Soc.* **2009**, *131*, 4570–4571.
[26] Ma, Y.; Wang, Y.; Li, H.; Guan, X.; Li, B.; Xue, M.; Yan, Y.; Valtchev, V.; Qiu, S.; Fang, Q. *Angew. Chem., Int. Ed.* **2020**, *59*, 19633–19638.
[27] Xie, Y.; Li, J.; Lin, C.; Gui, B.; Ji, C.; Yuan, D.; Sun, J.; Wang, C. *J. Am. Chem. Soc.* **2021**, *143*, 7279–7284.
[28] Wang, C.; Wang, Y.; Ge, R.; Song, X.; Xing, X.; Jiang, Q.; Lu, H.; Hao, C.; Guo, X.; Gao, Y. *et al. Chem. — A Eur. J.* **2018**, *24*, 585–589.
[29] Fang, Q.; Gu, S.; Zheng, J.; Zhuang, Z.; Qiu, S.; Yan, Y. *Angew. Chemie Int. Ed.* **2014**, *53*, 2878–2882.
[30] Smith, B. J.; Overholts, A. C.; Hwang, N.; Dichtel, W. R. *Chem. Commun.* **2016**, *52*, 3690–3693.
[31] Vitaku, E.; Dichtel, W. R. *J. Am. Chem. Soc.* **2017**, *139*, 12911–12914.
[32] Zhu, D.; Zhu, Y.; Yan, Q.; Barnes, M.; Liu, F.; Yu, P.; Tseng, C. P.; Tjahjono, N.; Huang, P. C.; Rahman, M. M. *et al. Chem. Mater.* **2021**, *33*, 4216–4224.
[33] Zhu, D.; Zhang, Z.; Alemany, L. B.; Li, Y.; Nnorom, N.; Barnes, M.; Khalil, S.; Rahman, M. M.; Ajayan, P. M.; Verduzco, R. *Chem. Mater.* **2021**, *33*, 3394–3400.
[34] Ding, S. Y.; Cui, X. H.; Feng, J.; Lu, G.; Wang, W. *Chem. Commun.* **2017**, *53*, 11956–11959.
[35] Biswal, B. P.; Chandra, S.; Kandambeth, S.; Lukose, B.; Heine, T.; Banerjee, R. *J. Am. Chem. Soc.* **2013**, *135*, 5328–5331.
[36] Haase, F.; Lotsch, B. V. *Chem. Soc. Rev.* **2020**, *49*, 8469–8500.
[37] Li, Z.; Feng, X.; Zou, Y.; Zhang, Y.; Xia, H.; Liu, X.; Mu, Y. *Chem. Commun.* **2014**, *50*, 13825–13828.
[38] Liu, M.; Guo, L.; Jin, S.; Tan, B. *J. Mater. Chem. A* **2019**, *7*, 5153–5172.
[39] Kuhn, P.; Antonietti, M.; Thomas, A. *Angew. Chemie Int. Ed.* **2008**, *47*, 3450–3453.
[40] Morris, R. E. *Chem. Commun.* **2009**, 2990–2998.
[41] Smith, B. J.; Parent, L. R.; Overholts, A. C.; Beaucage, P. A.; Bisbey, R. P.; Chavez, A. D.; Hwang, N.; Park, C.; Evans, A. M.; Gianneschi, N. C. *et al. ACS Cent. Sci.* **2017**, *3*, 58–65.
[42] Schiff, H. *Justus Liebigs Ann. Chem.* **1864**, *131*, 118–119.

[43] Kandambeth, S.; Dey, K.; Banerjee, R. *J. Am. Chem. Soc.* **2019**, *141*, 1807–1822.
[44] Citation report - 667 - Web of Science Core Collection. https://www.webofscience.com/wos/woscc/citation-report/1a313a00-7403-49a1-ab61-7e3b958b5071-4437528e.
[45] Dalapati, S.; Jin, S.; Gao, J.; Xu, Y.; Nagai, A.; Jiang, D. *J. Am. Chem. Soc.* **2013**, *135*, 17310–17313.
[46] Uribe-Romo, F. J.; Doonan, C. J.; Furukawa, H.; Oisaki, K.; Yaghi, O. M. *J. Am. Chem. Soc.* **2011**, *133*, 11478–11481.
[47] Stegbauer, L.; Schwinghammer, K.; Lotsch, B. V. *Chem. Sci.* **2014**, *5*, 2789–2793.
[48] Bunck, D. N.; Dichtel, W. R. *J. Am. Chem. Soc.* **2013**, *135*, 14952–14955.
[49] Fang, Q.; Zhuang, Z.; Gu, S.; Kaspar, R. B.; Zheng, J.; Wang, J.; Qiu, S.; Yan, Y. *Nat. Commun.* **2014**, *5*, 1–8.
[50] Jiang, L.; Tian, Y.; Sun, T.; Zhu, Y.; Ren, H.; Zou, X.; Ma, Y.; Meihaus, K. R.; Long, J. R.; Zhu, G. *J. Am. Chem. Soc.* **2018**, *140*, 15724–15730.
[51] Veldhuizen, H.; Vasileiadis, A.; Wagemaker, M.; Mahon, T.; Mainali, D. P.; Zong, L.; van der Zwaag, S.; Nagai, A. *J. Polym. Sci. Part A Polym. Chem.* **2019**, *57*, 2373–2377.
[52] Karak, S.; Kandambeth, S.; Biswal, B. P.; Sasmal, H. S.; Kumar, S.; Pachfule, P.; Banerjee, R. *J. Am. Chem. Soc.* **2017**, *139*, 1856–1862.
[53] Chandra, S.; Kandambeth, S.; Biswal, B. P.; Lukose, B.; Kunjir, S. M.; Chaudhary, M.; Babarao, R.; Heine, T.; Banerjee, R. *J. Am. Chem. Soc.* **2013**, *135*, 17853–17861.
[54] Zhuang, X.; Zhao, W.; Zhang, F.; Cao, Y.; Liu, F.; Bi, S.; Feng, X. *Polym. Chem.* **2016**, *7*, 4176–4181.
[55] Jadhav, T.; Fang, Y.; Liu, C. H.; Dadvand, A.; Hamzehpoor, E.; Patterson, W.; Jonderian, A.; Stein, R. S.; Perepichka, D. F. *J. Am. Chem. Soc.* **2020**, *142*, 8862–8870.
[56] Bi, S.; Meng, F.; Zhang, Z.; Wu, D.; Zhang, F. *Chem. Res. Chinese Univ. 2022 382* **2022**, *38*, 382–395.
[57] Yaghi, O. M.; O Keffe, M.; Ockwig, N. W.; Chae, H. K.; Eddaoudi, M.; Kim, J. *Nature* **2003**, *423*, 705–714.
[58] Diercks, C. S.; Yaghi, O. M. *Science* **2017**, *355*, eaal1585.
[59] Yang, Y.; Deng, D.; Zhang, S.; Meng, Q.; Li, Z.; Wang, Z.; Sha, H.; Faller, R.; Bian, Z.; Zou, X. *et al. Adv. Mater.* **2020**, *32*, 1908243.
[60] Zhang, B.; Mao, H.; Matheu, R.; Reimer, J. A.; Alshmimri, S. A.; Alshihri, S.; Yaghi, O. M. *J. Am. Chem. Soc.* **2019**, *141*, 11420–11424.
[61] Chen, L.; Gong, C.; Wang, X.; Dai, F.; Huang, M.; Wu, X.; Lu, C. Z.; Peng, Y. *J. Am. Chem. Soc.* **2021**, *143*, 10243–10249.
[62] Kang, X.; Han, X.; Yuan, C.; Cheng, C.; Liu, Y.; Cui, Y. *J. Am. Chem. Soc.* **2020**, *142*, 16346–16356.
[63] Segura, J. L.; Royuela, S.; Mar Ramos, M. *Chem. Soc. Rev.* **2019**, *48*, 3903–3945.
[64] Feriante, C. H.; Jhulki, S.; Evans, A. M.; Dasari, R. R.; Slicker, K.; Dichtel, W. R.; Marder, S. R. *Adv. Mater.* **2020**, *32*, 1905776.
[65] Zhu, D.; Verduzco, R. *ACS Appl. Mater. Interfaces* **2020**, *12*, 33121–33127.
[66] Braunecker, W. A.; Hurst, K. E.; Ray, K. G.; Owczarczyk, Z. R.; Martinez, M. B.; Leick, N.; Keuhlen, A.; Sellinger, A.; Johnson, J. C. *Cryst. Growth Des.* **2018**, *18*, 4160–4166.
[67] Wu, X.; Han, X.; Liu, Y.; Liu, Y.; Cui, Y. *J. Am. Chem. Soc.* **2018**, *140*, 16124–16133.
[68] Mitra, S.; Kandambeth, S.; Biswal, B. P.; Abdul Khayum, M.; Choudhury, C. K.; Mehta, M.; Kaur, G.; Banerjee, S.; Prabhune, A.; Verma, S. *et al. J. Am. Chem. Soc.* **2016**, *138*, 2823–2828.
[69] Li, J.; Zhang, F. Q.; Li, F.; Wu, Z.; Ma, C.; Xu, Q.; Wang, P.; Zhang, X. M. *Chem. Commun.* **2020**, *56*, 2747–2750.
[70] Paltrinieri, L.; Wang, M.; Sachdeva, S.; Besseling, N. A.; Sudhölter, E. J.; De Smet, L. C. *J. Mater. Chem. A* **2017**, *5*, 18476–18485.
[71] Biswal, B. P.; Kandambeth, S.; Chandra, S.; Shinde, D. B.; Bera, S.; Karak, S.; Garai, B.; Kharul, U. K.; Banerjee, R. *J. Mater. Chem. A* **2015**, *3*, 23664–23669.
[72] Chen, X.; Xia, L.; Pan, R.; Liu, X. *J. Colloid Interface Sci.* **2020**, *568*, 76–80.
[73] Castano, I.; Evans, A. M.; Li, H.; Vitaku, E.; Strauss, M. J.; Brédas, J.-L.; Gianneschi, N. C.; Dichtel, W. R. *ACS Cent. Sci.* **2019**, *5*, 1892–1899.
[74] Liu, W.; Li, X.; Wang, C.; Pan, H.; Liu, W.; Wang, K.; Zeng, Q.; Wang, R.; Jiang, J. *J. Am. Chem. Soc.* **2019**, *141*, 17431–17440.
[75] Wang, S.; Zhang, Z.; Zhang, H.; Rajan, A. G.; Xu, N.; Yang, Y.; Zeng, Y.; Liu, P.; Zhang, X.; Mao, Q. *et al. Matter* **2019**, *1*, 1592–1605.
[76] Calik, M.; Sick, T.; Dogru, M.; Döblinger, M.; Datz, S.; Budde, H.; Hartschuh, A.; Auras, F.; Bein, T. *J. Am. Chem. Soc.* **2016**, *138*, 1234–1239.
[77] Zhu, D.; Alemany, L. B.; Guo, W.; Verduzco, R. *Polym. Chem.* **2020**, *11*, 4464–4468.
[78] Maia, R. A.; Oliveira, F. L.; Nazarkovsky, M.; Esteves, P. M. *Cryst. Growth Des.* **2018**, *18*, 5682–5689.
[79] Ma, T.; Kapustin, E. A.; Yin, S. X.; Liang, L.; Zhou, Z.; Niu, J.; Li, L.-H.; Wang, Y.; Su, J.; Li, J. *et al. Science (80-.).* **2018**, *361*, 48–52.
[80] Liang, L.; Qiu, Y.; Wang, W. D.; Han, J.; Luo, Y.; Yu, W.; Yin, G.-L.; Wang, Z.-P.; Zhang, L.; Ni, J. *et al. Angew. Chemie Int. Ed.* **2020**, *59*, 17991–17995.
[81] Lee, G. Y.; Lee, J.; Vo, H. T.; Kim, S.; Lee, H.; Park, T. *Sci. Rep.* **2017**, *7*, 1–10.
[82] Yang, Y.; Faheem, M.; Wang, L.; Meng, Q.; Sha, H.; Yang, N.; Yuan, Y.; Zhu, G. *ACS Cent. Sci.* **2018**, *4*, 748–754.
[83] Wang, H.; Jiao, F.; Gao, F.; Lv, Y.; Wu, Q.; Zhao, Y.; Shen, Y.; Zhang, Y.; Qian, X. *Talanta* **2017**, *166*, 133–140.
[84] Vardhan, H.; Verma, G.; Ramani, S.; Nafady, A.; Al-Enizi, A. M.; Pan, Y.; Yang, Z.; Yang, H.; Ma, S. *ACS Appl. Mater. Interfaces* **2019**, *11*, 3070–3079.

[85] Li, L. H.; Feng, X. L.; Cui, X. H.; Ma, Y. X.; Ding, S. Y.; Wang, W. *J. Am. Chem. Soc.* **2017**, *139*, 6042–6045.
[86] Leng, W.; Ge, R.; Dong, B.; Wang, C.; Gao, Y. *RSC Adv.* **2016**, *6*, 37403–37406.
[87] Zhang, W.; Jiang, P.; Wang, Y.; Zhang, J.; Gao, Y.; Zhang, P. *RSC Adv.* **2014**, *4*, 51544–51547.
[88] Johnson, E. M.; Haiges, R.; Marinescu, S. C. *ACS Appl. Mater. Interfaces* **2018**, *10*, 37919–37927.
[89] Wang, J.; Yang, X.; Wei, T.; Bao, J.; Zhu, Q.; Dai, Z. *ACS Appl. Bio Mater.* **2018**, *1*, 382–388.
[90] Romero, J.; Rodriguez-San-Miguel, D.; Ribera, A.; Mas-Ballesté, R.; Otero, T. F.; Manet, I.; Licio, F.; Abellán, G.; Zamora, F.; Coronado, E. *J. Mater. Chem. A* **2017**, *5*, 4343–4351.
[91] Aiyappa, H. B.; Thote, J.; Shinde, D. B.; Banerjee, R.; Kurungot, S. *Chem. Mater.* **2016**, *28*, 4375–4379.
[92] Kundu, T.; Wang, J.; Cheng, Y.; Du, Y.; Qian, Y.; Liu, G.; Zhao, D. *Dalt. Trans.* **2018**, *47*, 13824–13829.
[93] Baldwin, L. A.; Crowe, J. W.; Pyles, D. A.; McGrier, P. L. *J. Am. Chem. Soc.* **2016**, *138*, 15134–15137.
[94] Mu, M.; Wang, Y.; Qin, Y.; Yan, X.; Li, Y.; Chen, L. *ACS Appl. Mater. Interfaces* **2017**, *9*, 22856–22863.
[95] Han, X.; Zhang, J.; Huang, J.; Wu, X.; Yuan, D.; Liu, Y.; Cui, Y. *Nat. Commun.* **2018**, *9*, 1–10.
[96] Leng, W.; Peng, Y.; Zhang, J.; Lu, H.; Feng, X.; Ge, R.; Dong, B.; Wang, B.; Hu, X.; Gao, Y. *Chem. — A Eur. J.* **2016**, *22*, 9087–9091.
[97] Chen, L.; Zhang, L.; Chen, Z.; Liu, H.; Luque, R.; Li, Y. *Chem. Sci.* **2016**, *7*, 6015–6020.
[98] Sun, Q.; Aguila, B.; Ma, S. *Mater. Chem. Front.* **2017**, *1*, 1310–1316.
[99] Yang, S.; Hu, W.; Zhang, X.; He, P.; Pattengale, B.; Liu, C.; Cendejas, M.; Hermans, I.; Zhang, X.; Zhang, J. *et al. J. Am. Chem. Soc.* **2018**, *140*, 14614–14618.
[100] Kushwaha, R.; Kaleeswaran, D.; Haldar, S.; Chakraborty, D.; Mullangi, D.; Borah, A.; Vinod, C. P.; Murugavel, R.; Vaidhyanathan, R. *ACS Appl. Nano Mater.* **2020**, *3*, 9088–9096.
[101] Waller, P. J.; Lyle, S. J.; Osborn Popp, T. M.; Diercks, C. S.; Reimer, J. A.; Yaghi, O. M. *J. Am. Chem. Soc.* **2016**, *138*, 15519–15522.
[102] Waller, P. J.; Alfaraj, Y. S.; Diercks, C. S.; Jarenwattananon, N. N.; Yaghi, O. M. *J. Am. Chem. Soc.* **2018**, *140*, 9099–9103.
[103] Li, X.; Zhang, C.; Cai, S.; Lei, X.; Altoe, V.; Hong, F.; Urban, J. J.; Ciston, J.; Chan, E. M.; Liu, Y. *Nat. Commun.* **2018**, *9*, 1–8.
[104] Kolb, H. C.; Finn, M.; Sharpless, K. B. *Angew. Chemie Int. Ed.* **2001**, *40*, 2004–2021.
[105] Nagai, A.; Guo, Z.; Feng, X.; Jin, S.; Chen, X.; Ding, X.; Jiang, D. *Nat. Commun. 2011 21* **2011**, *2*, 1–8.
[106] Huang, N.; Krishna, R.; Jiang, D. *J. Am. Chem. Soc.* **2015**, *137*, 7079–7082.
[107] Li, K.; Wong, N. K.; Strauss, M. J.; Evans, A. M.; Matsumoto, M.; Dichtel, W. R.; Adronov, A. *J. Am. Chem. Soc.* **2021**, *143*, 649–656.
[108] *ACS Appl. Mater. Interfaces* **2018**, *10*, 41350–41358.
[109] Dong, B.; Wang, L.; Zhao, S.; Ge, R.; Song, X.; Wang, Y.; Gao, Y. *Chem. Commun.* **2016**, *52*, 7082–7085.
[110] Qian, C.; Qi, Q.-Y.; Jiang, G.-F.; Cui, F.-Z.; Tian, Y.; Zhao, X. *J. Am. Chem. Soc.* **2017**, *139*, 6736–6743.
[111] Zhou, Z. B.; Tian, P. J.; Yao, J.; Lu, Y.; Qi, Q. Y.; Zhao, X. *Nat. Commun.* **2022**, *13*, 1–8.
[112] Qian, H. L.; Meng, F. L.; Yang, C. X.; Yan, X. P. *Angew. Chemie Int. Ed.* **2020**, *59*, 17607–17613.
[113] Cao, C.; Wang, H.; Wang, M.; Liu, Y.; Zhang, Z.; Liang, S.; Yuhan, W.; Pan, F.; Jiang, Z. *J. Memb. Sci.* **2021**, *630*, 119319.
[114] Zhang, Z.; Xiao, A.; Yin, C.; Wang, X.; Shi, X.; Wang, Y. *Chem. Commun.* **2022**, 7136–7139.
[115] Ma, D. L.; Qi, Q. Y.; Lu, J.; Xiang, M. H.; Jia, C.; Lu, B. Y.; Jiang, G. F.; Zhao, X. *Chem. Commun.* **2020**, *56*, 15418–15421.
[116] Cui, Y.; Miao, Z.; Liu, Q.; Jin, F.; Zhai, Y.; Zhang, L.; Wang, W.; Wang, K.; Liu, G.; Zeng, Y. *Chem. Res. Chinese Univ.* **2022**, *38*, 402–408.
[117] Liu, X.; Huang, D.; Lai, C.; Zeng, G.; Qin, L.; Wang, H.; Yi, H.; Li, B.; Liu, S.; Zhang, M. *et al. Chemical Society Reviews* **2019**, 5266–5302.
[118] Zhu, D.; Li, X.; Li, Y.; Barnes, M.; Tseng, C.-P.; Khalil, S.; Rahman, M. M.; Ajayan, P. M.; Verduzco, R. *Chem. Mater.* **2021**, *33*, 413–419.
[119] Nguyen, H. L.; Gropp, C.; Yaghi, O. M. *J. Am. Chem. Soc.* **2020**, *142*, 2771–2776.
[120] Garzón-Tovar, L.; Avci-Camur, C.; Rodríguez-San-Miguel, D.; Imaz, I.; Zamora, F.; Maspoch, D. *Chem. Commun.* **2017**, *53*, 11372–11375.
[121] Evans, A. M.; Ryder, M. R.; Ji, W.; Strauss, M. J.; Corcos, A.; Vitaku, E.; Flanders, N. C.; Bisbey, R. P.; Dichtel, W. *Faraday Discuss.* **2021**, *225*, 226–240.
[122] Emmerling, S. T.; Schuldt, R.; Bette, S.; Yao, L.; Dinnebier, R. E.; Kästner, J.; Lotsch, B. V. *J. Am. Chem. Soc.* **2021**, *143*, 15711–15722.
[123] Sick, T.; Rotter, J. M.; Reuter, S.; Kandambeth, S.; Bach, N. N.; Döblinger, M.; Merz, J.; Clark, T.; Marder, T. B.; Bein, T. *et al. J. Am. Chem. Soc.* **2019**, *141*, 12570–12581.
[124] Chen, X.; Addicoat, M.; Jin, E.; Zhai, L.; Xu, H.; Huang, N.; Guo, Z.; Liu, L.; Irle, S.; Jiang, D. *J. Am. Chem. Soc.* **2015**, *137*, 3241–3247.
[125] Langmuir, I. *J. Am. Chem. Soc.* **1918**, *40*, 1361–1403.
[126] Brunauer, S.; Emmett, P. H.; Teller, E. *J. Am. Chem. Soc.* **1938**, *60*, 309–319.
[127] Rouquerol, G. M. F.; Rouquerol, J.; Sing, K.; Llewllyn, P. *Adsorption by Powders and Porous Solids*; 2014.
[128] Osterrieth, J. W. M.; Rampersad, J.; Madden, D.; Rampal, N.; Skoric, L.; Connolly, B.; Allendorf, M. D.; Stavila, V.; Snider, J. L.; Ameloot, R. *et al. Adv. Mater.* **2022**, 2201502.

[129] Jagiello, J.; Olivier, J. P. *Carbon N. Y.* **2013**, *55*, 70–80.
[130] Etter, M.; Dinnebier, R. E. *Zeitschrift für Anorg. und Allg. Chemie* **2014**, *640*, 3015–3028.
[131] Bragg, W. H.; Bragg Apr, W. L.; H Bragg, B. W.; Professor of Physics, C. *Proc. R. Soc. London. Ser. A, Contain. Pap. a Math. Phys. Character* **1913**, *88*, 428–438.
[132] Debye, P.; Scherrer, P. *Nachrichten von der Gesellschaft der Wissenschaften zu GÃ¶ttingen, Mathematisch-Physikalische Klasse* **1916**, *1916*, 1–15.
[133] Holder, C. F.; Schaak, R. E. *ACS Nano* **2019**, *13*, 7359–7365.
[134] Scherrer, P. *Bestimmung der Größe und der Inneren Struktur von Kolloidteilchen mittels Röntgenstrahlung*, 2nd ed.; Göttinger Nachrichten Gesell., 1918; pp 98–100.
[135] Duer, M. J. *Introduction to solid-state NMR spectroscopy*; Blackwell, 2004; p 349.
[136] Laws, D. D.; Bitter, H.-M. L.; Jerschow, A. *Angew. Chemie Int. Ed.* **2002**, *17*, 3096–3129.
[137] Peng, H.; Raya, J.; Richard, F.; Baaziz, W.; Ersen, O.; Ciesielski, A.; Samorì, P. *Angew. Chemie Int. Ed.* **2020**, *59*, 19602–19609.
[138] Myers, A. L.; Prausnitz, J. M. *AIChE J.* **1965**, *11*, 121–127.
[139] Walton, K. S.; Sholl, D. S. *AIChE J.* **2015**, *61*, 2757–2762.
[140] Wang, P.; Peng, Y.; Zhu, C.; Yao, R.; Song, H.; Kun, L.; Yang, W.; Wang, P.; Peng, Y.; Zhu, C. *et al. Angew. Chemie Int. Ed.* **2021**, *60*, 19047–19052.
[141] Wang, J.; Zhuang, S. *Coord. Chem. Rev.* **2019**, *400*, 213046.
[142] Freund, R.; Zaremba, O.; Arnauts, G.; Ameloot, R.; Skorupskii, G.; Dincă, M.; Bavykina, A.; Gascon, J.; Ejsmont, A.; Goscianska, J. *et al. Angew. Chemie Int. Ed.* **2021**, *60*, 23975–24001.
[143] Qian, H. L.; Yang, C. X.; Wang, W. L.; Yang, C.; Yan, X. P. *J. Chromatogr. A* **2018**, *1542*, 1–18.
[144] Guan, Q.; Zhou, L. L.; Li, W. Y.; Li, Y. A.; Dong, Y. B. *Chem. — A Eur. J.* **2020**, *26*, 5583–5591.
[145] Zhao, X.; Pachfule, P.; Thomas, A. *Chem. Soc. Rev.* **2021**, *50*, 6871–6913.
[146] Skorjanc, T.; Shetty, D.; Valant, M. *ACS Sensors* **2021**, *6*, 1461–1481.
[147] Cui, F.-Z.; Xie, J.-J.; Jiang, S.-Y.; Gan, S.-X.; Ma, D.-L.; Liang, R.-R.; Jiang, G.-F.; Zhao, X. *Chem. Commun.* **2019**, *55*, 4550–4553.
[148] Bu, R.; Zhang, L.; Liu, X. Y.; Yang, S. L.; Li, G.; Gao, E. Q. *ACS Appl. Mater. Interfaces* **2021**, *13*, 26431–26440.
[149] Chen, Z.; Wang, K.; Hu, X.; Shi, P.; Guo, Z.; Zhan, H. *ACS Appl. Mater. Interfaces* **2021**, *13*, 1145–1151.
[150] Ascherl, L.; Evans, E. W.; Gorman, J.; Orsborne, S.; Bessinger, D.; Bein, T.; Friend, R. H.; Auras, F. *J. Am. Chem. Soc.* **2019**, *141*, 15693–15699.
[151] Chen, G.; Lan, H.-H.; Cai, S.-L.; Sun, B.; Li, X.-L.; He, Z.-H.; Zheng, S.-R.; Fan, J.; Liu, Y.; Zhang, W.-G. *ACS Appl. Mater. Interfaces* **2019**, *11*, 12830–12837.
[152] Das, G.; Biswal, B. P.; Kandambeth, S.; Venkatesh, V.; Kaur, G.; Addicoat, M.; Heine, T.; Verma, S.; Banerjee, R. *Chem. Sci.* **2015**, *6*, 3931–3939.
[153] Rodríguez, A.; Rico, E.; Sierra, C.; Rodríguez, O. *Sensors* **2020**, *20*, 1385.
[154] Zhang, Y.; Zhang, W.; Li, Q.; Chen, C.; Zhang, Z. *Sensors Actuators B Chem.* **2020**, *324*, 128733.
[155] Ko, W. C.; Kim, M. S.; Kwon, Y. J.; Jeong, J.; Kim, W. R.; Choi, H.; Park, J. K.; Jeong, Y. K. *J. Mater. Chem. A* **2020**, *8*, 19246–19253.
[156] Niu, F.; Shao, Z. W.; Zhu, J. L.; Tao, L. M.; Ding, Y. *J. Mater. Chem. C* **2021**, *9*, 8562–8569.
[157] Yuan, H.; Li, N.; Linghu, J.; Dong, J.; Wang, Y.; Karmakar, A.; Yuan, J.; Li, M.; Buenconsejo, P. J. S.; Liu, G. *et al. ACS Sensors* **2020**, *5*, 1474–1481.
[158] S., Y.; Li, X.; Zhu, J.; Zhang, G.; Van Puyvelde, P.; Van der Bruggen, B. *Chem. Soc. Rev.* **2019**, *48*, 2665–2681.
[159] Han, X. H.; Gong, K.; Huang, X.; Yang, J. W.; Feng, X.; Xie, J.; Wang, B. *Angew. Chemie Int. Ed.* **2022**, *61*, e202202912.
[160] Lyu, H.; Li, H.; Hanikel, N.; Wang, K.; Yaghi, O. M. *J. Am. Chem. Soc.* **2022**, *144*, 12989–12995.
[161] IPCC,; Masson-Delmotte, V.; Zhai, P.; Pirani, A.; Connors, S.; Péan, C.; Berger, S.; Caud, N.; Chen, Y.; Goldfarb, L. *et al. Climate change 2021: The physical science basis. contribution of working group I to the sixth assessment report of the intergovernmental panel on climate change*; Cambridge University Press: Cambridge, United Kingdom and New York, NY, USA, 2021.
[162] Dlugokencky, E.; Dr. Pieter Tans, NOAA/GML (gml.noaa.gov/ccgg/trends/),; Dr. Ralph Keeling, Scripps Institution of Oceanography (scrippsco2.ucsd.edu/), Trends in atmospheric carbon dioxide. https://gml.noaa.gov/ccgg/trends/.
[163] Bui, M.; Adjiman, C. S.; Bardow, A.; Anthony, E. J.; Boston, A.; Brown, S.; Fennell, P. S.; Fuss, S.; Galindo, A.; Hackett, L. A. *et al. Energy Environ. Sci.* **2018**, *11*, 1062–1176.
[164] Zeng, Y.; Zou, R.; Zhao, Y. *Adv. Mater.* **2016**, *28*, 2855–2873.
[165] Sekizkardes, A. K.; Altarawneh, S.; Kahveci, Z.; Islamoğlu, T.; El-Kaderi, H. M. *Macromolecules* **2014**, *47*, 8328–8334.
[166] Islamoğlu, T.; Gulam Rabbani, M.; El-Kaderi, H. M. *J. Mater. Chem. A* **2013**, *1*, 10259–10266.
[167] Fu, Y.; Wang, Z.; Fu, X.; Yan, J.; Liu, C.; Pan, C.; Yu, G. *J. Mater. Chem. A* **2017**, *5*, 21266–21274.
[168] Mahato, M.; Nam, S.; Tabassian, R.; Oh, S.; Nguyen, V. H.; Oh, I. K. *Adv. Funct. Mater.* **2022**, *32*, 2107442.
[169] Zu, Y.; Li, J.; Li, X.; Zhao, T.; Ren, H.; Sun, F. *Microporous Mesoporous Mater.* **2022**, *334*, 111779.
[170] Zhao, S.; Dong, B.; Ge, R.; Wang, C.; Song, X.; Ma, W.; Wang, Y.; Hao, C.; Guo, X.; Gao, Y. *RSC Adv.* **2016**, *6*, 38774–38781.
[171] Popp, N.; Homburg, T.; Stock, N.; Senker, J. *J. Mater. Chem. A* **2015**, *3*, 18492–18504.

[172] Das, S. K.; Wang, X.; Ostwal, M. M.; Lai, Z. *Sep. Purif. Technol.* **2016**, *170*, 68–77.
[173] Huang, N.; Chen, X.; Krishna, R.; Jiang, D.; Huang, N.; Chen, X.; Jiang, D.; Krishna, R. *Angew. Chemie Int. Ed.* **2015**, *54*, 2986–2990.
[174] Wang, Y.; Kang, C.; Zhang, Z.; Usadi, A. K.; Calabro, D. C.; Baugh, L. S.; Yuan, Y. D.; Zhao, D. *ACS Sustain. Chem. Eng.* **2022**, *10*, 332–341.
[175] Gomes, R.; Bhaumik, A. *RSC Adv.* **2016**, *6*, 28047–28054.
[176] Kaleeswaran, D.; Vishnoi, P.; Murugavel, R. *J. Mater. Chem. C* **2015**, *3*, 7159–7171.
[177] Halder, A.; Karak, S.; Addicoat, M.; Bera, S.; Chakraborty, A.; Kunjattu, S. H.; Pachfule, P.; Heine, T.; Banerjee, R. *Angew. Chem. Int. Ed.* **2018**, *57*, 5797–5802.
[178] Wang, Y.; Liu, Y.; Li, H.; Guan, X.; Xue, M.; Yan, Y.; Valtchev, V.; Qiu, S.; Fang, Q. *J. Am. Chem. Soc.* **2020**, *142*, 3736–3741.
[179] Bai, L.; Phua, S. Z. F.; Lim, W. Q.; Jana, A.; Luo, Z.; Tham, H. P.; Zhao, L.; Gao, Q.; Zhao, Y. *Chem. Commun.* **2016**, *52*, 4128–4131.
[180] Fan, H.; Mundstock, A.; Feldhoff, A.; Knebel, A.; Gu, J.; Meng, H.; Caro, J. *J. Am. Chem. Soc.* **2018**, *140*, 10094–10098.
[181] Silvestre-Albero, A. M.; Juárez-Galán, J. M.; Silvestre-Albero, J.; Rodríguez-Reinoso, F. *J. Phys. Chem. C* **2012**, *116*, 16652–16655.
[182] Yang, J.; Acharjya, A.; Ye, M. Y.; Rabeah, J.; Li, S.; Kochovski, Z.; Youk, S.; Roeser, J.; Grüneberg, J.; Schwarze, M. *et al. Angew. Chem., Int. Ed.* **2021**, *60*, 19797–19803.
[183] Dautzenberg, E.; Lam, M.; Li, G.; de Smet, L. C. P. M. *Nanoscale* **2021**, *13*, 19446–19452.
[184] Karak, S.; Kumar, S.; Pachfule, P.; Banerjee, R. *J. Am. Chem. Soc.* **2018**, *140*, 5138–5145.
[185] Sun, D.; Kim, D. P. *ACS Appl. Mater. Interfaces* **2020**, *12*, 20589–20595.
[186] Mo, J.; Chen, H.; Lin, T. Method for preparing covalent organic framework material by mechanical ball milling method. 2020.
[187] Chen, L.; Zhou, C.; Yang, H.; Lin, J.; Ge, Y.; Zhou, W.; Lu, C.; Tan, L.; Dong, L. *Chem. Commun.* **2021**,
[188] Feriante, C.; Evans, A. M.; Jhulki, S.; Castano, I.; Strauss, M. J.; Barlow, S.; Dichtel, W. R.; Marder, S. R. *J. Am. Chem. Soc.* **2020**, *23*, 18637–18644.
[189] Zhang, Y.; Položij, M.; Heine, T. *Chem. Mater.* **2022**, *34*, 2376–2381.
[190] van Meerten, S. G.; Franssen, W. M.; Kentgens, A. P. *J. Magn. Reson.* **2019**, *301*, 56–66.
[191] Yuan, Y. C.; Sun, B.; Cao, A. M.; Wang, D.; Wan, L. J. *Chem. Commun.* **2018**, *54*, 5976–5979.
[192] Kubelka, P.; Munk, F. *Zeitschrift für Tech. Phys.* **1931**, *12*, 593–601.
[193] Tauc, J. *Mater. Res. Bull.* **1968**, *3*, 37–46.
[194] Talu, O. *Adv. Colloid Interface Sci.* **1998**, *76-77*, 227–269.
[195] Cessford, N. F.; Seaton, N. A.; Düren, T. *Ind. Eng. Chem. Res.* **2012**, *51*, 4911–4921.
[196] An, X.; Zhao, K.; Zhang, W.; Yang, J.; Liao, Y.; Wang, L.; Fu, D. *Fuel* **2022**, *309*, 122175.
[197] Cai, X.; Gharagheizi, F.; Bingel, L. W.; Shade, D.; Walton, K. S.; Sholl, D. S. *Ind. Eng. Chem. Res.* **2021**, *60*, 639–651.
[198] Gharagheizi, F.; Sholl, D. S. *Ind. Eng. Chem. Res.* **2022**, *61*, 727–739.
[199] Lee, S.-P.; Mellon, N.; Shariff, A. M.; Leveque, J.-M. *New J. Chem.* **2018**, *42*, 15488–15496.
[200] Lee, S.-P.; Mellon, N.; Shariff, A. M.; Leveque, J.-M. *J. Nat. Gas Sci. Eng.* **2018**, *50*, 139–146.
[201] Liu, B.; Yu, L.; Wang, H.; Ma, X.; Zeng, Z.; Li, L. *Chem. Eng. J.* **2022**, *435*, 135069.
[202] Kundu, A.; Sillar, K.; Sauer, J. *Chem. Sci.* **2020**, *110*, 643–655.
[203] Stegbauer, L.; Hahn, M. W.; Jentys, A.; Savasci, G.; Ochsenfeld, C.; Lercher, J. A.; Lotsch, B. V. *Chem. Mater.* **2015**, *27*, 7874–7881.
[204] Lan, J.; Cao, D.; Wang, W.; Smit, B. *ACS Nano* **2010**, *4*, 4225–4237.
[205] Hammett, L. P. *Chem. Rev.* **1935**, *17*, 125–136.
[206] Hammett, L. P. *J. Am. Chem. Soc.* **1937**, *59*, 96–103.
[207] Hansch, C.; Leo, A.; Unger, S. H.; Kim, K. H.; Nikaitani, D.; Lien, E. J. *J. Med. Chem.* **1973**, *16*, 1207–1216.
[208] Hansch, C.; Leo, A.; Taft, R. W. *Chem. Rev.* **1991**, *91*, 165–195.
[209] Keenan, S. L.; Peterson, K. P.; Peterson, K.; Jacobson, K. *J. Chem. Educ.* **2008**, *85*, 558–560.
[210] Schultz, D.; Nitschke, J. R. *J. Am. Chem. Soc.* **2006**, *128*, 9887–9892.
[211] Schoustra, S. K.; Dijksman, J. A.; Zuilhof, H.; Smulders, M. M. *Chem. Sci.* **2021**, *12*, 293–302.
[212] Hesse, M.; Meier, H.; Zeeh, B. *Spectroscopic Methods in Organic Chemistry*, 2nd ed.; Georg Thieme Verlag, 2008; p 58.
[213] Dautzenberg, E.; Lam, M.; Nikolaeva, T.; Franssen, W. M.; van Lagen, B.; Gerrits-Benneheij, I. P.; Kosinov, N.; Li, G.; de Smet, L. C. *J Phys Chem C,* **2022**, *126*, 21338–21347.
[214] Baer, D. R.; Artyushkova, K.; Brundle, C. R.; Castle, J. E.; Engelhard, M. H.; Gaskell, K. J.; Grant, J. T.; Haasch, R. T.; Linford, M. R.; Powell, C. J. *et al. J. Vac. Sci. Technol. A Vacuum, Surfaces, Film.* **2019**, *37*, 031401.
[215] Easton, C. D.; Kinnear, C.; McArthur, S. L.; Gengenbach, T. R. *J. Vac. Sci. Technol. A Vacuum, Surfaces, Film.* **2020**, *38*, 023207.
[216] Liu, Y.; Dikhtiarenko, A.; Xu, N.; Sun, J.; Tang, J.; Wang, K.; Xu, B.; Tong, Q.; Heeres, H. J.; He, S. *et al. Chem. — A Eur. J.* **2020**, *26*, 12134–12139.
[217] Altarawneh, S.; Islamoğlu, T.; Sekizkardes, A. K.; El-Kaderi, H. M. *Environ. Sci. Technol.* **2015**, *49*, 4715–4723.

[218] Dautzenberg, E.; van Hurne, S.; Smulders, M. M.; de Smet, L. C. *Comput. Phys. Commun.* **2022**, 108494.
[219] Principe, I. A.; Fletcher, A. J. *Adsorption* **2020**, *26*, 723–735.
[220] Zhai, Y.; Liu, G.; Jin, F.; Zhang, Y.; Gong, X.; Miao, Z.; Li, J.; Zhang, M.; Cui, Y.; Zhang, L. *et al. Angew. Chemie - Int. Ed.* **2019**, *58*, 17679–17683.
[221] Li, Z.; Ding, X.; Feng, Y.; Feng, W.; Han, B. H. *Macromolecules* **2019**, *52*, 1257–1265.
[222] Kohl, A.; Nielsen, R. *Gas Purification*, 5th ed.; Gulf Publishing Company: Houston, Texas, 1997.
[223] Rabbani, M. G.; El-Kaderi, H. M. *Chem. Mater.* **2011**, *23*, 1650–1653.
[224] Sekizkardes, A. K.; Altarawneh, S.; Kahveci, Z.; Islamoğlu, T.; ; El-Kaderi, H. M. *Macromolecules* **2014**, *47*, 8328–8334.
[225] Altarawneh, S.; Behera, S.; Jena, P.; El-Kaderi, H. M. *Chem. Commun.* **2014**, *50*, 3571–3574.
[226] Rabbani, M. G.; Reich, T. E.; Kassab, R. M.; Jackson, K. T.; El-Kaderi, H. M. *Chem. Commun.* **2012**, *48*, 1141–1143.
[227] Rabbani, M. G.; El-Kaderi, H. M. *Chem. Mater.* **2012**, *24*, 1511–1517.
[228] Nandi, S.; Kumar Singh, S.; Mullangi, D.; Illathvalappil, R.; George, L.; Vinod, C. P.; Kurungot, S.; Vaidhyanathan, R.; Nandi, S.; Mullangi, D. *et al. Adv. Energy Mater.* **2016**, *6*, 1601189.
[229] Patra, B. C.; Khilari, S.; Satyanarayana, L.; Pradhan, D.; Bhaumik, A. *Chem. Commun.* **2016**, *52*, 7592–7595.
[230] Byrd, E. F.; Scuseria, G. E.; Chabalowski, C. F. *J. Phys. Chem. B* **2004**, *108*, 13100–13106.
[231] Dautzenberg, E.; Claassen, F.; de Smet, L. C. *Microporous and Mesoporous Materials,* **2023**, *350*, 112318.
[232] Commission, E.; Centre, J. R.; Olivier, J.; Guizzardi, D.; Schaaf, E.; Solazzo, E.; Crippa, M.; Vignati, E.; Banja, M.; Muntean, M. *et al. GHG emissions of all world : 2021 report*; Publications Office, 2021.
[233] Gui, B.; Liu, X.; Cheng, Y.; Zhang, Y.; Chen, P.; He, M.; Sun, J.; Wang, C. *Angew. Chemie Int. Ed.* **2021**,
[234] Altundal, O. F.; Altintas, C.; Keskin, S. *J. Mater. Chem. A* **2020**, *8*, 14609–14623.
[235] Simon, C. M.; Smit, B.; Haranczyk, M. *Comput. Phys. Commun.* **2016**, *200*, 364–380.
[236] Iacomi, P.; Llewellyn, P. L. *Adsorption* **2019**, *25*, 1533–1542.
[237] Lee, S.; Lee, J. H.; Kim, J. *Korean J. Chem. Eng.* **2018**, *35*, 214–221.
[238] ISO Central Secretary, *ISO 9241-11:2018(en): Ergonomics of human-system interaction — Part 11: Usability: Definitions and concepts*; Standard, 2018.
[239] Lam, M. Influence of pore size and methylation on the physicochemical properties of imine-linked covalent organic frameworks. M.Sc. thesis, Wageningen Universtiy & Research, 2021.
[240] Zhu, D.; Zhang, J.-J.; Wu, X.; Yan, Q.; Liu, F.; Zhu, Y.; Gao, X.; Rahman, M. M.; Yakobson, B. I.; Ajayan, P. M. *et al. Chem. Sci.* **2022**,
[241] Tran, L. D.; Presley, K. F.; Streit, J. K.; Carpena-Núñez, J.; Beagle, L. K.; Grusenmeyer, T. A.; Dalton, M. J.; Vaia, R. A.; Drummy, L. F.; Glavin, N. R. *et al. Chem. Mater.* **2022**, acs.chemmater.1c02565.
[242] Yang, J. G. S. *Nat. Commun.* **2022**, *13*, 1–10.
[243] Chavez, A. D.; Evans, A. M.; Landers, N.; Bisbey, R. P.; Vitaku, E.; Chen, L. X.; Dichtel, a. R.; Chavez, D.; Evans, A. M.; Flanders, N. C. *et al. Chem. — A Eur. J.* **2018**, *24*, 3989–3993.
[244] Sharma, A.; Jindal, J.; Mittal, A.; Kumari, K.; Maken, S.; Kumar, N. *Environ. Chem. Lett.* **2021**, *19*, 875–910.
[245] Singh, H.; Tomer, V. K.; Jena, N.; Bala, I.; Sharma, N.; Nepak, D.; De Sarkar, A.; Kailasam, K.; Pal, S. K. *J. Mater. Chem. A* **2017**, *5*, 21820–21827.
[246] Sachdeva, S.; Venkatesh, M. R.; Mansouri, B. E.; Wei, J.; Bossche, A.; Kapteijn, F.; Zhang, G. Q.; Gascon, J.; de Smet, L. C.; Sudhölter, E. J. *Small* **2017**, *13*, 1–6.
[247] Xia, B.; Matavž, A.; Tu, M.; Rubio-Giménez, V.; Tietze, M. L.; Marreiros, J.; Ceyssens, F.; Cresens, C.; Wauteraerts, N.; Kubarev, A. *et al. Adv. Funct. Mater.* **2022**, *32*, 2204065.
[248] Bürgi, T. *Nanoscale* **2015**, *7*, 15553–15567.
[249] Ryu, J. H.; Messersmith, P. B.; Lee, H. *ACS Appl. Mater. Interfaces* **2018**, 7523–7540.
[250] Lee, H.; Dellatore, S. M.; Miller, W. M.; Messersmith, P. B. *Science (80-.).* **2007**, *318*, 426–430.
[251] Svoboda, J.; Král, M.; Dendisová, M.; Matějka, P.; Pop-Georgievski, O. *Colloids Surfaces B Biointerfaces* **2021**, *205*, 111897.
[252] Liu, X.-H.; Mo, Y.-P.; Yue, J.-Y.; Zheng, Q.-N.; Yan, H.-J.; Wang, D.; Wan, L.-J. *Small* **2014**, *10*, 4934–4939.
[253] Liu, X.-H.; Guan, C.-Z.; Ding, S.-Y.; Wang, W.; Yan, H.-J.; Wang, D.; Wan, L.-J. *J. Am. Chem. Soc.* **2013**, *135*, 10470–10474.
[254] Dey, K.; Pal, M.; Rout, K. C.; Kunjattu, S. S.; Das, A.; Mukherjee, R.; Kharul, U. K.; Banerjee, R. *J. Am. Chem. Soc.* **2017**, *139*, 13083–13091.

About the author

“It does not matter how slowly you go

as long as you do not stop”

— Confucius

Overview of completed training activities

Discipline specific activity	Organising Institute	Year
Advanced organic chemistry	VLAG & ORC	2018-2022
Molecular life sciences	VLAG & ORC	2018-2022
CHAINS 7^{th} conference*	NWO	2019
CHAINS 8^{th} conference	NWO	2020
EuroMOF conference 2021 Krakow*	DECHEMA	2020
CHAINS 9^{th} conference**	NWO	2021
MOF2022 Dresden*	DECHEMA	2022
Micromeritics seminar on physisorption	Mircomeritics B.V.	2022
Bronkhorst customer product training	Bronkhorst B.V.	2022

General courses	Organising Institute	Year
VLAG PhD week	VLAG	2019
Scientific Artwork	WUR Library	2019
Effective behaviour in professional surroundings	WGS	2019
Presenting with impact	WGS	2020
Career Prespectives	WGS	2022

Teaching activities	Year
Bio-organic chemistry	2019-2021
Organic chemistry 1	2020-2021
Organic chemistry 1	2021
Bio-organic chemistry for life sciences	2020-2021
Supervision of MSc students	2019-2021

Other activities	Year
Preparation of research proposal	2018
Colloquia & Material Science Meetings	2018-2022
PhD study tour to Israel*	2019
Organisation of PhD study trip during pandemic	2020-2022

* poster presentation, ** talk

Acknowledgments

“As long as I don't write about the government, religion, politics, and other institutions,

I am free to print anything”

— Pierre-Augustin Beaumarchais

After years of work, thousands of words, and hours of formatting, I can write the most-read part of my thesis, which is most likely also the chapter that can disappoint the most. I am extremely grateful for all the openness, support, and appreciation that I received not only over the last four years. I would have never been able to master a PhD without the help on many people. This one is for all of you!

My first address goes to my promoter and daily supervisor **Louis de Smet** for the freedom and independence I got in nearly all aspects. We are both very perfectionistic, but in different ways that complemented each other. Nowadays, almost everybody tells me how much I have grown over the last years, and you also contributed to me becoming a stronger person.

My supervision team was completed by **Han Zuilhof**, who did not only contributed to my successful PhD, but also took care of me when I got sick in the middle of the Israeli desert. **Han**, thank you for your visible and invisible contributions that helped me growing.

To all members of my thesis committee (**Monique van der Veen, Rob Ameloot, Harry Bitter, Arne Thomas**) a big *Thank You* for the time and effort you spent in evaluating my thesis.

Another thank you goes to my paranymphs **Arne** and **Sybren** who helped me a lot and support me on stage. I am glad to have you there, sharing the day with me, and making sure that I remain as little nervous as possible. My inofficial third paranymph **Andriy** was a huge help, finalising my thesis and going through all bureaucratic steps. Thank you guys, I am glad to have such good friends at my side!

During a PhD, you do not always work alone on a project, but there are more people involved that put a lot of effort to support me. My Master students **Mees Vos** and **Milena Lam** both worked very dedicated on parts of my project and I am very grateful for the time that we spent together. Both of you are amazing people and I am happy that we managed to keep in touch every now and then. **Jochem Janssen**, you had a difficult internship, because the pandemic kicked in. Thank you for being so open for pragmatic solutions in that time.

A big thank you to the entire group of BCT, in particular **Marlene Führer, Nazila Masoud, Tomas van Haasterecht** and **Harry Bitter**. In my first two years, I was allowed to access your physisorption equipment. I learned all the basics and even a bit more from you and you were still welcoming me in guest shifts when the pandemic made it difficult to perform research.

Katharina Peikert, Luca Lucarelli, and **Jouk Hamelik**, I thank you for your open ears, and for your genuine interest in me and my work beyond your own responsibilities.

Next to the physisorption measurements, solid-state NMR soon became one of my standard techniques. This would have not been possible without **Tatiana Nikolaeva, Wouter Franssen** and **Yangzhang Luo**. I am grateful for all the lessons you taught me and I really enjoyed our collaboration. **Tatiana**, you even trusted me so much that you gave me independent user access, which facilitated my work a lot. I am really happy that our collaboration resulted together with **Wouter** in a publication.

I am thankful for the training on the diffuse reflection measurements that I got from **Rob Koehorst** and all the brainstorming we did together on the analysis of my data. Even after your retirement, you and your colleague **Cor Wolfs** were still always open for my questions, which I do not take for granted.

Barend van Lagen, many thanks for measuring my samples on the PXRD on a daily basis and **Guanna Li** for the DFT-computed structures that were needed to analyse the diffractograms. For their help with my PXRD analysis, I thank **Nikolay Kosinov** and **Ilse Gerrits-Benneheij**. Without the help of all of you, my work would not have been possible!

There was a point in my PhD where I needed programming knowledge. Thank you **Simon van Hurne** for helping me out, explaining to me the example code and developing together with me the idea of programming our own software so that future PhDs without this knowledge would not be as lost as I was. Thank you **Maarten Smulders** and **Louis** for supporting this idea!

Next to this more research-related support, much more is needed to successfully work on a PhD project. **Frank Claassen** and **Hans Beijleveld**, thank you both for your support with purchasing our own physisorption instrument and the measurements you did for me. **Frank**, thank you in particular for all the measurements you made when I could not perform lab work after my little surgery. It was a lot of fun with you guys when we had drinks at Proost. **Barend**, you have been a huge support for me in all these years. Thank you for always thinking along with me to find the best experimental proof for all questions and also for our private chats. **Elly Geurtsen** and **Aleida Ruisch**, without you, ORC would not be the same. Thank you for always finding solutions for my organisational questions and booking a date for me for the first time in the new system Hora Finita. **Henny Li**, thank you for purchasing all my orders and for the fun times during game nights. I will always have fond memories of our Bio-Organic Chemistry practicals that were a lot of fun thanks to our teaching staff **Anne-Marie Franssen, Dieuwertje Streefkerk, Hendra Willemsen, Judith Firet** and **Tjerk Sminia**. I learned a lot during these weeks and really enjoyed our conversations in the few moments when no student had a question. **Judith** and **Tjerk**, you taught me the relevant things for each practical and were always

available for questions as well as to help me out when I could not be at several places simultaneously. **Tjerk**, thank you for taking me (and some others) to the highest waterfall in the Netherlands and guiding me to many beautiful places. **Annelies van Bok**, we first met online in a break-out room for a small coffee break. It was always great to talk to you and get advises from somebody who was a step further in finishing her PhD. Thank you for your support in all those times with words and with actions.

For all interesting discussions about chemistry in general or in particular my research challenges, I thank **Maarten Smulders, Fedor Miloserdov**, and **Maurice Franssen**. Knowing that there are people around that I could ask for help, gave me a lot of security. **Maurice**, I really enjoyed when you walked by to our Friday evening drinks and games and all the lunch conversations that we had over the last years.

Dieuwertje, I am so happy that you joined ORC during my PhD. Since you also made some of my building blocks in your PhD, you were always my first address to discuss synthetic problems. Thank you for always making time for my questions and for all the help you provided. Usually, our conversations did not stop at chemistry. Instead, we continued to discuss many other items, like the honey badger. Thank you for all the advices, all the pep talks, and all the laughter.

During my PhD, I was surrounded by many other PhDs who shared the good and the less good moments with me. To my first office mates **Alyssa, Fred, Pepijn, Jay**, and **Sevil**, thank you for introducing me to ORC and all the small chats that we had in breaks. I was not the only one starting at that time and it was great for me to share all four years with **Alyssa, Jay, Lucas**, and **Sybren**. **Alyssa**, you are incredibly supportive. Thank you for the uncounted times when you helped me with my research. **Lucas**, even though we never made it to a second PhD trip, it was great trying to organise it with you! **Jordi** and **Ian**, thank you for organising the first PhD trip to Israel and welcoming me even though I joined last minute and messed up your finances. **Pepijn**, thank you for going extra mile with me and always offering two more inches. I will never forget our PhD trip to Isreal and the desert adventures (**Michel**). **Esther**, you are such a lovely person and I enjoyed all of our conversations. Thank you for bringing me to the next accommodation when I was sick and sleeping in the back of the van! **Jorick**, you will always remain my personal Merlin. Thanks for all thoughtful conversations. You are a true friend! **Rafael**, thanks for deepening my understanding of physisorption, and **Thijmen** thank you for understanding my time struggles so well. **Daniele**, it was always fun having you around for a coffee, and **Ariadni, Irene**, and **Clementina** thanks for the nice chats. **Julian**, I will miss your detailed descriptions of delicious food. Having the French croissants for a Christmas breakfast remains one of

my highlights!
Later, I moved offices, so I want to thank **Alice, Annemieke, Bas, Sybren**, and **Simon** for their warm welcome and the fun we had during work. **Alice**, nobody can type on a keyboard as you can. I truly miss the sounds. **Andriy**, our (not-so-)secret office mate, I always enjoyed listening to you while working! **Shauni, Marieke, Hamit**, and **Sjoerd**, I had many good, supportive, funny, and thoughtful conversations and I wish all of you just the best for the future. **Carolina**, the same goes for you. We will meet in Zürich! **Martijn**, you are such a cheerful and intelligent guy that it was always fun to chat with you about work, life, karate, piano, climbing,... Thank you for being an adopted ORC member! Now, **Sybren** and **Jordi**, all, that is left to say, is: “It is done!”

Für zahlreiche Lernsessions während meines Bachelor- und Master-Studiums bedanke ich mich bei **Simon Thölke, Carsten Hackler** und **Isabel Arndt**. Für das Ende deiner eigenen Promotion wüsche ich dir, **Simon**, nur das allerbeste. Danke auch für all die Telefonate und dass ich mit dir und **Arne** nochmal einen “privaten AK” zum diskutieren hatte, der immer spontan verfügbar war.

Auf der Arbeit verbringen wir ein Drittel des Tages und sogar die Hälfte unserer wachen Zeit, daher gibt es kaum etwas wichtigeres, als sich an diesem Ort wohl zu fühlen. Ich danke **Jan-Michael Stepper** mit der iSQUARED AG dafür, Teil eines handverlesenen Teams sein zu dürfen, in welchem neben der fachlichen Kompetenz auch der menschliche Aspekt nicht zu kurz kommt. Bei meinen neuen Kollegen, insbesondere dem R&D Team **Arne, Michael, Robin, Roman, Stephan**, möchte ich mich für die offene und herzliche Aufnahme in eure Mitte bedanken. Ich freue mich schon auf die Zeit mit euch während und auch nach der Arbeit und möchte hiermit auch die denkwürdige Fahrweise von Tim würdigen!

Karate has been my second home for 20 years now. The lessons I learned there were not only physical, but also philosophical and mental, which had a huge impact on my mindset and my life. To my childhood trainer **Bernd**: thank you for teaching me the spirit and beauty of karate. To **Dirk** and **Ludwig**, thank you for teaching me all the lessons that went way beyond sport. You are both amazing people who always support others.
Ludwig, du bist der typische “Rheinländer”: offen und herzlich. Dein direktes Feedback über mich hat mich sehr weitergebracht. Dank dir ist aus dem schüchternen Entlein nun eine Kampfziege geworden! And also in the Netherlands, karate has become my second home. **Bas** and **Rudy** thank you for your support. **Constantijn, Herman, Christian**, and **Martijn**, I had a lot of fun training with you guys and also going for beers to Arnhem. Thanks for keeping an eye on my well-being and taking me as I am. I

will always remember “Nein, Ellen, nein!”.
Representative for my SKA family, I thank **Eefje, Claudia, Jon**, and **Sjors**. I felt home faster than I ever did before in this group. **Claudia**, you came back from Italy and dragged me right into the middle of the group. **Eefje**, I had a lot of fun training hard together with you. **Sjors** and **Jon**, you made me the fittest Ellen ever and I am a little bit afraid that I might not feel challenged enough for fitness in Switzerland. My gratitute goes beyond those people mentioned, but listing all would have exceed the limits of this chapter.

Danke **Claudia** und **Sven** für eure offene und herzliche Art, und dass ihr mich mit allen Stärken und Schwächen unterstützt. Es macht immer Spaß etwas mit euch zu unternehmen, zum Beispiel Motorradtouren, Kinobesuche oder Spieleabende.

Niklas, Quantität sagt nichts über Qualität. Du bist einer der intelligensten und ehrgeizigsten Menschen, die ich kenne. Deine Anrufe zu Chemiefragen während des Studiums waren nie leicht zu beantworten und haben mir immer sehr viel Spaß gemacht! Mit den Bravo Hits hat es zwar nicht geklappt, aber dafür haben wir beide bald unserer Titel.

Sevil, you have been my partner in crime during the PhD for so many years. It was a pleasure to be in an office with you and I appreciated every single conversation and every coffee. We have shared so many experiences, game nights, and hours. Thank you for being the positive and open person that you are and thank you for being my go-to person especially during the finalisation of the booklet.

Ich wäre nicht bis hierher gekommen ohne die Unterstützung meiner gesamtem Familie. Liebe **Sippschaft**, es ist alles andere als selbstverständlich, dass ihr nahezu geschlossen zu meiner Verteidigung kommen werdet, obwohl alles auf Englisch stattfinden wird und es um Chemie geht. Danke, dass ihr 30 Jahre lang immer auf meine speziellen kulinarischen Eigenheiten Rücksicht genommen habt. Danke, dass ihr immer Verständnis hattet, wenn ich nicht zu allen Familienfeiern kommen konnte. Es bedeutet mir viel eine so große und tolle Familie zu haben, die alle hinter mir stehen!

Dennis, unserer Freundschaft hat ihren Lauf erst vorsichtig im Informatik-Unterricht und später dann schneller im Mathe- und Physik-LK aufgenommen. Unvergessen wird für mich immer unsere Kommunikation während einer Physik-Klausur bleiben. Danke für deine Geduld, wenn ich bei jedem Treffen am Anfang rede wie ein Wasserfall und dafür, dass ich mit dir über Mathe reden/nerden kann.

Vanessa, wir sind jetzt seit fast 15 Jahren befreundet und obwohl ich jetzt weiter weg wohne hoffe ich, dass es noch viele Jahre mehr werden. Du bist immer für mich da, wenn ich dich brauche und dafür kann ich dir gar nicht genug danken. Danke, dass du mit größter Geduld alle meine Schwächen akzeptierst und dass wir so gut über alles bis ins letzte Detail reden können. Ich bin immer für dich da!

Alice, you are one of the most loving and caring persons I have ever met. After our bonding car trip on the campus roads, you have whirled through my life as a little Italian tornado. We have had great fun nights and we had serious conversations. You took care of me after my surgery and taught me how to make real Italian lasagna. Thank you for all the love and support I received from you.

Andriy, four years ago, you were the "biggest challenge" and now you are one of my closest friends. I really enjoyed all our discussions and you taught me that disagreement can be appreciated. Thank you for always being there, all the help, advice, and also for fooling around. You know, I will always follow you to France secretly. A special thanks for your morale support during "the hornet story".

Sybren, we started at roughly the same time and we finish at roughly the same time and I really enjoyed sharing this journey with you. You have a golden heart and I am extremely thankful for the time and space that you gave me. You never needed many words to say the right things at the right time. Later, I even joined your "party office" to work closer together with Simon and you, and our shared humour only made it funnier. You are a great pool teacher with a lot of patience. After all, you kept your promise that I will score one count myself!

Arne, unsere Freundschaft bedeutet mir unglaublich viel. Für dich gibt es bei der Frage nach Unterstützung kein *ob*, sondern nur ein *wie* und du schaffst es immer genau die richtigen Fragen zu stellen. Getreu den zukünftigen Serien-Hits "Arne macht schlau" und "Arne macht heil" hast du mir nicht nur alles repariert, sondern auch beigebracht, die entsprechenden Probleme selbst zu lösen. Danke für deine Ruhe, deine Geduld, deine Offenheit und für deinen Pragmatismus. Und danke, dass du jeden meiner Sprüche noch einmal kontern kannst.

So bleibt mir am Schluss nur noch, mich bei meinen Eltern **Jutta** und **Arno**, sowie meiner Schwester **Lena** zu bedanken. Ihr habt mir unzählige Male den Rücken freigehalten (Stichwort Weihnachtsgeschenke), wenn ich durch Studium oder Promotion zu eingespannt war. Danke, dass ich immer meinen eigenen Kopf haben (zum Beispiel beim Essen) und mir meinen Weg suchen durfte, ohne jemals an eurer Unterstützung zweifeln zu müssen.

The research presented in this thesis was financially supported by the Dutch Research Councile (NWO START-UP grant 740.018.004).

Financial support from Wageningen University for printing this thesis is gratefully acknowledged.

Printed by Ipskamp, Enschede, The Netherlands

Design and layout by author

Cover by Roman Tenger and Ellen Dautzenberg